

Designing a DNA-encoded library of aptamer-like oligomers that target an antibody drug.

By

Quy Son Bui

*A thesis submitted to McGill University in partial fulfillment of the requirements of the degree of
Master of Science*

Department of Chemistry, McGill University

Montréal, Québec, Canada

June, 2023

© Quy Son Bui, 2023

Abstract

Aptamers are oligonucleotide sequences that have shown promise as alternatives to antibodies due to their high binding affinities with various targets. While aptamers possess some advantages over their protein counterparts, including the ease of chemical modification and the ability to undergo *in vitro* selection from a randomized pool, their limited chemical diversity, stemming from the four canonical nucleosidic bases, restricts their binding capabilities. Many methods have been used to broaden the chemical space of aptamers including SOMAmer technology and or click-SELEX, but methods rely on nucleosidic monomers that are compatible with DNA polymerases or ligases. Previously, the Sleiman and McKeague labs introduced Aptamer-Like ENcoded OligoMERS (Alenomers) to address the limited chemical diversity of aptamers. This approach incorporates synthetic, non-nucleosidic building blocks into sequence-defined oligo strands to expand the range of molecular interactions. The proof-of-concept study made use of the thrombin binding aptamer (TBA) as a template, a well-known stable G-quadruplex. We also include a DNA code strand that is covalently linked to the oligomer through a nucleoside-based branching unit to identify the corresponding oligo strand. Solid-phase phosphoramidite synthesis and the split-and-pool strategy were used to create a combinatorial library of nearly 300,000 alenomers. Libraries were subject to biomolecule selection, separation, and code amplification. Alenomers identified from next-generation sequencing of the DNA code showed improvements in binding affinity and serum stability, underpinning our strategy as an effective method to identify new and useful sequence-defined oligomer for biomolecule binding.

The goal of this thesis was to study the important parameters of the alenomer library structure and design that can be tuned for efficient aptamer function. First, we identified a model aptamer that

binds to a protein target with high affinity but lacks the common G-quadruplex structure. We next identified a suitable library template design, including positions suitable for modification, the length of the code, the spacer between the aptamer, and the types of branching unit. New types of monomer phosphoramidites were also synthesized and their coupling ability was tested. Finally, the compatibility of library synthesis protocol to the new design was examined. This work expands the monomer library approach, making it more generalizable to diverse aptamer structures and designs – and thus can be applied widely to identify highly stable and functional aptamers.

Résumé

Les aptamères sont des séquences d'oligonucléotides qui ont montré leur potentiel comme alternatives aux anticorps en raison de leur grande affinité de liaison avec diverses cibles. Bien que les aptamères présentent certains avantages par rapport à leurs homologues protéiques, tels que la facilité de modification chimique et la capacité de sélection *in vitro* à partir d'un pool aléatoire, leur diversité chimique reste limitée aux quatre bases nucléosidiques canoniques, ce qui restreint leur affinité avec leur cible. De nombreuses méthodes ont été utilisées pour élargir l'espace chimique des aptamères, notamment la technologie SOMAmer et le click-SELEX, mais ces méthodes reposent sur des monomères nucléosidiques compatibles avec les ADN polymérases ou les ligases. Les laboratoires Sleiman et McKeague ont par le passé introduit des oligomères encodés semblables aux aptamères (Alénomères) pour pallier cette diversité chimique limitée. Cette approche intègre des monomères synthétiques et non nucléosidiques dans des oligomères avec un contrôle précis de la séquence pour étendre la gamme d'interactions moléculaires. Une étude de preuve de concept a utilisé un aptamère de la thrombine (TBA) en tant que modèle, un quadruplex G bien connu et stable. Un brin de code ADN est lié de manière covalente à l'oligomère par le biais d'un nucléoside ramifié pour identifier l'oligomère modifié correspondant. La synthèse par phosphoramidite en phase solide et une stratégie de fractionnement et de combinaison ont permis la création d'une bibliothèque combinatoire de près de 300 000 alénomères. Ces bibliothèques ont été soumises à une étape de sélection, suivie d'une séparation et une amplification. Les alénomères ainsi obtenus, identifiés à partir du séquençage de nouvelle génération du code ADN, ont une affinité de liaison et une résistance à la dégradation dans le sérum élevées, ce qui confirme que notre stratégie est efficace pour identifier de nouveaux oligomères à séquence contrôlée se liant à des biomolécules.

L'objectif de cette thèse était d'étudier quels paramètres de la structure et de la conception de la bibliothèque d'aléomères peuvent être ajustés pour assurer une fonction efficace. Tout d'abord, nous avons identifié un aptamère modèle qui se lie à une cible protéique avec une grande affinité tout en ne présentant pas de structure en quadruplex G. Ensuite, nous avons identifié une conception de appropriée de la bibliothèque d'aléomères, identifiant les positions adaptées à la modification, la longueur du code, l'espaceur entre l'aptamère et les types d'unités de ramification nécessaires à une synthèse efficace. De nouveaux types de phosphoramidites ont également été synthétisés et leur capacité de couplage a été testée. Enfin, la compatibilité du protocole de synthèse de la bibliothèque avec la nouvelle conception a été examinée. Ce travail étend l'approche de notre bibliothèque d'aléomères, la rendant plus généralisable à des structures et des conceptions d'aptamères diverses, et peut donc être largement appliqué pour identifier des aptamères hautement stables et fonctionnels.

Acknowledgements

First and foremost, I would like to give my most sincere gratitude to Prof. Hanadi Sleiman and Prof. Maureen McKeague for their helpful guidance, great motivation, continuous encouragement, and support throughout my time at McGill University. I want to express appreciation to Dr. Donatien de Rochambeau for his valuable work on the same topic and experimental methods that are extremely helpful to this whole work. I would also like to gratefully appreciate Dr. Daniel Saliba, Dr. Eiman Osman, Dr. Quentin Laurent and Dr. Alex Prinzen for their crucial guidance, constructive discussions, suggestions, and their enthusiastic assistants during the time this work was implemented. I want to give my gratitude to Abdelrahman Elmanzalawy, Fangzhou Zhao, Tyler Brown, Jathavan Ashohan and Shiyuan Liu for their special experimental assistants and constructive discussions. In addition, I would like to give a thank to all members of Sleiman and McKeague groups, all the staff from MC2 McGill chemistry characterization and all of the staff from McGill University. Finally, I would like to express to the deepest appreciation to my family members, especially, my parents Dinh Quy Bui, Thuy Ha Tran, and my brother Quy Minh Bui for their greatest supports and encouragement.

List of abbreviations

Alenomer	aptamer-liked encoded oligomer
Å	Angstrom
ASO	antisense oligonucleotide
BU	branch unit
CD	circular dichroism
CEP	<i>N,N'</i> -diisopropylcyanoethylphosphoramidite
CPG	controlled pore glass
CuAAC	Cu(I)-catalyzed azide–alkyne cycloaddition
CV	column volume
DCM	dichloromethane
DEL	DNA-encoded library
DIPEA	<i>N,N</i> -diisopropylethylamine
DMAP	4-dimethylaminopyridine
DMF	dimethylformamide
DMSO	dimethyl sulfoxide
DMT	dimethoxytrityl
DNA	deoxyribonucleic acid
ds	double-stranded
DX	double crossover
EDC/EDC-Cl	<i>N</i> -ethyl- <i>N'</i> -(3-dimethylaminopropyl)carbodiimide hydrochloride
EDTA	ethylenediaminetetraacetic acid
ELISA	enzyme-linked immunosorbent assay
ESI	electrospray ionization
Et	ethyl
EtOAc	ethyl acetate
ETT	5-(ethylthio)-1H-tetrazole
FA/FP	fluorescent anisotropy/fluorescent polarization
FAM	fluorescein

FANA	2'-deoxy-2'-fluoro-arabinonucleic acid
FDA	The United States Food and Drug Administration
HPLC	high-performance liquid chromatography
HOBt	hydroxybenzotriazole
ITC	isothermal titration calorimetry
K_A	association equilibrium constant
K_D	dissociation equilibrium constant
k_{off}	dissociation rate constant / off-rate
k_{on}	association rate constant / on-rate
Lev	levulinyl
LNA	locked nucleic acid
LOOPER	ligase-catalyzed oligonucleotide polymerization
MD	molecular dynamic
Me	methyl
MeOH	methanol
mRNA	messenger RNA
NGS	next-generation sequencing
NMR	nuclear magnetic resonance
NTP	nucleoside triphosphate
OBOC	one-bead-one-compound
OMe	methoxy
PAGE	polyacrylamide gel electrophoresis
PBS	phosphate-buffered saline
PCR	polymerase chain reaction
PD-1	programmed cell death protein 1
PEG	polyethylene glycol
PKA	protein kinase A
PO	phosphate linkage
PS	phosphorothioate linkage
PS2	phosphorodithioate linkage
PX	paranemic crossover

RBF	round bottom flask
RISC	RNA-induced silencing complex
RNA	ribonucleic acid
rt	room temperature
RU	response unit
SELEX	systematic evolution of ligands by exponential enrichment
siRNA	small interfering RNA
SOMAmer	slow off-rated modified aptamer
SPR	surface plasmon resonance
SPS	solid-phase synthesis
SST	single-stranded DNA tile
TBA	thrombin-binding aptamer
TBDMS	<i>tert</i> -butyldimethylsilyl
TBE buffer	tris/borate/EDTA buffer
TBTU	O-(benzotriazol-1-yl)-N,N,N',N'-tetramethyluronium Tetrafluoroborate
t-Bu	<i>tert</i> -butyl
TdT	terminal deoxynucleotidyl transferase
TEA	triethylamine
THF	tetrahydrofuran
TLC	thin-layer chromatography
TNA	threose nucleic acid
UBP	unnatural base pair
XNA	xeno nucleic acid

Table of Contents

Chapter 1: Introduction

1.1 Nucleic acids	16
1.1.1 Introduction to nucleic acids.....	16
1.1.2. Nucleic acids synthesis.....	20
1.1.2.1 Solid-phase synthesis	20
1.1.2.2. Other type synthesis	22
1.1.3. Nucleic acids applications	23
1.1.3.1. DNA nanotechnology	23
1.1.3.2. Gene silencing.....	27
1.1.3.3. DNA-encoded libraries.....	29
1.2. Aptamers and ribozymes	34
1.2.1. Introduction to aptamer	34
1.2.1.1. Aptamer and antibodies	34
1.2.1.2. SELEX.....	35
1.2.2. Aptamer binding characterization	36
1.2.2.1. Aptamer binding equilibrium and kinetics.....	36
1.2.2.2. Aptamer binding thermodynamics	37
1.2.2.3. Methods for aptamer characterization	38
1.2.3. Chemical modifications of aptamers	43
1.2.3.1. Pre-SELEX and post-SELEX modification	44
1.2.3.2. Modification of the sugar ring	45
1.2.3.3. Modification of phosphate linkage.....	46
1.2.3.4. Modification of nucleobases.....	49
1.2.4 Ribozyme and DNAzyme	54

1.2.5. Aptamers and ribozymes applications.....	55
1.2.5.1. Therapeutics	55
1.2.5.2. Riboswitches	56
1.2.5.3. Biosensors	57
1.3. Previous work: Alenomers	59
Chapter 2: Results & Discussion	
2.1. Author contribution	65
2.2. Introduction	66
2.3. Identification of a non-G-quadruplex aptamer scaffold.....	67
2.4. Design of the library member scaffold.....	71
2.4.1. The design and synthesis of model constructs	71
2.4.2. Binding comparison of model constructs	76
2.4.2.1. Fluorescent anisotropy binding assay.....	77
2.4.2.2 SPR binding assay.....	80
2.4.2.3. Conclusion for binding study	85
2.4.4. Identification of potential positions in the aptamer that tolerate modifications.	85
2.5. Modified monomer amidites synthesis	88
2.5.1. Synthesis of phosphoramidites from TBA library	88
2.5.2. Synthesis of a new class of phosphoramidites	90
2.6. Library synthesis protocol	93
2.7. Conclusions and future work	97
2.7.1. Conclusion.....	97
2.7.2. Future work.....	98
2.7.2.1. For CH1S-3-based alenomer library	98
2.7.2.2. Further technique generalization	98
2.7.2.3. Technique improvement.....	99

2.8. Experimental Section.....	100
2.8.1 Chemicals	100
2.8.2. Instrumentation	101
2.8.3. Small molecule synthesis	102
2.8.4. Solid phase synthesis	113
2.8.5. Gel electrophoresis	115
2.8.6. LC-MS	116
2.8.7. Fluorescence anisotropy	118
2.8.8. Surface plasmon resonance	124
References.....	129

List of Figures

Figure 1: Ribonucleotide and deoxyribonucleotide structures	17
Figure 2: Double helix structure of double-stranded DNA	18
Figure 3: B-form, A-form and Z-form double-stranded DNA structure.	19
Figure 4: Oligonucleotide solid-phase synthesis cycle in the synthesizers.	21
Figure 5: DX, TX and PX structures.	24
Figure 6 : DNA origami and DNA wireframe.....	25
Figure 7: Self-assembly of single-stranded tile motif into a DNA brick structure	26
Figure 8: Other strategies to create DNA nanostructures	27
Figure 9: Working mechanism of ASO and siRNA.....	28
Figure 10: DNA-encoded library synthesis methods	31
Figure 11: General workflow for DEL screening and analysis process.....	32
Figure 12: General procedure of a SELEX cycle.	36
Figure 13: Principle of fluorescent anisotropy.....	39
Figure 14: General set up and working principle of a SPR instrument.	42
Figure 15: A typical cycle of an SPR experiment with immobilized aptamer and small molecule	43
Figure 16: 2'-modified oligonucleotide structures	45
Figure 17: XNA structures.....	46
Figure 18: Structures of common PS sulfurization agents.....	48
Figure 19: Phosphorothioate diastereomer structures and EMAMer	49
Figure 20: SOMAMers with 5-modified uridine.....	50
Figure 21: A cycle of Click-SELEX.	52
Figure 22: LOOPER library synthesis with oligonucleotide fragments and DNA ligase.	53
Figure 23: Unnatural base pairs	54
Figure 24: Representative ribozymes and their structures.	55
Figure 25: SAM riboswitch 'ON' and 'OFF 'states.	57
Figure 26: An example of an E-AB that recognize L-tryptophan.....	59
Figure 27: TBA alenomer library design with monomer structures.....	61
Figure 28: Alenomer library synthesis protocol.....	62
Figure 29: TBA-based alenomer library screening process with thrombin and other controls	63
Figure 30: TBA alenomer library screening result and evaluation	64

Figure 31: The TBA-based oligomer structure with seven modified positions	68
Figure 32: FA experiment set-up on a 96-well plate.....	69
Figure 33: Predicted 2D structures and FA binding assay of PD4S and CD63-1	70
Figure 34: Trastuzumab-binding aptamer CH1S-3	71
Figure 35: Structures of BU and BU2 phosphoramidites.....	72
Figure 36: Synthetic route of BU phosphoramidite.....	73
Figure 37: Design structures of test strands.....	74
Figure 38: Strand-by-strand synthesis strategy of CH1S-3-3	75
Figure 39: Denaturing PAGE of the crude products for the synthesis of CH1S-3-2 and CH1S-3-3	76
Figure 40: Fluorescent anisotropy result for the binding of branched constructs to trastuzumab	78
Figure 41: Hybridization binding test of CH1S-3-3	79
Figure 42: The set-up of two types of SPR assays (made by Biorender).....	81
Figure 43: SPR sensograms of the binding of immobilized trastuzumab with branched constructs	82
Figure 44: SPR sensorgrams of the binding of trastuzumab with poly(A) constructs	84
Figure 45: Mutation study of CH1S-3	87
Figure 46: Nine synthetic phosphoramidites included in TBA alenomer library study.	89
Figure 47: Synthetic route of Alk and Sug from PT1.....	89
Figure 48: Synthetic route of Phe from PT2a	89
Figure 49: Synthetic routes of Et , COO , Prop and Ser phosphoramidites.....	91
Figure 50: Crude PAGE result of the coupling of modified amidites	92
Figure 51: Lev20T sequence from 5' to 3' (right) and synthesis procedure from 3' to 5'(left)	93
Figure 52: N-acetyl and N-benzoyl cytidine nucleoside structures	94
Figure 53: Single member synthesis	95
Figure 54: Denature PAGE of single member library synthesis using N-Bz and N-Ac DMT-protected cytidine.....	96
Figure 55: Diagram of the sample in each well of the 96-well plate	119

List of Tables

Table 1: Calculated K_D values of three constructs on FA assay	78
Table 2: Calculated K_D values of CH1S-3-1 , CH1S-3-3 and CH1S-3-3-HYB	79
Table 3: SPR binding kinetics data of branched constructs with immobilized trastuzumab.....	82
Table 4: SPR binding kinetics and affinity data of immobilized constructs with trastuzumab.....	84

CHAPTER 1: INTRODUCTION

1.1 Nucleic acids

1.1.1 Introduction to nucleic acids

Nucleic acids are a class of biopolymer molecules that function primarily as genetic carriers in most living organisms. The building blocks of nucleic acids are nucleotides, which consist of three main components: a pentose sugar ring, a nitrogen-containing nucleobase and a phosphate group¹ (**Figure 1a**). In ribonucleic acid (RNA) the sugar ring is ribose while deoxyribose nucleic acid (DNA) contains a 2-deoxyribose ring. There are two types of nucleobases that attach at the C1 position of the sugar: purine-based (adenine and guanine) and pyrimidine-based (thymidine, cytosine, and uracil) nucleobases. A phosphodiester linkage connects the C3' and C5' of consecutive nucleotides. As a result, each nucleic acid strand has a directionality, determined by the direction from C5' to C3' of the sugar-phosphate backbone (**Figure 1b**).

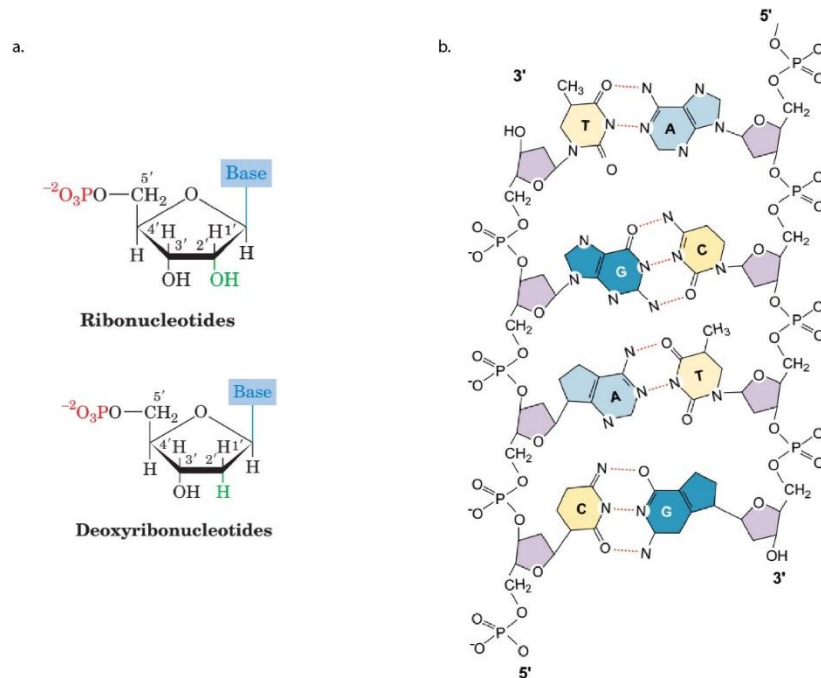


Figure 1: a. | Ribonucleotide and deoxyribonucleotide structures. (adapted from reference 1) ¹ ; **b.** |

Double-stranded oligodeoxyribonucleotide structure. (adapted from reference 2) ²

Nucleic acids were first discovered inside the nuclei of human white blood cells in 1869 by Swiss doctor Friedrich Miescher. ³ By the 1910s, many studies had revealed that nucleotides composed of a sugar, a nitrogen-containing base and a phosphorus-based linkage, are the monomers of nucleic acids. ⁴ In 1944, DNA was found to be the molecule containing genetic information by Avery, Macleod and McCarty. The X-ray structure of DNA was found in a famous X-ray experiment by Watson, Crick and Franklin in 1953. ⁵

DNA has a 2-deoxyribose backbone and the nucleobases are adenine (A), thymine (T), cytosine (C) and guanine (G). DNA occurs in natural systems mostly as double-stranded, where two single-stranded DNA wrap around each other to form a double helix ⁶ (**Figure 2a**). The two complementary strands in a DNA double helix are antiparallel or have opposite 5'-to-3' directionality. The base of nucleotide in each strand is connected to one from the other strand

through a specific hydrogen bonding pattern called Watson-Crick base pair. In Watson-Crick base pair, a purine and a pyrimidine interact with each other through a system of specific hydrogen bonds: adenine and thymine pairs to through two hydrogen bonds, while the connection between cytosine and guanine are three hydrogen bonds. This Watson-Crick base pair gives DNA specific complementarity, which is an important property for most DNA functions. The double helix structure is stabilized mainly by π -stacking between nucleobases, while base-pairing is a lesser contributor to the stability of the helix. ⁷ The spaces around a base pair are not similar in size and therefore are divided into major or minor grooves. These two types of grooves have different hydrogen-bond acceptor or donor patterns, therefore are important sites for protein binding and recognition (**Figure 2b**).

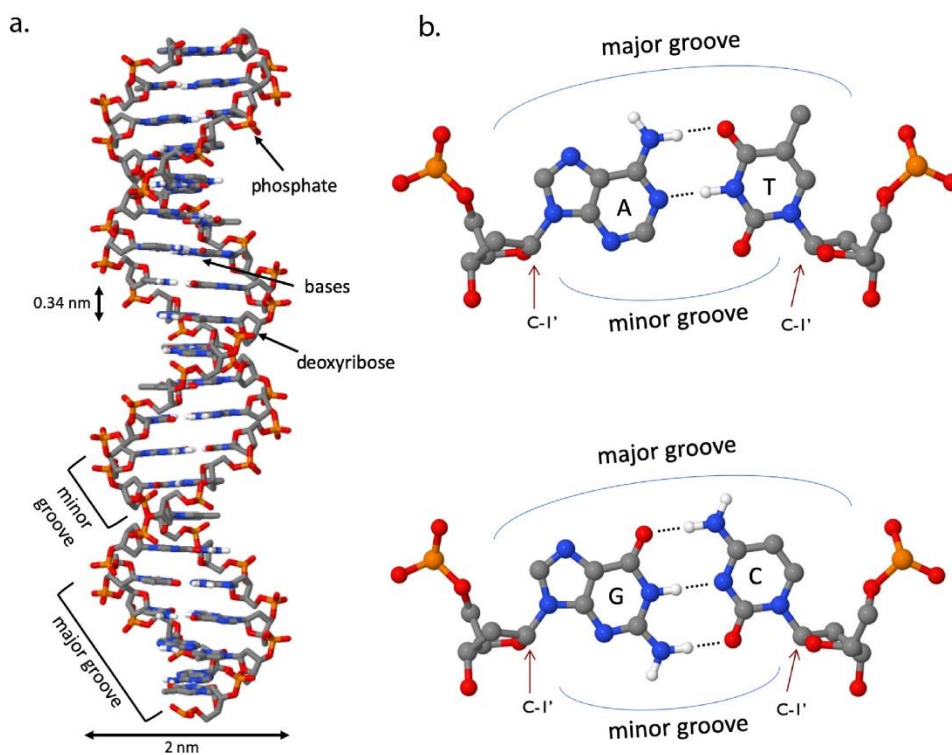


Figure 2: a. | Double helix structure of double-stranded DNA. (adapted from reference 6) ⁶ ; b. | Major and minor grooves structure in a base pair. (adapted from reference 6) ⁶

There are three major polymorphic forms of DNA double helix: A-, B- and Z-form ⁸ (**Figure 3**). In the most common B-form, the helix is right-handed and contains 10.5 nucleotides per helical turn. ⁹ The diameter of the helix is 1.9 nm, while the length of one turn is about 3.4 nm. ^{9, 10} The A-form DNA is also right-handed, but includes more base pairs in a turn and more compress to the axis than B-form. ⁹ Z-form is left-handed and rarer than the other two forms.

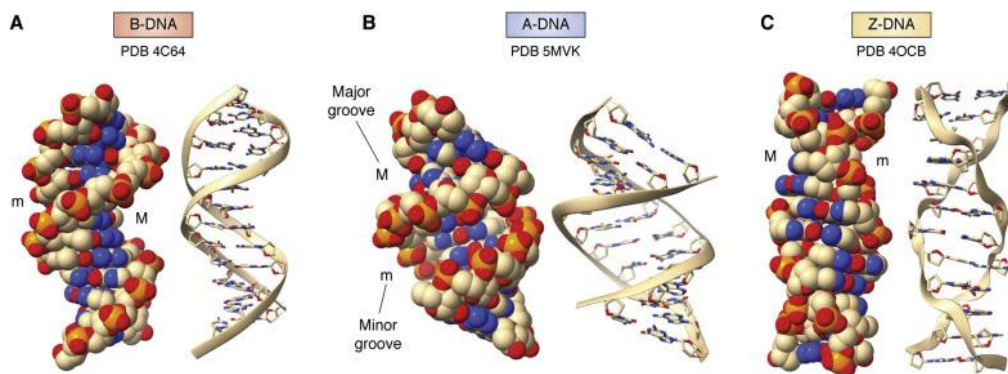


Figure 3: B-form, A-form, and Z-form double-stranded DNA structure. (adapted from reference 8) ⁸

RNA contains a ribose sugar backbone and the four nucleobases are adenine (A), guanine (G), uracil (U) and cytidine (C). Unlike DNA, RNA mostly exists as single-stranded in nature with various secondary structures such as stem, hairpin loop or bulges. ¹¹ RNA can also form RNA/RNA homo-duplexes or RNA/DNA hetero-duplexes, in which the uracil nucleobase can form Watson-Crick base pairing with adenine in a similar hydrogen bond system as A-T pair in DNA. Generally, the stability of the duplexes decreases by the order: RNA/RNA, RNA/DNA and DNA/DNA, with the heteroduplex stability highly dependent on the composition of both ribose and deoxyribose nucleotides. ^{12, 13} The presence of the 2'-hydroxyl group makes RNA more susceptible to basic conditions or enzymatic degradation, as the deprotonated hydroxyl group can undergo nucleophilic attack to phosphate linkage and cleave the RNA strand. Besides the vital role

in gene transcription and translation, RNA also participates in many other biological functions, including catalysis in ribozymes or molecular recognition in riboswitches.

1.1.2. Nucleic acids synthesis

1.1.2.1 Solid-phase synthesis

The solid phase synthesis (SPS) was pioneered in 1963 when Merrifield used the approach to synthesize oligopeptides.¹⁴ The growing peptide was covalently linked to a polymeric support to facilitate the purification of the final strand. The synthesis of oligonucleotides using SPS was also developed after this, and started thriving when phosphoramidites were used as the phosphorus-containing intermediates in the process.¹⁵ Currently, short to medium oligonucleotides can be synthesized using automated SPS with phosphoramidite chemistry depending on the size of the resin pore (the 1000 Å CPG can provide good synthesis of oligonucleotide with the length up to 100 bases). In most SPS protocols, the nucleoside phosphoramidites are protected at the 5'-end with a dimethyl trityl (DMT) group. The nucleobases (except thymine and uracil) and the 2'-hydroxyl group of ribose phosphoramidites also need to be protected to prevent unwanted nucleophilic reactions. The amino groups of A, G and C are protected as amide derivatives. The 2'-hydroxy group is normally protected with *tert*-butyldimethylsilane (TBDMS).

The synthesis occurs on the surface of a functionalized solid support, usually controlled pore glass (CPG), in a 3' to 5' direction.¹⁶ **(Figure 4)** A synthesis cycle starts with the deprotection of the existing DMT in the growing strand in acidic conditions, leaving the free 5'-hydroxyl group. The protected amidite of the next nucleotide is then added by the synthesizer, and couple to the 5'-hydroxyl group in the presence of a weak acid activator. Since the coupling yield is not 100%, the uncoupled free hydroxyl group is then capped as an ester, to prevent the growing of truncated

sequence. P (III) is oxidized to the more stable P (V) to prevent the reverse cleavage of the newly formed linkage. Finally, the DMT protecting group is removed under acidic conditions to leave the 5'-hydroxyl group for a new cycle.

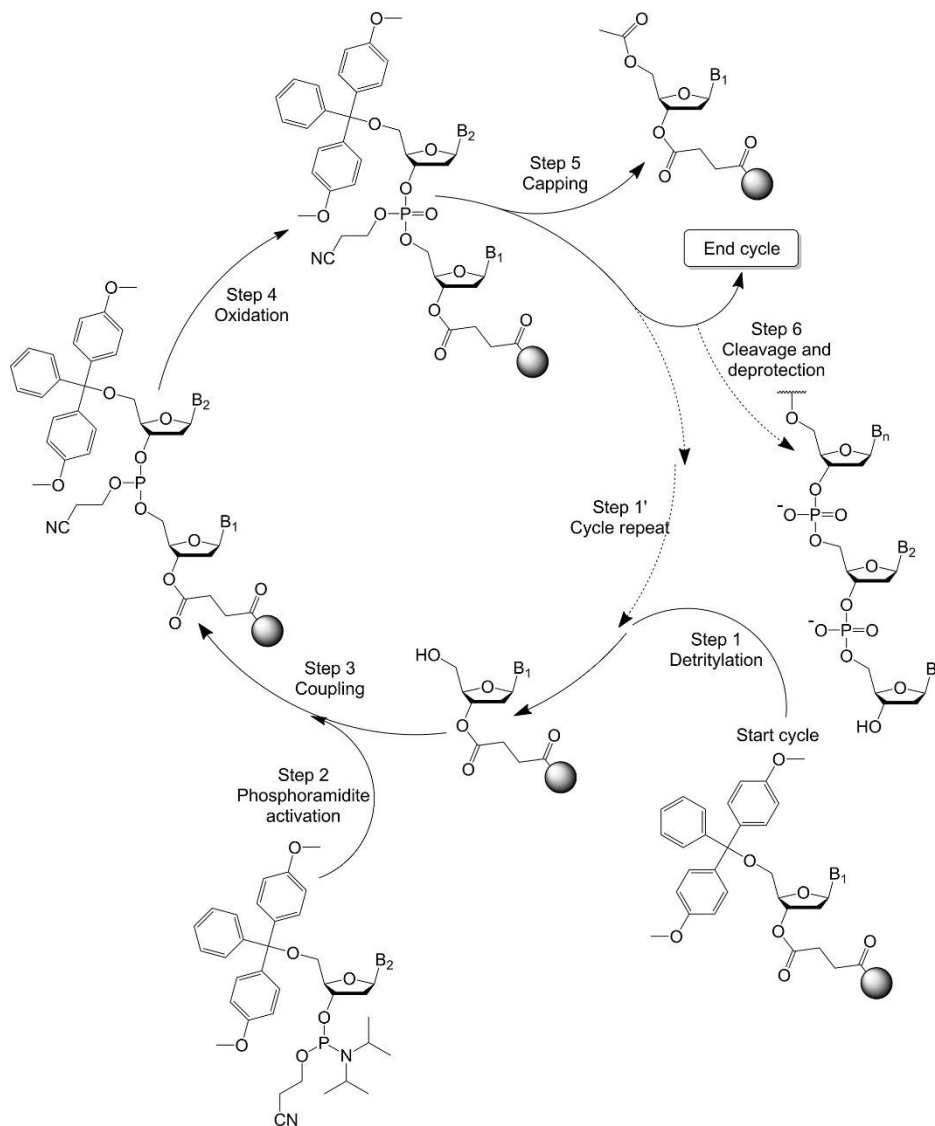


Figure 4: Oligonucleotide solid-phase synthesis cycle in the synthesizers. (adapted from reference 16) ¹⁶

Once the strand growing is complete, the solid-supported oligonucleotide is incubated in an aqueous base (normally ammonium hydroxide) to deprotect the nucleobases and the cyanoethyl group in the phosphodiester linkage. The oligonucleotide strands are also cleaved from the solid

support to the solution phase in this step. TBDMS deprotection with fluoride treatment is carried out after the basic deprotection to avoid base-catalyzed RNA cleavage. The final strand can be purified by gel electrophoresis or high-performance liquid chromatography (HPLC) and characterized by mass spectrometry.

1.1.2.2. Other type synthesis

1.1.2.2.1. Liquid-phase synthesis

Oligonucleotides can also be synthesized in a homogeneous phase with the solution. Technically, removing the heterogeneous support facilitates the distribution and accessibility of the reagents. Moreover, liquid phase synthesis does not require excess amounts of expensive reagents as well as an automated synthesizer.¹⁷ This reduces the price of oligonucleotides synthesis and therefore can help with scaling up the synthesis procedure. In liquid-phase synthesis, a soluble polymeric support from which the strand can grow is needed to facilitate the post-synthesis purification. Polyethylene glycol (PEG) is one of the most frequently used support in liquid-phase synthesis because the support facilitates the ether precipitation and filtration, which helps lower the cost of the total synthesis process.¹⁷ Most of the liquid-phase synthesis also utilize phosphoramidite chemistry similar to SPS. In a synthesis cycle, instead of capping the truncated strand, the growing oligonucleotides can be separated from reaction mixture in each cycle by precipitation, extraction, or chromatography.¹⁸⁻²⁰ However, these removals of reagents and by-products make the synthesis more laborious and not environmentally friendly. Recently, there are some advances in liquid-phase synthesis protocol to facilitate the isolation of the fully grown strands, such as using organic-solvent nanofiltration^{21, 22} or Aliphase support²³.

1.2.2.2. Enzymatic synthesis

The SPS and liquid-phase synthesis methods are efficient to synthesize short- to medium-chain oligonucleotide. However, as the coupling yield of a single phosphoramidite is not 100%, the synthesis yield will decrease dramatically when the strand becomes very long. Also, the separation method would significantly affect the amount of desired strand one can get. Therefore, current SPS technique should only be used with oligonucleotide strands that have smaller than 200 nucleotides²⁴. Longer DNA strands can be synthesized by assembling short oligonucleotide fragments with enzyme such as ligases or polymerase. Furthermore, to synthesize sequence-controlled oligonucleotide, many enzymes that do not require templates or primers were examined. For example, terminal deoxynucleotidyl transferase (TdT) – a DNA polymerase that allow template-independent synthesis – was used to incorporate free nucleoside triphosphates dNTPs into a free 3' hydroxyl end²⁵.

1.1.3. Nucleic acids applications

Besides being genetic carriers in living organisms, nucleic acids have many other applications in various fields. This section covers main applications of nucleic acids, such as nanotechnology and therapeutics: functional nucleic acids will be discussed separately in section 1.2.

1.1.3.1. DNA nanotechnology

With its well-defined and programmable structure, DNA is a promising material for bottom-up assembly. The field of DNA nanotechnology was pioneered in 1982 by Nadrian Seeman.^{26, 27}

Inspired by the Holliday junction structure in the homologous recombination that happens in meiotic cell cycles, he constructed a four-arm junction made from four different oligonucleotide strands around. Ten years later, the same group showed the double-crossover (DX molecule)

consisting of two double-stranded DNA connected through two crossover points can be used to make a more rigid structure than the single-crossover Holliday junction.²⁸ The triple-crossover (TX)²⁹ and paranemic crossover (PX)³⁰ molecules were designed by the same group a few years later. These crossover structures can also be assembled in a periodic way to form a larger architecture. For example, Winfree, Seeman and colleagues created DX molecules, which they called DNA tiles, that can self-assemble through sticky ends into nano-scale pattern crystals.³¹

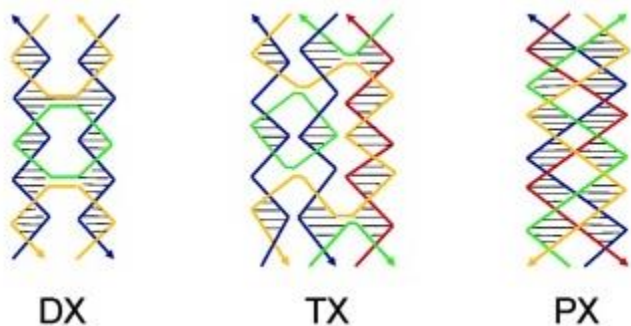


Figure 5: DX, TX and PX structures. (adapted from reference 27)²⁷

Since then, many studies have more complex DNA architectures using different strategies including DNA origami and DNA bricks. In DNA origami, the folding of a long, single-stranded DNA scaffold into a defined shape is controlled by many other shorter oligonucleotide strands.³²
³³ The 2D DNA origami structure can be folded into 3D by simply shifting the position of the crossover between two antiparallel helices by less than a turn.³⁴ The DNA origami structures can be built from either cylinder models or wireframe models. In the cylinder models, a filled structure is composed of tightly packed cylinders made of origami helices.³⁴ In the wireframe model, a porous, hollow structure is designed using vertices and edges, which are brought together by scaffold-staple crossovers.³⁵ Theoretically, programmable DNA origami can be used to address any shape, with the recent Mona Lisa DNA portrait³⁶ as an example. However, the need for a

large number of different DNA strands makes this method impractical for building large, complicated architectures.

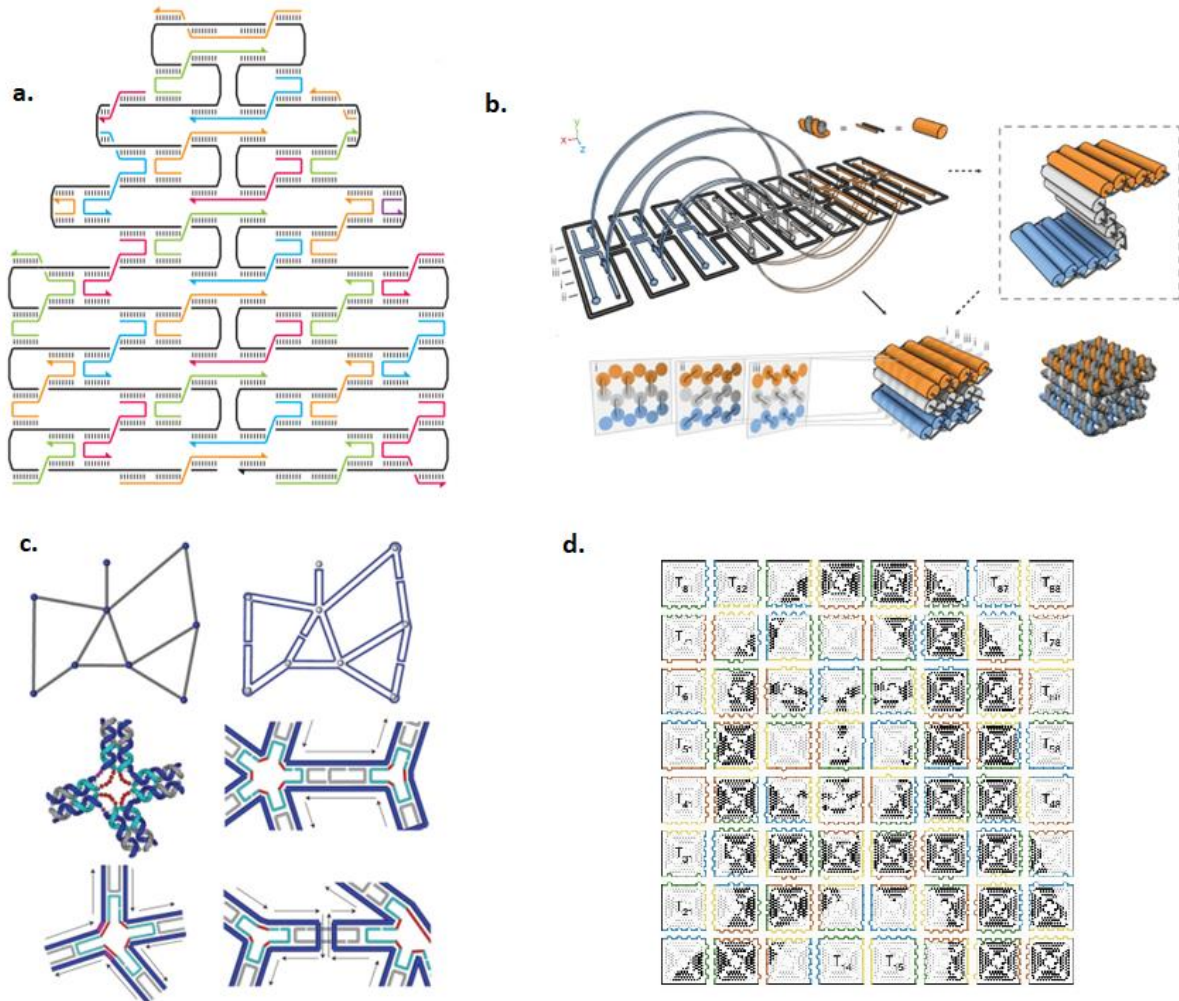


Figure 6 : DNA origami and DNA wireframe. **a.** | DNA origami scaffold and staples design. (adapted from reference 33)³³ ; **b.** | 3D DNA origami with stacked helices design. (adapted from reference 34)³⁴ ; **c.** | DNA wireframe with lines and vertices design. (adapted from reference 35)³⁵ ; **d.** | Mona Lisa portrait made from DNA origami. (adapted from reference 36)³⁶

On the other hand, DNA bricks utilize the assemblies of single-stranded DNA tiles (SSTs) which has two “head” and two “tail” domains that were complementary with others “tail” and “head”.³⁷ A strand’s head could be designed to specifically bind to a tail domain of another strand, therefore creating the self-assembly of many SSTs into a large object. The 3D version of DNA tile, also called DNA brick, is made by decreasing the length of each domain, therefore changing the helical turn.³⁸ Arbitrary shapes created by DNA SST or DNA bricks can be constructed by designing the SSTs as “pixels” on a pre-designed molecular canvas.

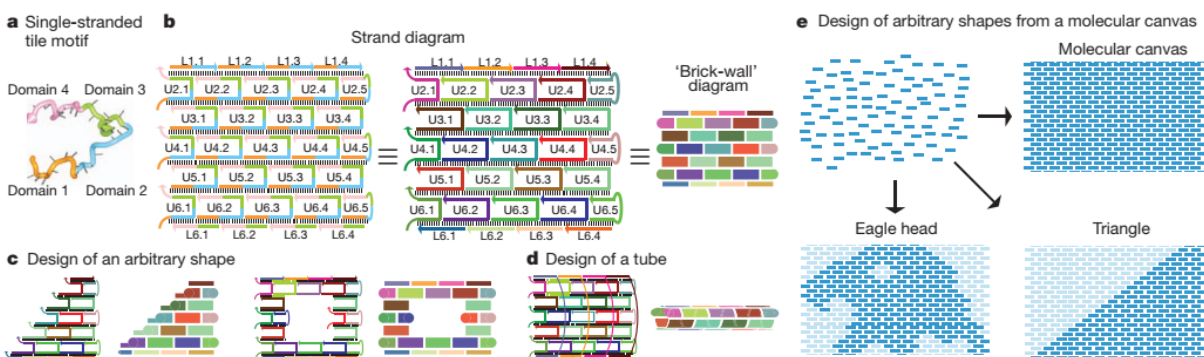


Figure 7: Self-assembly of single-stranded tile motif into a DNA brick structure. (adapted from reference

37)³⁷

There are many other strategies that have been utilized to create nanostructures, such as gold nanoparticle assemblies templated by DNA,³⁹⁻⁴¹ or metal-DNA junctions held together by metal-ligand interactions, as well as DNA hybridization.⁴²⁻⁴⁴ Many reports of minimal DNA assemblies have appeared, where the least possible number of DNA strands is used. For example, the Sleiman group has developed DNA minimal nanotubes with controlled length by stepwise assembly.^{45, 46}

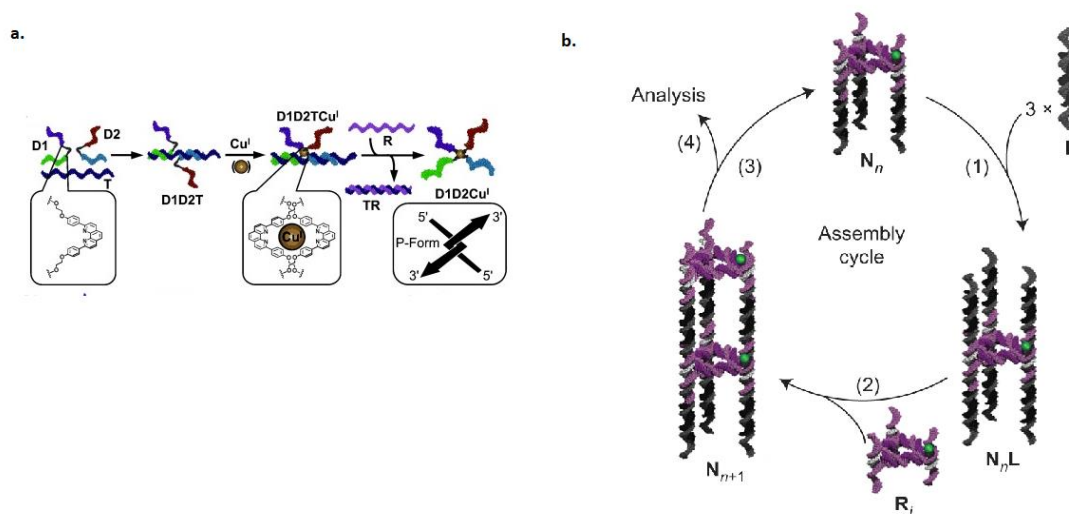


Figure 8: Other strategies to create DNA nanostructures **a.** | Cu(I)-mediated DNA junctions. (adapted from reference 44) ⁴⁴ ; **b.** | Stepwise assembly of DNA minimal nanotube. (adapted from reference 46) ⁴⁶

Due to DNA's biocompatibility, biodegradability and low toxicity, DNA nanostructures have many advantages compared to other nanomaterials, especially in biomedical applications. For example, many DNA nanostructures have been used as delivery vehicles for oligonucleotide therapeutic agents, intercalated drugs or nanoparticles. ⁴⁷⁻⁴⁹ Moreover, DNA nanotechnology can also be used to create dynamic nanodevices such as a thermoresponsive DNA flexor ⁵⁰ or the pH-responsive DNA nano-switch ⁵¹.

1.1.3.2. Gene silencing

Gene silencing is a promising oligonucleotide therapy, where the oligonucleotide strands are used to produce the therapeutic effect. Instead of directly binding to the proteins, which is the case for biologics and small molecules, gene silencing inhibits protein production, therefore controlling the target expression. Two of the most frequently used gene silencing agents are antisense oligonucleotides and small interfering RNAs. Antisense oligonucleotide (ASO) is a short, single-

stranded DNA that is complementary to a sequence in mRNA and interferes with its activity by several mechanisms, one being the RNase H-mediated cleavage of ASO/mRNA duplex. ⁵² Other inhibition methods including altering pre-mRNA splicing or sterically blocking ribosome translation are often employed in ASO with modified backbones. ⁵³ On the other hand, the activity of small interference RNA (siRNA) is operated through the RNA interference process. The first step is the cleavage of long dsRNA to the short siRNA duplex by Dicer enzyme. When siRNA duplex enters the cell, it can form a complex with multiple proteins to form RISC (RNA-induced silencing complex). ⁵⁴ One of the siRNA strands, also called antisense strand, guides RISC to the target mRNA, and the proteins in RISC will catalyze the cleavage of the mRNA. ⁵⁵

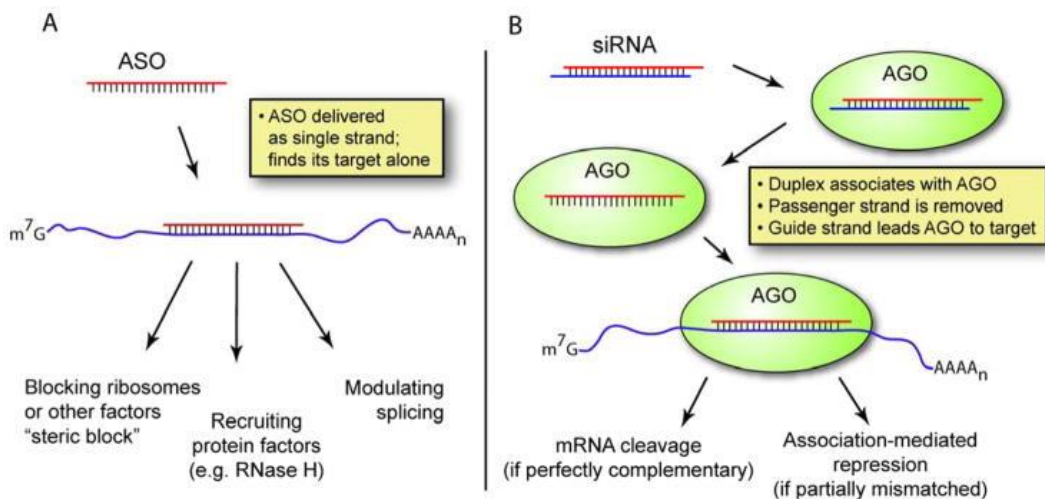


Figure 9: Working mechanism of ASO and siRNA **a.** | Mechanism of ASO. (adapted from reference 54) ⁵⁴ ; **b.** | Mechanism of siRNA. (adapted from reference 54) ⁵⁴

Gene silencing is a promising therapeutical strategy as it can target the expression of many undruggable proteins. By the end of 2022, eighteen oligonucleotide-based therapeutics have been approved by FDA, nine of which are ASOs and siRNAs. ⁵⁶ However, the main limitations of gene

silencing agents are their low *in vivo* stability and their poor cellular uptake. These problems can be tackled by chemical modifications, bio-conjugation or using delivery vehicles.

1.1.3.3. DNA-encoded libraries

The accuracy of base pairing as well as the fidelity in PCR and sequencing techniques make DNA a great “barcoding” tool, with DNA-encoded libraries (DEL) as the most popular application. In the DEL approach, each compound is tagged by a unique oligonucleotide “barcode”, enabling all members of the library to be synthesized and screened simultaneously in a single solution.⁵⁷ The coding power and amplifiability of DNA enable the information of library to be stored and decoded after the screening process. The technique was pioneered by Brenner and Lerner in 1990s, when they prepared tripeptide library encoded by single-stranded DNA.^{58, 59} According to Neri, DELs can be divided into two subgroups: single- and dual-pharmacophore libraries.⁶⁰ In single-pharmacophore libraries, a single molecule is attached to one DNA fragment, while in double-pharmacophore one, two molecules are tagged with a double-stranded DNA in an individual member of the library.

There are two common ways to synthesize a single-pharmacophore library, either by DNA-recorded or DNA-templated synthesis. In DNA-recorded synthesis, after each building block coupling step, a DNA fragment encoding that block is also enzymatically attached to the nascent coding strand. A “split-and-pool” procedure is usually used to yield a combinatorial library.^{60, 61} The coding DNA used in this method is normally double-stranded, but some studies also reported the use of single-stranded fragments in encoding DNA-recorded libraries.^{62, 63} On the other hand, DNA-templated libraries are synthesized by pools of pre-encoded DNA templates. The building blocks contain the compound and its anticodon sequence, and the complementary codon-anticodon pairing directs the coupling of the building block to the template. A novel universal strategy has

been developed with templates containing poly-inosine that can bind to any of the four bases, enabling the creation of random combination of building blocks in a rapid and simple way.⁶⁴ The dual-pharmacophore library, also known as encoded self-assembling combinatorial (ESAC) library, was pioneered by Neri *et al.* in 2004.⁶⁵ The two sub-libraries of two building blocks, each of which linked with the coding strands that were able to hybridize with ones in the other sub-library, were synthesized. The building blocks were linked only by the complementary pairing of the two coding strands, leading to the need of re-synthesizing two-component compounds with proper covalent linkers for hit evaluation. A d-spacer was added in a later study to prevent the hybridization mismatch of the two DNA strands.⁶⁶

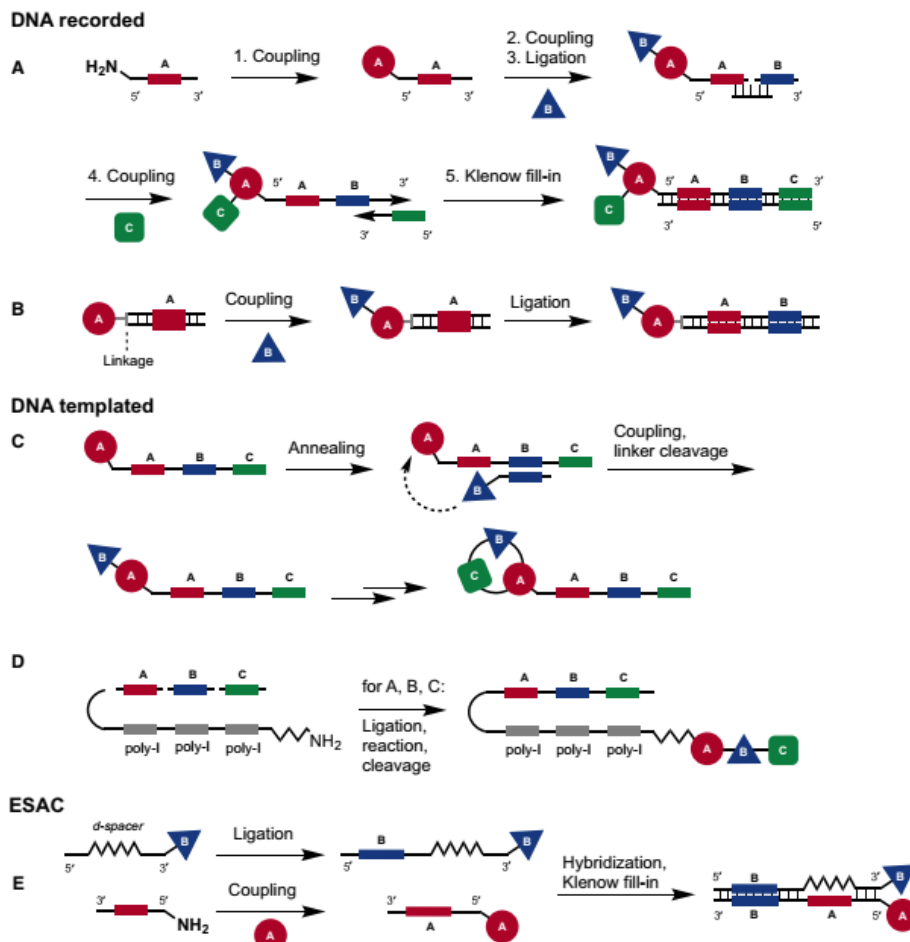


Figure 10: DNA-encoded library synthesis methods. (adapted from reference 60)⁶⁰

Figure 11 shows the common steps in the affinity-based screening and analysis of a DEL toward a biochemical target.⁶⁷ In contrast to general high-throughput screening protocol, a DEL exists as a mixture, so all the screening experiments happen in parallel within a single tube. The target, which is in many cases protein, is mixed with library mixture in an appropriate condition. In solid-phase selections, the targets are often tagged with an oligohistidine or biotin for immobilization on solid supports^{68,69}, and the unbound compounds are washed away after the affinity capture. In the next step, the barcodes are amplified using PCR and decoded by sequencing to yield the binders' information. The sequence frequency, which represents the relative number of a barcode sequence

found after decoding, can be used to estimate the abundance of the corresponding compound.⁶⁰ The enrichment step can be repeated through several cycles, and the degree of repetition of building blocks in the hits is statistically analyzed. The most frequently appearing building blocks will be used to build the off-DNA compounds for re-validation using biochemical assays.

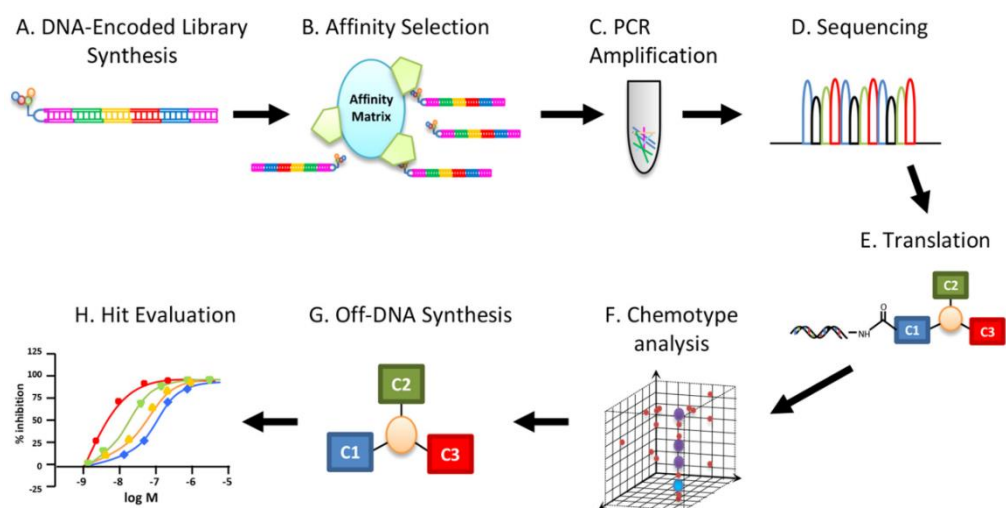


Figure 11: General workflow for DEL screening and analysis process. (adapted from reference 67)⁶⁷

DELs provide an inexpensive and rapid method for screening of large libraries (which can reach 10^6 members) without the need for expensive automated systems. In addition, the screening can happen in a single tube as the library exists as a mixture. The DEL members also do not need to be prepared in high concentration thanks to the amplification ability of DNA coding strands. However, compared to other screening methods, there are still various limitations that prevent DELs to be widely applied. First, the requirement of DNA-compatible coupling reactions for building blocks significantly reduces the choices of library synthetic routes. Moreover, the non-equal yields between coupling reactions may create a bias in the library. Second, most current DEL screening techniques are only based on physical affinity between the target and ligands. As a result, many site-selective biological functions need to be studied from the post-screening off-DNA

validation. Third, for many DEL-targeting proteins, the solid-phase immobilization techniques require pure proteins in their active forms. However, many proteins cannot be isolated or denature in the isolation process, leading to the need for *in vivo* DEL screening protocols.

Recently, many advances in DEL have been created to overcome these problems. A wide variety of DEL-compatible reactions have been found, including metal-catalyzed⁷⁰⁻⁷³ or photoredox^{74, 75} coupling reactions. In addition, many screening strategies targeting biological properties have been developed. For example, during the selection of FTase, protein kinase A (PKA), and caspase 3 enzyme with DNA-encoded peptide substrates, Jetson and Krusemark used additional enzymes to selectively biotinylate the products, which helps isolate the successful products later.⁷⁶ The “one-bead-one-compound” (OBOC) techniques are also utilized frequently to create functional DELs. In OBOC-DELs, each library member is attached to a bead, often through a cleavable linker, that also contains its own DNA code. In 2019, Cochrane and colleagues created the first activity-based screening DEL to identify phosphodiesterase autotaxin inhibitor.⁷⁷ In their OBOC-DEL, microfluidics was used to separate each bead in a droplet, and the compound was cleaved from the bead to interact with the target in the same droplet. The droplets were sorted based on the fluorescent signal intensity that showed the inhibition of the library compound. The non-immobilization screening techniques are also examined to broaden the scope of targets for DEL. For example, the solution-phase DNA-encoded dynamic chemical library (DEDL) utilized photo-driven crosslinking to lock up the highest affinity combination of pharmacophores in a dynamic equilibrium.^{57, 78} For example, Petersen *et al.* reported an *in vivo* DEL screening targeting protein with the assistance of another integrated “bait” protein that helps discriminate the hits and the non-binders.⁷⁹

1.2. Aptamers and ribozymes

1.2.1. Introduction to aptamer

1.2.1.1. Aptamer and antibodies

Aptamers, or nucleic acid aptamers, are short single-stranded oligonucleotide sequences that bind specifically to a target.⁸⁰ Each aptamer often has a functional structure that may include various secondary structures such as stem-loop or G-quadruplex. There is a wide variety of targets reported for DNA or RNA aptamers, from small molecules, and proteins to cells and viruses. The interactions responsible for the binding between an aptamer and its target include non-covalent interactions such as hydrophobic effect, electrostatic interaction, hydrogen-bonding or π - π stacking.⁸¹

Aptamers can be considered the “nucleic acid version” of antibodies. In fact, while having binding affinity comparable with antibodies, aptamers have many advantages over antibodies. As therapeutics, aptamers are generally non-immunogenic. Their small size allows them to penetrate efficiently into many biological areas that antibodies might be too large to access.⁸² In addition, since aptamers can be chemically synthesized, their production process is cheaper, and also able to avoid viral or bacterial contamination that often occurs in antibody manufacturing.⁸² Aptamers can undergo *in vitro* selection and endure various chemical modifications, which can facilitate the screening and optimization process. Their storage conditions are also more tolerable than antibodies, as aptamers can refold to their original form simply by heating and cooling.⁸³ However, there are still some significant drawbacks that prevent aptamers from being widely applied. First, unmodified aptamers lack the chemical diversity that is observed in antibodies (both DNA and RNA consist of only 4 nucleotides compared to 20 amino acids in antibodies). This shortage limits

the available non-covalent interactions, reducing the binding affinity and specificity of aptamers to their targets. Moreover, the charged nature of the phosphodiester backbone prevents the diffusion of aptamers into the interior of cells. Aptamers are also labile to nuclease degradation, decreasing *in vivo* efficiency when compared to antibodies.⁸⁴ As a result, until 2021, only one aptamer drug has been approved by FDA.^{85,86} These disadvantages can be addressed by chemical modification, which will be discussed in more detail in section 1.2.3.

1.2.1.2. SELEX

Aptamers for a specific target can be identified from a pool of oligonucleotides through an *in vitro* selection process called SELEX (Systematic Evolution of Ligands by EXponential enrichment). A general SELEX protocol starts with the generation of a randomized DNA or RNA library.⁸⁷ **(Figure 12)** The oligonucleotide library can be generated from either solid-phase synthesis with phosphoramidite chemistry, or from enzymatic synthesis with polymerase and deoxyribose triphosphates or ribose triphosphates (dNTPs or NTPs). A SELEX library design usually contains two parts: primer regions at both ends and a random region in the middle. Primer regions, which are similar among library members, are used for amplification. On the other hand, random regions are the “actual aptamer” part and are variable between strands. In the next step, the target is incubated with the library and some oligonucleotides will bind to the target. The target-bound complexes are isolated, in many cases through immobilization of the target, and the non-binding sequences are washed away. Finally, the binders are amplified by the polymerase chain reaction (PCR) to create a new pool that is ready for another selection round. The binder information can also be identified in each round by sequencing using Sanger sequencing or Next-Generation Sequencing (NGS).

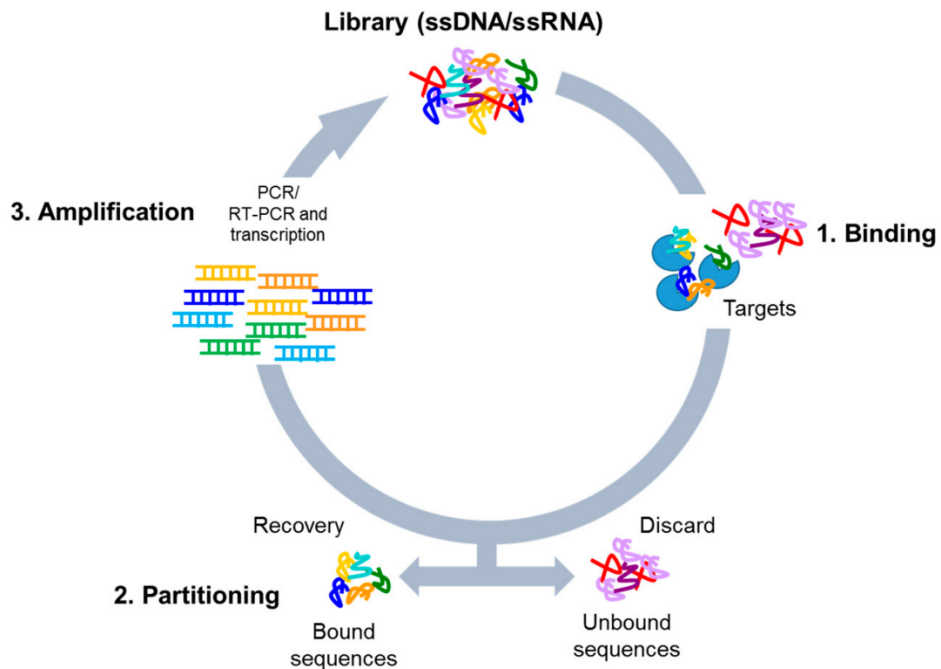
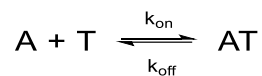


Figure 12: General procedure of a SELEX cycle. (adapted from reference 88)⁸⁸

1.2.2. Aptamer binding characterization

1.2.2.1. Aptamer binding equilibrium and kinetics

When an aptamer (A) binds to a target (T) in 1:1 ratio, there is an equilibrium between A, T and the aptamer-target complex AT:



In equilibrium, k_{on} represents the rate-constant of the association reaction (forward reaction) and k_{off} represents the rate-constant of the dissociation reaction (reverse reaction). The association and dissociation constants, K_A or K_D respectively, are calculated as follows:

$$K_A = \frac{1}{K_D} = \frac{[AT]}{[A][T]}$$

[A], [T] and [AT] represent the concentration at equilibrium of A, T and AT, respectively. When the K_D value is low (or the K_A value is high), the formation of AT will be more favored, therefore the binding affinity of the aptamer to the target will be stronger. In addition, if $[T] = [AT]$, $K_D = [A]$. Therefore, K_D can be considered as the concentration of free aptamer when the target is half-saturated.

In terms of kinetics, the rate constants k_{off} and k_{on} values highly depend on the free energy of the transition state, which cannot be isolated during the binding process. Therefore, these kinetics data are difficult to observe, and highly sensitive methods such as surface plasmon resonance (SPR) are required to observe the kinetic behavior of aptamer binding. In addition, the kinetic properties can also be used to study the binding affinity of aptamer. Theoretically, K_D can be calculated from rate constants:

$$K_D = \frac{k_{\text{off}}}{k_{\text{on}}}$$

As a result, lower K_D is also characterized by low k_{off} and high k_{on} . In other words, high-affinity aptamers are likely to display a low value of rate of dissociation (slow off-rate) and high value of rate of rate of association (fast on-rate). Slow off-rate can be achieved by stabilizing the aptamer-target complex (AT), and this strategy can be utilized to optimize better aptamer binders. For example, Gold *et al.* created high-affinity SOMAmer (Slow Off-rate Modified Aptamer) in which nucleobases were modified with hydrophobic moieties to mimic amino acid side chains, therefore generating a more stable oligonucleotide-protein complex.⁸⁹

1.2.2.2. Aptamer binding thermodynamics

The Gibbs free energy of binding process between aptamer and target can be calculated as:

$$\Delta G = \Delta H - T\Delta S$$

The binding process is spontaneous thermodynamically if $\Delta G < 0$, which is favored by more negative ΔH and more positive ΔS . As a result, the aptamer binding can be driven by either enthalpy or entropy factor. The change in enthalpy is the total energy change when an aptamer binds to its target, resulting in forming new non-covalent interactions in the aptamer-target complex. Moreover, solvent also contributes to the net ΔH value, as the interaction between solvent and aptamer or target is disrupted during the binding process. On the other hand, the total entropy change indicates the variation in the degree of freedom of the system consisting of aptamer, target, and solvent, with a more positive value meaning the system is more chaotic. Generally, the formation of a more ordered complex from free molecules contributes negatively to the system ΔS .

⁹⁰ To compensate for this entropic loss, in some aqueous systems, the binding is driven majorly by water entropy – water molecules are released from interaction with oligonucleotide or the target.

91

1.2.2.3. Methods for aptamer characterization

1.2.2.3.1. Fluorescent anisotropy (FA)

A fluorophore when excited by a polarized light will also emit polarized light with different intensities in the planes that are parallel, versus perpendicular, to the excited plane. A fluorescent anisotropy (FA) value is calculated based on the parallel (I_{\parallel}) and perpendicular intensities (I_{\perp}) as following formula:

$$\text{Anisotropy} = \frac{I_{\parallel} - I_{\perp}}{I_{\parallel} + 2I_{\perp}}$$

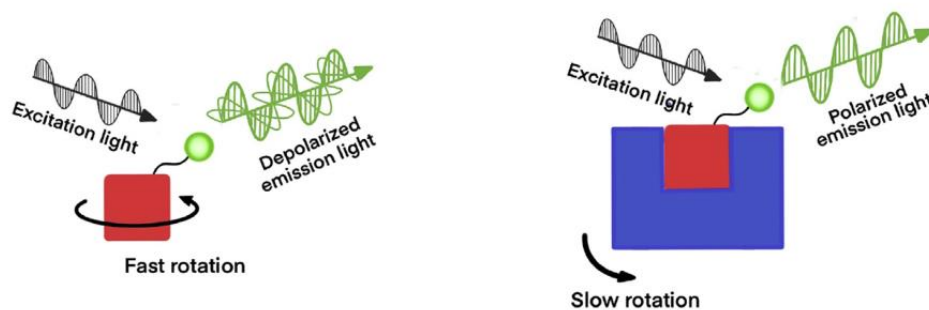


Figure 13: Principle of fluorescent anisotropy. (adapted from reference 92)⁹²

Physically, FA represents the rotational speed of the fluorophore with respect to its fluorescent lifetime.⁹² Therefore, the value of FA depends heavily on the volume and the degree of freedom for rotation around the fluorophore. The larger the volume, the slower the fluorophore can rotate, which leads to the more polarized emitted light and therefore the FA value is higher. The maximum anisotropy can also be calculated based on the angle between the absorption and emission dipole moments as follow⁹³:

$$\text{Maximum anisotropy} = \frac{2}{5} \left(\frac{3 \cos^2 \beta - 1}{2} \right)$$

Therefore, the maximum theoretical anisotropy value is 0.4, obtained when $\beta = 0$.

FA assay is a frequently used method to study the binding affinity of aptamers to proteins. In most of the FA assays, the fluorophore-labelled aptamer is incubated with the protein in a homogeneous solution. Since the aptamer is generally smaller than the protein, the binding will generally increase the anisotropy of the fluorophore. Therefore, by monitoring the change in fluorophore anisotropy over a range of protein concentrations, one can fit the data to the binding curve and therefore get the affinity values such as dissociation constant K_D . A competitive assay between non-labelled and labelled aptamer is also often used to examine the specificity of the binding.⁹² The localization of

fluorophore in the aptamer is also important. Ideally, the fluorophore should be attached close to the binding site so that the binding can have enough effect on the fluorophore's local rotation. Examples of proteins used FA assays to study the binding with their aptamers are thrombin ⁹⁴, vascular endothelial growth factor (VEGF) ⁹⁵, CD63 ⁹⁶ and immunoglobulin E (IgE) ⁹⁷.

Unlike with proteins, the study of aptamer-small molecule binding using FA assay is more complicated. Since in most cases the aptamers have a larger size than the small molecule, having the fluorophore attached to the aptamer might not yield enough significant anisotropy change to be observed. To overcome this problem, the attachment site needs to be examined very carefully to produce the best signal. For example, Zhao *et al.* identified the proper label site of ochratoxin A aptamer by screening the anisotropy signal of many different fluorophore positions. ⁹⁸ On the other hand, attaching the fluorophore to the small molecule might change the molecule's nature, as the fluorophore might have the same size as the small molecule. In that case, additional competitive assay with non-labelled small molecules can give the actual binding data of the target. ^{99, 100} Some molecules that have the aptamer binding studied by FA are ochratoxin A ⁹⁸, ATP ¹⁰⁰ or cocaine ¹⁰¹.

Fluorescent anisotropy provides a simple, cost-effective homogeneous method to measure the binding affinity for a wide range of targets. However, there are some general limitations with the FA assays. First, the method might not be sensitive enough to study the kinetic properties of many aptamer-ligand systems. Second, the attachment of fluorophore to either the aptamer or target might interfere with binding interactions. Moreover, the binding lifetime and the location of fluorophore can affect the result significantly.

1.2.2.3.2. Surface plasmon resonance (SPR)

Surface plasmon resonance (SPR) is a phenomenon that takes place in the surface of a thin metal sheet placed in the boundary of a dielectric medium is excited by light photon.¹⁰² At a certain angle of the incident light, there is a coincidence between the energy of the evanescent wave caused by the total reflection and the plasmon energy in the surface of the metal, SPR occurs. At that angle when the resonance happens, called SPR angle, the reflection is minimal, and a “dip” will appear in the detector. Since the SPR phenomenon is very sensitive to the refractive index near the surface of the metal sheet, a change at the metal surface can be tracked by recording the “dip” response. As a result, SPR can be used to monitor the binding event of the aptamer to its target that occurs on the metal surface.

A general SPR experiment requires an SPR chip, which is usually a thin gold film, which has the analyte anchored in the surface (**Figure 14**). A prism with a high refractive index is connected to one side without the analyte of the chip, and the other side is a flow channel with the dielectric medium (water or buffer solution). In many SPR instruments, a second blank flow channel is used as a reference channel to eliminate noise signals. As the incident light hits the film through the prism, the change in mass concentration near the film surface can be monitored by the change of SPR angle, and the detector will record that signal as a response unit (RU).

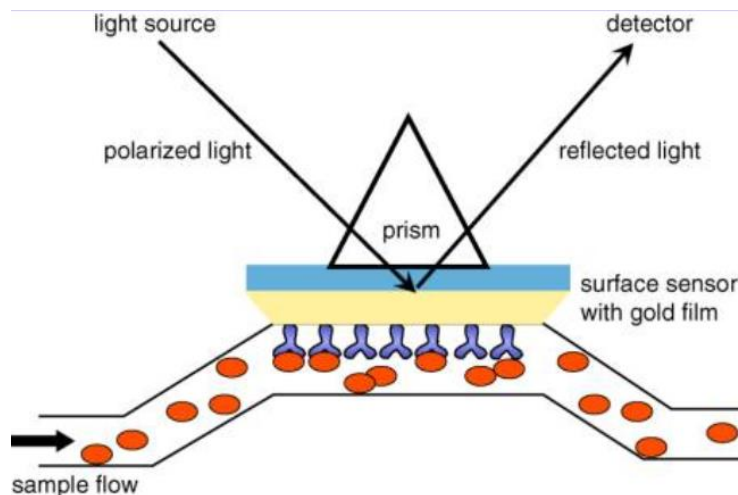


Figure 14: General set up and working principle of a SPR instrument. (adapted from reference 102) ¹⁰²

A typical cycle of an SPR experiment for an aptamer binding assay is shown in **Figure 15**. For the analytes that are not attached to the gold film, the first step is the analyte capture. This analyte can be either aptamer or the target, which is often conjugated with a linker that can bind with another linker covalently attached to the gold film. Some common linker pairs are poly(A)/poly(T) ¹⁰³ and biotin/streptavidin ¹⁰⁴. Next, the flow channel brings the ligand into contact with the thin film. The binding increases the RU signal (association step) until it reaches a maximum value where the equilibrium occurs. After this, the buffer is flown to detach the bound ligand and generate a new cycle (dissociation step). Normally, there are two ways to analyze the SPR data. The affinity analysis fits the equilibrium response unit at different ligand concentrations to the binding curve to generate the binding constant value such as K_D . On the other hand, the kinetic analysis fits the signal in association and dissociation steps to find out k_{on} and k_{off} , respectively, and one can find the K_D values based on these rate constant values.

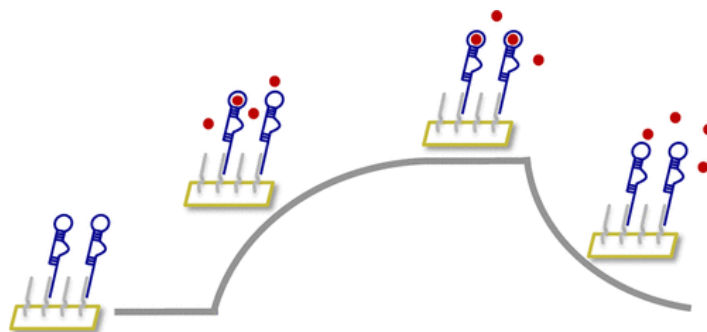


Figure 15: A typical cycle of an SPR experiment with immobilized aptamer and small molecule. (adapted from reference 103) ¹⁰³

One of the most important advantages of SPR compared to other methods is its very high sensitivity, which enables real-time kinetic studies. Second, the technique is totally label-free, which reduces the cost and the labor to prepare any fluorescent probes. However, SPR requires expensive instruments with expensive gold film chips, that in some cases are not reusable. Moreover, the linker may affect the folding and binding of the aptamer, especially the poly(A) or poly(T) linker. ¹⁰³ It is worth noting that since the technique is heterogeneous, the measurement results may not be consistent with other homogeneous methods such as FA or isothermal titration calorimetry (ITC). For example, Potty and colleagues identified a significant difference between the K_D value of VEGF binding with its aptamer when measured by FA and when measured by SPR, with a possible explanation due to different binding modes observed in solution and in immobilized conditions. ¹⁰⁵

1.2.3. Chemical modifications of aptamers

As mentioned above, there are several obstacles preventing aptamers from being applied as widely as antibodies. Two of the most significant disadvantages of aptamers are the lack of chemical

diversity and their liability to nuclease degradation. With the tolerance of many chemical reactions, modified aptamers are often used to ease those obstacles.

1.2.3.1. Pre-SELEX and post-SELEX modification

Generally, there are two strategies to make a chemical modification of aptamer: either before or after the SELEX process. In pre-SELEX modification, the modified nucleotides or other building blocks are introduced into the initial library. These modifiers can be incorporated either through solid-phase or enzymatic synthesis. The great advantage of this approach is the ability to create a highly diverse aptamer library, which includes theoretically all possible combinations of all available monomers. Also, the binders are fully identified by the selection process, which removes the time and cost needed for the laborious post-SELEX optimization. However, there are several large trade-offs for this strategy. First, an appropriate library generation protocol for the modified building blocks must be employed. Second, the modified monomers must be recognized by polymerases. Although some polymerases have been reported to tolerate a few base-modified nucleotides,¹⁰⁶ there are still large limitations on the number and composition of building blocks that can be used. Moreover, to maintain the fidelity of the amplification and sequencing process, each monomer must be recognized specifically by its sequence. This can be eased by the research in unnatural base pairs (UBPs), which aims to expand the genetic alphabet of aptamers.¹⁰⁷

On the other hand, post-SELEX modification is an optimization process of the selected binders. Normally, the selected candidates from a canonical oligonucleotide pool will undergo many mutations for structure-affinity or structure-activity studies. As a result, there is no polymerase-compatible requirement for modification to be introduced into the aptamer. However, there is a risk of the mutants losing the binding affinity from the original aptamer, as chemical modifications

can significantly change the oligonucleotide folded structure.¹⁰⁸ In addition, synthesizing a large number of individual mutants and testing each of them is a tedious and costly task.

Different types of chemical modification have different suitability for either strategy. In the next few sections, examples of different types of modified oligonucleotides and their improvement from the original aptamers will be discussed.

1.2.3.2. Modification of the sugar ring

RNA strands can undergo enzymatic cleavage in specific sites by RNase due to their nucleophilic 2'-hydroxyl group.¹⁰⁹ As a result, the ribose 2' position is a frequent target for modification to make more nuclease-stable aptamers. Some remarkable examples with replacement of the 2'-hydroxyl group by 2'-fluoro, 2'-amino or 2'-O-methyl showed both improved nuclease resistance and great binding affinity.¹¹⁰⁻¹¹² In addition, several polymerases can tolerate 2'-fluoro and 2'-amino NTPs, while fewer enzymes can recognize and incorporate 2'-O-methyl NTPs.¹¹³ The first and only aptamer drug that was accepted by FDA, Pegaptanib, consists of 2'-fluoro and 2'-O-methyl nucleotides that help increase the stability to nucleases.⁸⁶

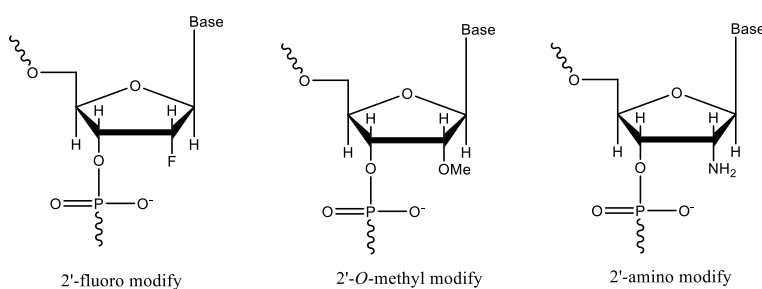


Figure 16: 2'-modified oligonucleotide structures

In broader terms, “xeno” nucleic acids (XNAs) are nucleic acid analogues in which the ribose or deoxyribose ring was replaced by other chemical moieties. Various engineered polymerases have

been able to transcribe XNA from DNA or reversely synthesize DNA from XNA,¹¹⁴ enabling the SELEX of many types of XNA aptamers. Moreover, since the structures of nucleobases are maintained, many XNAs can form duplexes with complementary DNA or RNA.¹¹⁵ Some of them can even form a more stable hetero-duplex with DNA/RNA than the homo-duplex itself,¹¹⁶⁻¹¹⁸ which can increase the fidelity of transcription and PCR process. A frequently studied XNA, locked nucleic acid (LNA), has the 4'-carbon and 2'-O of ribose sugar covalently linked through a methylene group. Although this locked conformation enhances nuclease resistance and thermal stability, its steric hindrance restricts the flexibility of the aptamers.^{119, 120} To minimize this limitation, aptamers are often selected from a mixture of LNA and other residues, e.g., chimeric DNA/LNA aptamers can target the TAR RNA element from the HIV virus with high affinity.¹¹⁹ Beside LNA, aptamers of other XNAs such as threose nucleic acid (TNA) or 2'-deoxy-2'-fluoroarabinose nucleic acid (FANA) also show great nuclease resistance and high binding affinity (sometimes even greater than the ribose analogues) to various targets.¹²¹⁻¹²³

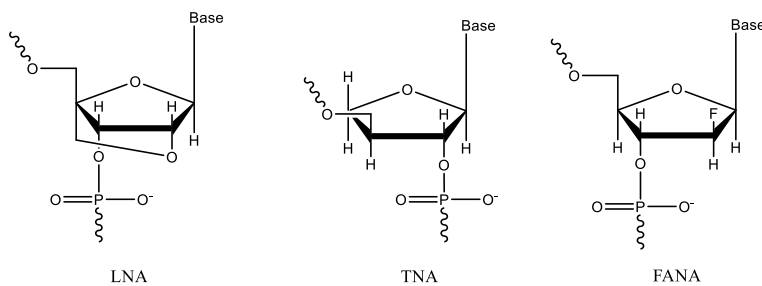


Figure 17: XNA structures

1.2.3.3. Modification of phosphate linkage

Sulfurization of the phosphate linkage (PO) into the phosphorothioate (PS) is probably the most common method to increase the nuclease resistance of nucleic acids.¹²⁴ In PS linkage, an oxygen atom in PO is replaced by a sulfur atom, therefore creating a chiral center at the phosphorus atom.

As a result, the PS linkage exists as two enantiomers: left-handed (Sp) and right-handed (Rp), and PS oligonucleotides are diastereomer mixtures. The Sp stereoisomers are more stable in duplex form while Rp ones offer more nuclease resistance,¹²⁵ so a mixture of stereoisomers can offer a balance of the benefit between the two stereoisomers. The oligonucleotides can be sulfurized in solid-phase synthesis, in which the sulfurizing agents such as the Beaucage reagent or 3-((dimethylamino-methylidene)amino)-3H-1,2,4-dithiazole-3-thione (DDTT) are added instead of the oxidizing agent.¹²⁶ While most of the sulfurizing agents yield a mixture of Sp and Rp PS linkages, a sulfur-containing phosphorylation reagent was found by the Baran group recently can help synthesize stereo-defined PS linkages through a P(V)-based synthesis protocol.¹²⁷ The stereochemistry of PS linkage can also be controlled in enzymatic synthesis using polymerases that prefer alpha-S thiotriphosphate substrates.¹²⁸ Overall, PS modifications have been implemented to increase nuclease resistance in many aptamers with a wide range of structures and targets.¹²⁹⁻¹³² Beside PS, phosphorodithioate (PS2) modification can be created by replacing both non-bridge oxygen atoms to sulfur on the phosphate linkage. The non-chirality of PS2 center prevents the formation of racemic mixtures in the modified aptamer. Many dithio-aptamers express great nuclease assistance; some of them even have higher binding affinity than the PS-modified strands with the same sequence.¹³³ However, di-sulfurization of aptamers might alter the specificity depending on the modified positions.¹³³

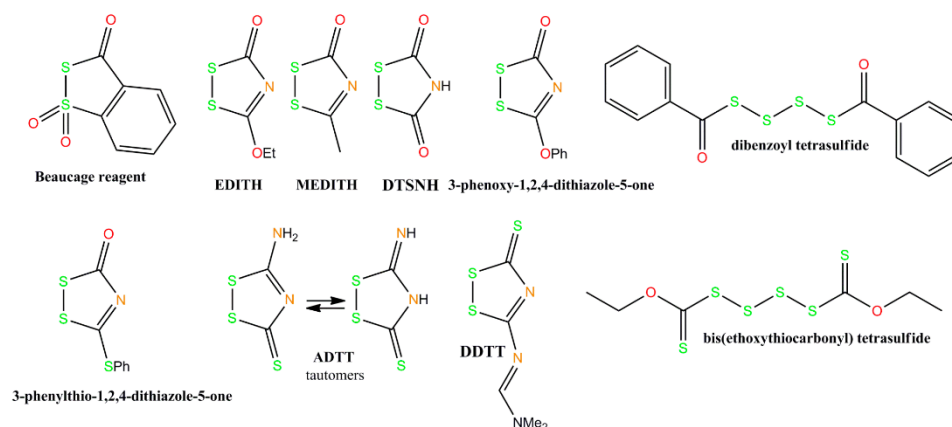


Figure 18: Structures of common PS sulfuration agents. (adapted from reference 126) ¹²⁶

Recently, Chen *et al.* reported a study of modified aptamer which they called “ensemble modified aptamers” (EMAmer). ¹³⁴ In EMAmer, hydrophobic moieties are attached directly to the sulfur atom in PS linkage through a nucleophilic substitution reaction. As a result, the modified sites can be controlled by controlling the sulfuration of the original aptamer. EMAMers were shown to bind to seven proteins, and a sensor based on an EMAmer library was constructed to identify some unknown proteins with high accuracy.

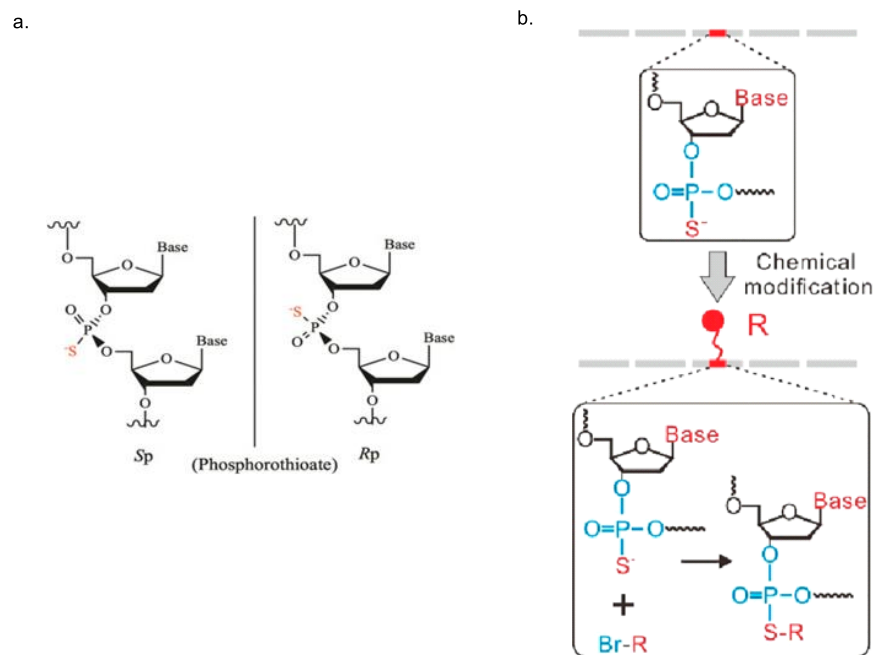


Figure 19: a. | Phosphorothioate diastereomer structures. (adapted from reference 124)¹²⁴ ; b. | EMAMer modification on PS bond. (adapted from reference 134)¹³⁴

1.2.3.4. Modification of nucleobases

While modification of the sugar and phosphate bonds mainly aims to increase the stability of the aptamers, changing the nucleobases widens the aptamer chemical diversity, which can directly affect the binding affinity. Therefore, pre-SELEX modification of the nucleobases is preferred as it will utilize the selection process with the modifiers.¹³⁵ As discussed above, to undergo SELEX, the modified nucleobases must be recognized by polymerase and must be able to form Watson-Crick base pairs normally with complementary natural nucleobases.

Modifications at the C5 position of pyrimidines and at the N7 or C8 position of purines are the most common since those positions do not participate in base-pair hydrogen bonding and can be tolerated by many polymerases.^{136, 137} Moreover, the modified moieties at those positions will likely protrude from the major groove, with greater access to the target.¹³⁷ For a protein target,

aromatic and hydrophobic modification groups are frequently incorporated since they resemble the side chains of many amino acids.¹³⁸ One notable example of this approach is the Slow Off-rate Modified Aptamer (SOMAmer) that was first reported in 2010 by Larry Gold and colleagues.⁸⁹ By adding hydrophobic moieties into the 5-position of uridine, they were able to select high-affinity and high-specificity aptamers with several “difficult” protein targets. Furthermore, adjustment of the SELEX protocol to select binders with slow off-rate allows them to select high-quality SOMAmers for a huge number of human proteins with success rate above 90%.

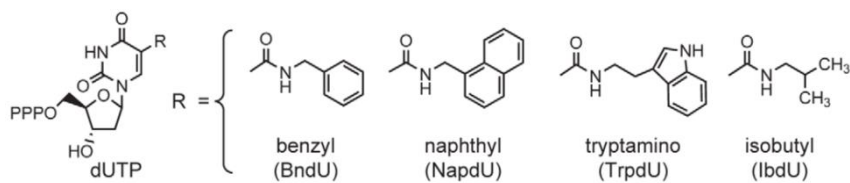


Figure 20: SOMAmers with 5-modified uridine. (adapted from reference 89)⁸⁹

Uridine derivatives can also be found in X-aptamers – a next-generation of thioaptamers that was created by Gorenstein group.¹³⁹ The X-aptamer library is the fully mono-sulfurized library that was synthesized in bead support with one-bead-one-compound strategy. The library contains amino-uridine that can be conjugated with drug-like appendages. The X-aptamers with small molecular drug ADDA conjugated were selected with CD44 protein, and the binders showed significant increase of nuclease stability as well as an enhancement in binding affinity depending on the position of the drug-like moiety.

In a recent report, the Soh group integrated modified uracil into their aptamer library and used a multiparameter particle display screening technique to target glycosylated proteins.¹⁴⁰ The aptamers were hybridized with magnetic beads to form monoclonal aptamer particles, which were then incubated with different fluorescently tagged targets. The combination of fluorescent signals

could distinct the binding affinity of the aptamer to each individual molecule. In the aptamer, the uracil bases were attached to indole moieties to resemble tryptophan. The modified aptamers were reported to have great selectivity against different protein glycoforms and could be used to discriminate the glycoproteins in research or clinical applications.

The modifications can also be introduced after library generation, e.g., through click chemistry. In the click-SELEX method, developed by the Mayer group, a library of single-stranded DNAs is generated, in which deoxythymine (dT) is replaced by 5-ethynyldeoxyuridine (EdU).¹⁴¹ An azide moiety, usually hydrophobic or aromatic, is attached to the triple bond through copper-catalyzed alkyne-azide cycloaddition (CuAAC) reaction before the target binding step. The amplification of the binders with EdU yields a new modified library, and the azide must be “clicked” again to start a new cycle. Click-SELEX has been able to select a few high-affinity modified aptamers, also called clickmers, against several targets including streptavidin or 3 Green Fluorescent Protein (3GFP).^{142, 143} However, there are still some limitations that need to be improved for this method. First, only one azide moiety can be “clicked” into the modified thymidine in one cycle. Also, because the clicked product still needs to be read by the polymerase in the first round of PCR, the size of the azide moieties needs to be compatible with the enzyme. Moreover, the appearance of PCR by-products may prevent the enrichment of the binders, although this problem can be eased by reducing the number of modification on a single strand.¹⁴²

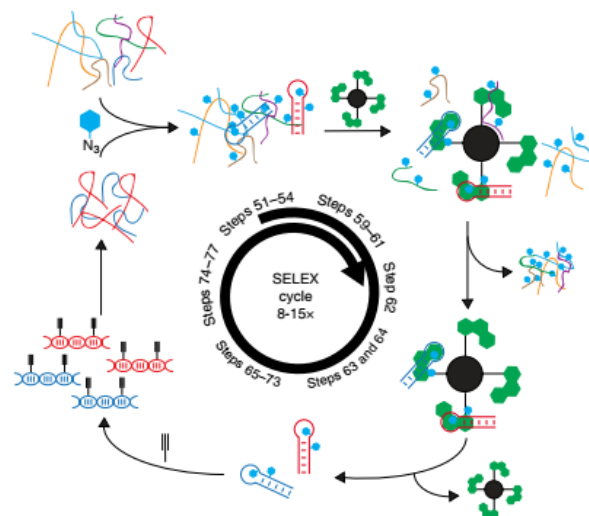


Figure 21: A cycle of Click-SELEX. (adapted from reference 141) ¹⁴¹

To overcome the requirement for polymerase compatibility in library synthesis, the Hili and Liu groups came up with the idea of using the enzyme ligase in a technique called Ligase-Catalyzed Oligonucleotide Polymerization (LOOPER). ¹⁴⁴ They synthesized short fragments of 5'-phosphorylated oligonucleotides (containing 3 or 5 nucleotides), in which one of the nucleotides has a modified nucleobase and the rest act as an anti-codon for the modifier. A template DNA library with a reading frame containing the codon is synthesized, and the fragments are annealed to the template and ligated together by T3 or T4 ligase. ¹⁴⁵⁻¹⁴⁷ The double strand is then separated and incubated with the target. The PCR and sequencing step of the binders will yield another template library, which will be ready for the next selection round. Besides the advantage of not using polymerase to incorporate modified nucleotides, LOOPER allows the attachment of many types of modification for an individual nucleobase in a single strand. However, the use of a fragment consisting of three to five nucleotides instead of a single modified nucleotide in library synthesis can decrease the randomness and the diversity of the initial library. In addition, the high cost of ligase and extensive time for LOOPER-SELEX are also major problems for scaling up the

protocol. Nevertheless, some high-affinity aptamers were able to be selected from LOOPER, including the first non-G-quadruplex thrombin binding aptamer with nanomolar dissociation constant value.¹⁴⁸

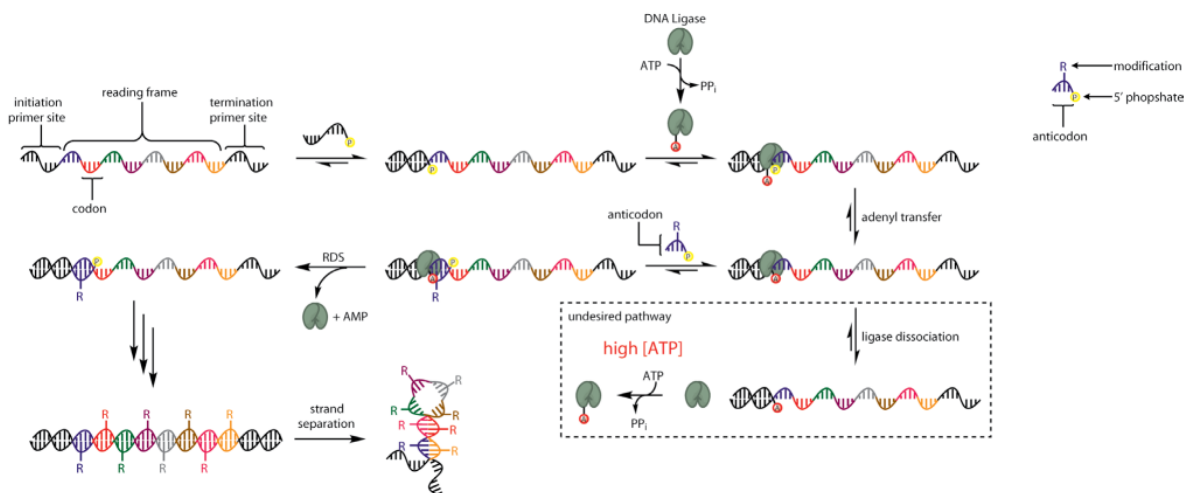


Figure 22: LOOPER library synthesis with oligonucleotide fragments and DNA ligase. (adapted from reference 144)¹⁴⁴

Introducing new base pairs is one of the most direct ways to expand the chemical diversity of the aptamer. However, the discovery of new base pairs is not straightforward because of the strict requirements for high PCR fidelity and efficiency. One successful example is the Ds-Px pair created by the Hirao group.¹⁴⁹ Since both bases do not contain any hydrogen bonding units, the pairing between them relies mostly on shape complementary. Nevertheless, the Ds-Px base pair was shown to undergo PCR efficiently,¹⁴⁹ and aptamers with Ds nucleobases were selected against vascular endothelial cell growth factor-165 (VEGF-165) and interferon- γ (IFN- γ) with much higher affinity than natural aptamers.¹⁵⁰ A few years later, the Benner group also found an unnatural hydrogen-bonding base pair dZ-dP that is totally orthogonal to the other two canonical Watson-Crick pairs. A SELEX protocol for expanded genetic information systems (AEGIS-

SELEX) was developed by the same group to yield high-affinity aptamers against breast cancer cell ¹⁵¹ and T cell receptor-CD3 ϵ ¹⁵².

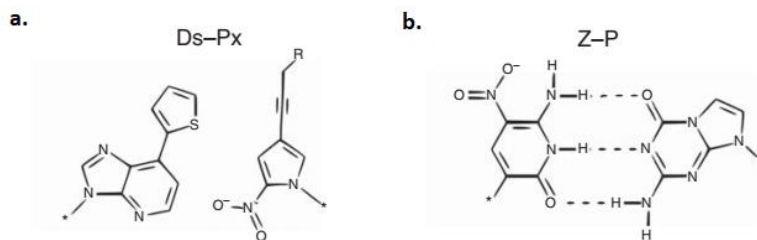


Figure 23: Unnatural base pairs (adapted from reference 153) **a.** | Ds-Px base pair structures ¹⁵³; **b.** | Z-P base pair structures ¹⁵³

1.2.4 Ribozyme and DNAzyme

Nucleic acid enzymes, another class of functional nucleic acids, are nucleic acid molecules that can perform specific catalytic activities for certain biochemical or chemical reactions. Because of their limited chemical space as compared to proteins, nucleic acid enzymes usually need co-factors, which in most cases are metal ions, to facilitate their catalytic activities. However, the 3D conformation and Watson-Crick base pairing enable them to interact specifically with other nucleic acid substrates, therefore increasing the selectivity and stabilizing the catalyst-substrate complex. Nucleic acid enzymes can be divided into ribozymes (enzymatic RNA) and DNAzymes (enzymatic DNA). Ribozymes were first found in 1980s from independent works by Thomas Cech and Sidney Altman. ¹⁵⁴ The discovery of many naturally occurring ribozymes later provided evidence for the “RNA world” theory, in which RNA is thought to pre-exist DNA and protein in the prebiotic world. ¹⁵⁵

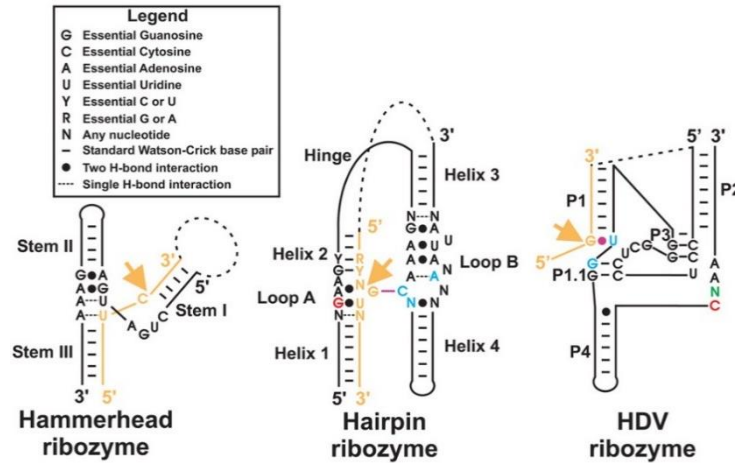


Figure 24: Representative ribozymes and their structures. (adapted from reference 155) ¹⁵⁵

Unlike ribozymes, there is still no evidence that DNAzymes can be found in nature. However, a huge number of DNAzymes have been discovered from DNA pools through *in vitro* selection over many years. Artificial ribozymes or DNAzymes can be selected by SELEX in a similar manner to aptamers, but the catalytic products need to be isolated from the pools to be amplified for the following round. For example, the SELEX library design of self-cleaving DNAzymes or ribozymes often contains a biotinylated primer that is used to immobilize the unreacted substrates. ¹⁵⁶ Another frequently used strategy is to isolate the catalytic products from the pool by preparative gel electrophoresis. ¹⁵⁷ Numerous enzymatic nucleic acids that catalyze a wide variety of reactions have been *in vitro*-selected by SELEX, including ribozymes catalyzing the Diel-Alder reaction, ¹⁵⁸ ¹⁵⁹ or an amide-hydrolysis-mediating DNAzyme ¹⁶⁰.

1.2.5. Aptamers and ribozymes applications

1.2.5.1. Therapeutics

Aptamers can be used as drugs in therapy in the same way as antibodies. Unlike siRNAs or ASOs, where nucleic acids are used to control protein expression, aptamers bind to and interfere with the

protein activity directly, mainly by blocking protein-protein interactions.¹⁶¹ As drugs, aptamers possess many advantages over antibodies, such as no batch-to-batch variation and less immunogenicity.¹⁶² Moreover, aptamers have lower production costs, a longer shelf life and easier maintenance. However, aptamers are easily degraded by nucleases. Moreover, because of their small sizes, aptamers are often excreted by renal filtration.¹⁶³ As a result, many aptamer drugs being tested in therapy contain chemical modifications. Nevertheless, the toxicity of the modification also needs to be considered; for example, LNA has been found to cause cell toxicity¹⁶⁴. Until 2022, besides one aptamer that has been approved by the FDA, there are also some candidates in clinical trials. For example, E10030, an aptamer targeting platelet-derived growth factor (PDGF), is undergoing phase III trial.¹⁶⁵ In addition, many other aptamers are still in earlier clinical trials, such as ARC-1779¹⁶⁶, ARC1905¹⁶⁷ or REG1(RADAR)¹⁶⁸.

1.2.5.2. Riboswitches

A riboswitch is a mRNA segment that can regulate the expression of the same mRNA upon binding to a specific ligand. Riboswitches were discovered in 2002 in the 5'-untranslated region of bacterial mRNAs¹⁶⁹⁻¹⁷², presenting the earliest evidence that aptamers can be found in nature. Riboswitches can also be found in eukaryotic cells, such as the *THIC* TPP riboswitches found in many plant species.¹⁷³ Most riboswitches contain two main parts: an aptamer platform where the ligand binds and changes the conformation (and therefore the activity) of an expression platform. Riboswitch aptamers can specifically target many types of metabolites including metal ions, nucleotides and their derivatives, amino acids or coenzymes.¹⁷⁴ The binding of metabolites to aptamer platform can also induce a conformational change in the other platform that regulates gene expression through various mechanisms. For example, in the bound state (the 'ON' state), the transcription terminator sequences, which appear in many riboswitches, such as SAM-riboswitches, force the

termination of transcription by RNA polymerase.^{175, 176} On the other hand, in the absence of the ligand (the ‘OFF’ state), an anti-terminator sequence is released and helps the transcription to continue beyond the terminator. Some riboswitches, including the plant TPP riboswitch, alter RNA 3'-end splicing by changing the flexibility and accessibility of the splice site in their ‘ON’ state.¹⁷³ As another example, the *glimS* riboswitch also acts as a ribozyme and performs self-cleavage upon binding of the metabolite.¹⁷⁷ Besides acting as a natural sensor for mRNA, riboswitches can be engineered to perform other applications. For example, many riboswitches have been utilized as molecular biology tools to target transcription or translation regulation of certain proteins in gene therapy.¹⁷⁸

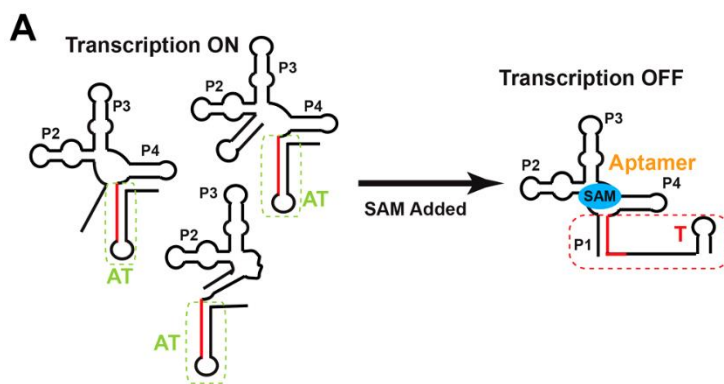


Figure 25: SAM riboswitch ‘ON’ and ‘OFF’ states. (adapted from reference 176)¹⁷⁶

1.2.5.3. Biosensors

Aptamers and enzymatic nucleic acids are utilized in many biosensing systems. A typical biosensor contains two main elements: a bioreceptor that recognizes the sensing target and a transducer that reports the signal.^{179, 180} As bioreceptors, nucleic acids possess advantages over other types of molecules such as monoclonal antibodies. Since some aptamers undergo conformational change upon ligand binding, they can induce a signal with high sensitivity. For example, electrochemical aptamer-based sensors (E-AB), one of the most common classes of

applied aptamer sensors, use a redox tag attached to the aptamer that is immobilized to a conducting support to report the structural change with the appearance of the target.¹⁸¹ E-AB is also built in many real-time sensors, such as in the Microfluidic Electrochemical Detector for *In vivo* Continuous monitoring (MEDIC) which continuously tracks the therapeutic agent concentration in blood and has the potential to be applied in personalized therapy.¹⁸² In addition, many aptamer sensors use fluorescent reporters to monitor the signal. For example, fluorescent resonance energy transfer (FRET)-based sensors, where the signal is detected by the distance between a dye and a quencher, have been developed for many types of targets like heavy metal ions,¹⁸³ dopamine,¹⁸⁴ *Tat* protein¹⁸⁵ or lysozyme.¹⁸⁶ Another advantage of using nucleic acids for biosensors is the ability for amplification of the probe sequence or signal. For example, an ultra-sensitive biosensor for a wide range of targets has been developed utilizing rolling circle amplification (RCA).¹⁸⁷ With a circular template, RCA can amplify isothermally a short DNA probe into a long, linear strand with repetitive tandem sequence that can facilitate the detection. Ribozymes and DNazymes that require cofactors such as metal ions to perform catalytic activity can be used to sense such ions. The selectivity can be achieved by tuning the catalytic activity to the conformational change. For example, He *et al.* reported a DNzyme that can recognize Na⁺ and K⁺.¹⁸⁸ In addition, the binding of a high amount of potassium cation will misfold the DNzyme strand and inhibit the catalytic activity, leading to the discrimination between the two cations.

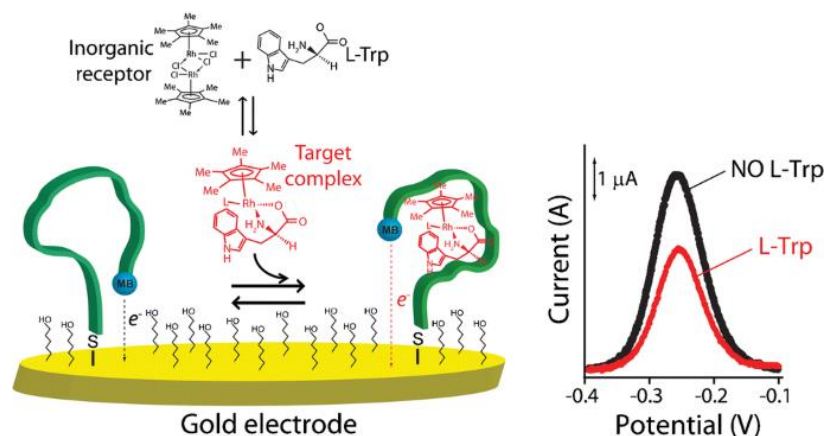


Figure 26: An example of an E-AB that recognize L-tryptophan. (adapted from reference 181) ¹⁸¹

1.3. Previous work: Alenomers

Most of the chemical modification methods discussed in section 1.2.3, such as SOMAMers, click-SELEX or use of XNA, are still relatively conservative modifications required to maintain compatibility with the enzymes. Although some strategies do not need polymerase to generate the pre-SELEX modified library (e.g., LOOPER by using ligase, or X-aptamer by using SPS), there is still a requirement for enzymatic reactions in the PCR and sequencing steps. As a result, the range of modification is still highly limited, as none of these methods can produce the aptamers with non-nucleosidic modifications.

Recently, the Sleiman and McKeague groups developed a method, called aptamer-liked encoded oligomer or alenomers, which can overcome the aforementioned problems. ¹⁸⁹ An alenomer molecule consists of two strands: the “aptamer” strand and the code strand. These strands are covalently attached through an uracil-based branching unit. The “aptamer” strand consists of both conventional nucleosidic and synthetic non-nucleosidic building blocks connected through phosphodiester linkages. The code strand consists of only nucleotides, in which each monomer in

the “aptamer” is encoded by a codon combination of three nucleotides in the code strand. The “aptamer” strand will be the one that binds to the target, while the code strand containing the aptamer identification will undergo amplification and sequencing later. Two regions flanking the code strand act as the primer regions for PCR amplification.

Previously, the two groups have used the alenomer approach to optimize the thrombin-binding aptamer (TBA).¹⁸⁹ A library of alenomers was prepared in which the “aptamer” strand is a modified TBA. The thermodynamically stable G-quadruplex structure was conserved, and all of the other positions were modified by both conventional or synthetic monomers. The code strand and the aptamer strand were covalently connected by a uridine-based branch unit (**BU**). The **BU** was inserted in the reversed primer region for a better PCR efficiency.

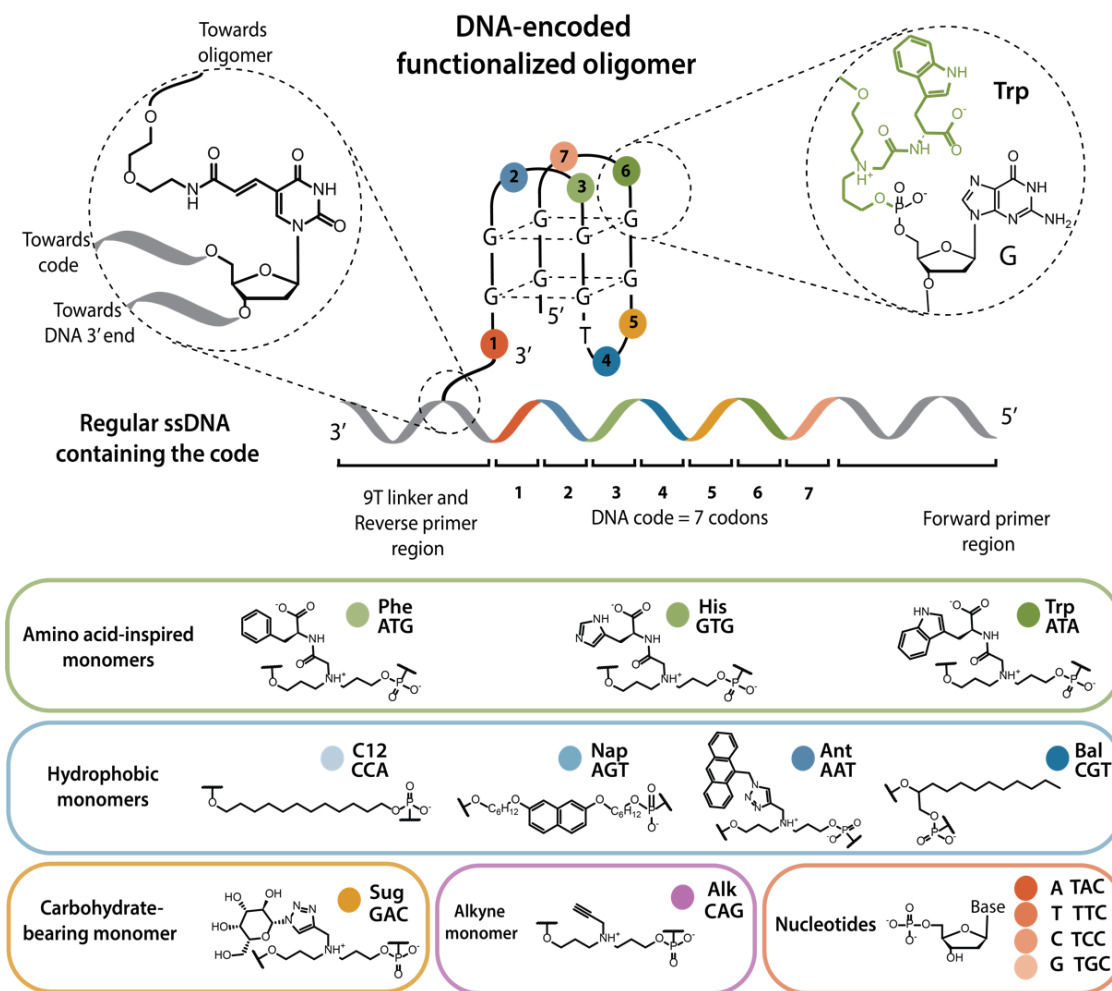


Figure 27: TBA alenomer library design with monomer structures. (adapted from reference 189)¹⁸⁹

The library was synthesized by solid-phase synthesis with natural or synthetic monomer phosphoramidites. The two strands were synthesized in parallel, using two orthogonal 5'-protecting groups: dimethoxytrityl (DMT) and levulinyl (Lev). The deprotection of DMT group requires acidic treatment (dichloroacetic acid 3% in DCM), while the cleavage of Lev protecting group requires hydrazine treatment (hydrazine 0.5 M in pyridine/acetic acid buffer). A split-and-pool strategy was utilized to create more than 300,000 alenomers with their distinct codes.

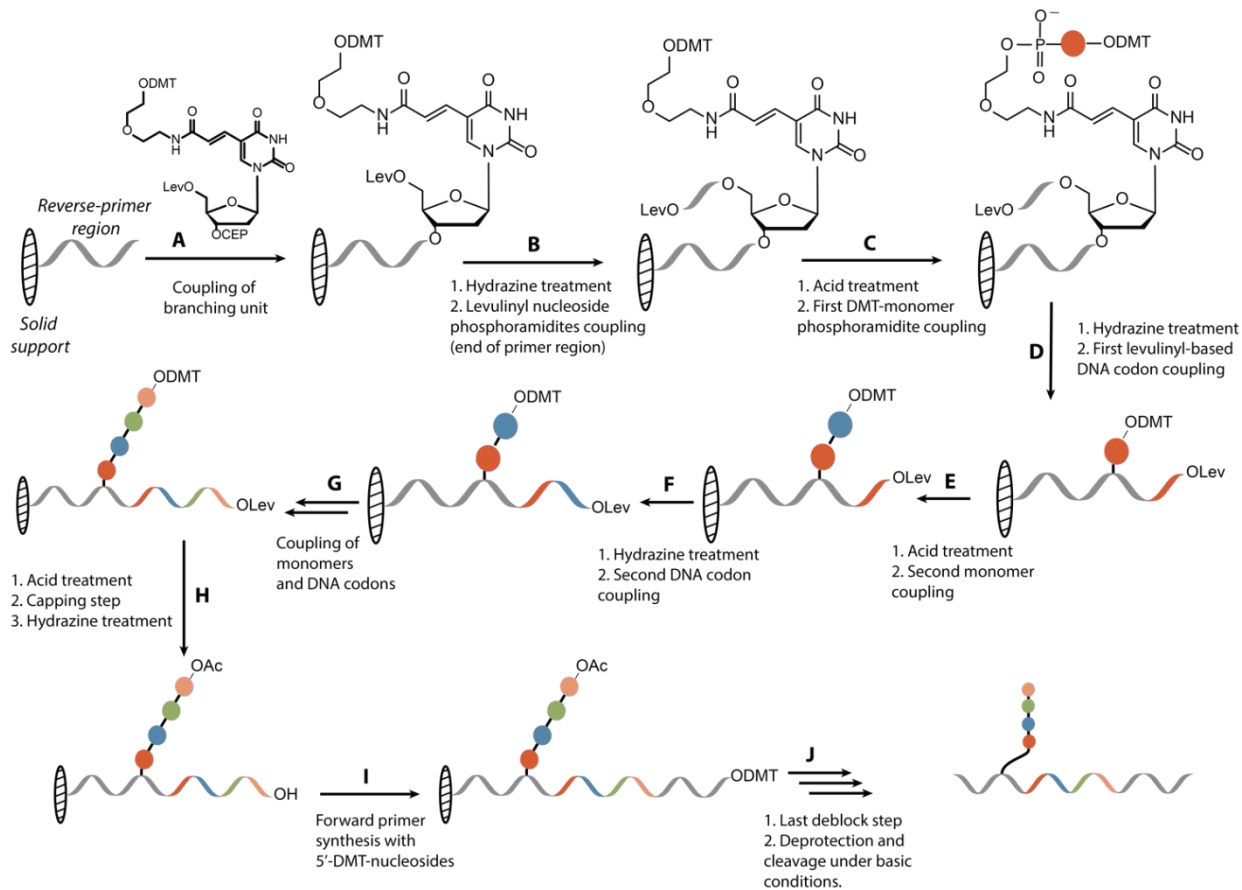


Figure 28: Alenomer library synthesis protocol. (adapted from reference 189) ¹⁸⁹

The screening process was done in a similar way as a normal DNA-encoded library screening process. Prior to the screening, the library was eluted through a blank column and a streptavidin-immobilized column to eliminate all non-specific binding oligomers. The remaining pool was then incubated with solid matrix with immobilized thrombin, and the non-binders were eluted out of the column. In the next few steps, weak binders were removed from the solid support by competitive elution using thrombin or unmodified TBA. Finally, the remaining strong binders were totally removed from the column by heat. The elution fractions from competitive binding and the final elutions were all undergone PCR and next-generation sequencing to identify the code

information in each portion. From the sequencing data, the abundance and frequency of the monomers in each elution were compared to identify the strongest-binder sequence.

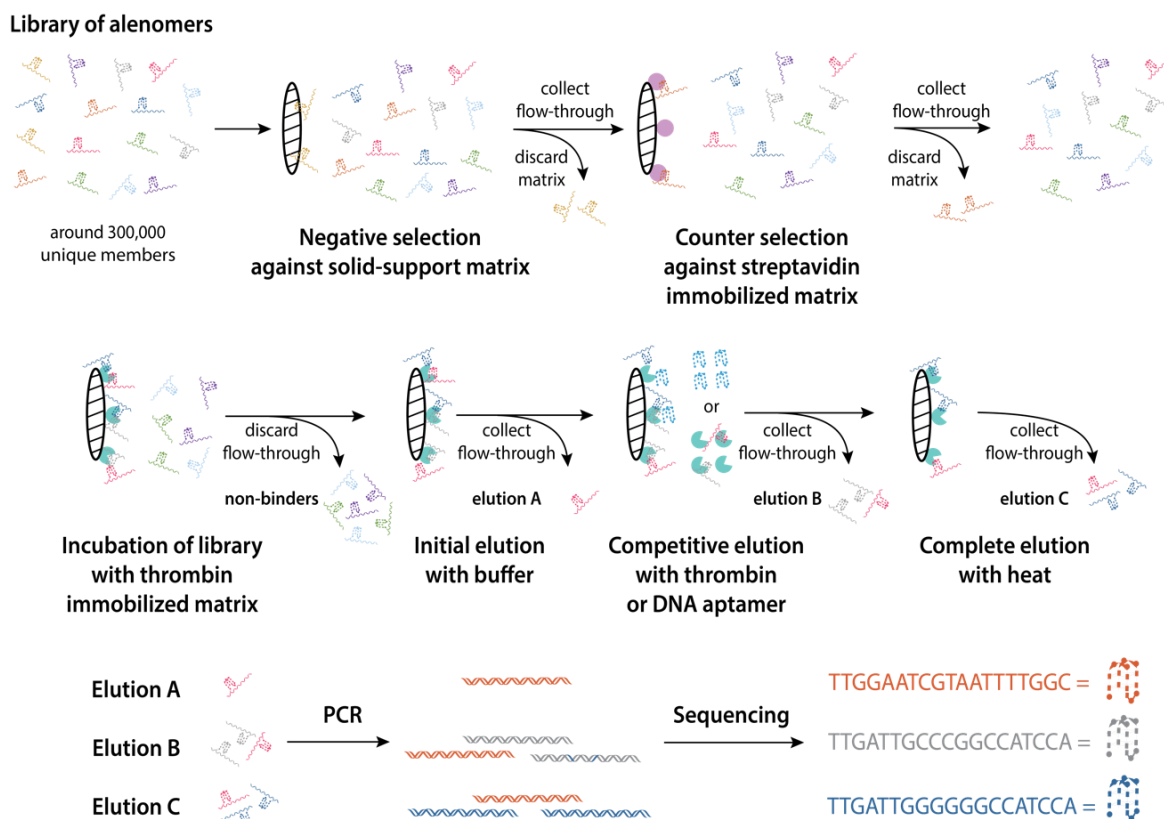


Figure 29: TBA-based alenomer library screening process with thrombin and other controls. (adapted from reference 189)¹⁸⁹

The strongest-binding strands were synthesized again without the code strands for more detailed study. The sequences of those binders, including the best binders **AlenA** and **AlenB**, were illustrated in **Figure 30**. The fluorescent anisotropy experiment (**Figure 30D**) resulted in a higher thrombin binding affinity of **AlenA** and **AlenB** compared to the original TBA, which has K_D value of 11 ± 8 nM (not shown in **Figure 30**). The SPR kinetic analysis (**Figure 30B** and **30C**) also showed a longer off-rate of **AlenB** to the original aptamer. For the stability, **AlenA** obtained similar

half-life in serum as the unmodified TBA, while the stability of **AlenB** improved more the ten times.

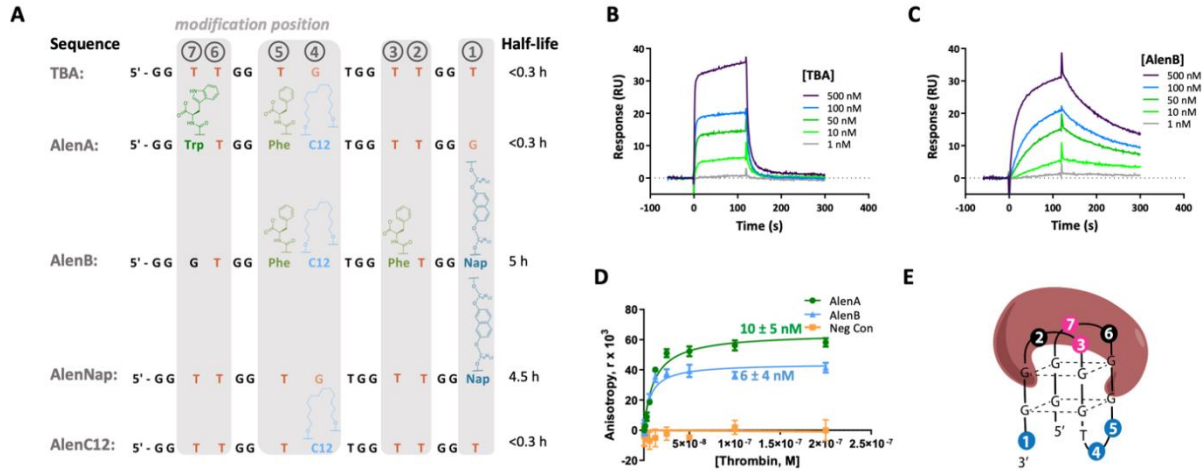


Figure 30: TBA alenomer library screening result and evaluation (adapted from reference 189)¹⁸⁹ **a.** | The sequence name, composition, and serum stability of the three most popular alenomers identified in screening along with comparison model TBA aptamer; **b.** | SPR sensorgrams of increasing concentrations of the thrombin binding DNA aptamer (**TBA**) interacting with thrombin immobilized to a gold chip; **c.** | SPR sensorgrams of increasing concentrations of the alenomer **AlenB** interacting with thrombin immobilized to a golden chip; **d.** | Binding isotherms of alenomers **AlenA** and **AlenB** interacting with thrombin obtained using fluorescence anisotropy; **e.** | An exemplary alenomer library member interacting with thrombin.

CHAPTER 2: RESULTS & DISCUSSION

2.1. Author contribution

Son Q. Bui codesigned, carried out and analyzed the data of all experiments except those listed below. **Son Q. Bui** wrote and edited this thesis. **Prof. Hanadi Sleiman** and **Prof. Maureen McKeague** codesigned the project, guided interpretation of data, discussed of results and helped editing the thesis.

Small molecule synthesis:

Abdelhralman Elmanzalawy synthesized of **3**, **4**, **5** and **BU** amidites following the original work of **Dr. Donatien de Rochambeau**. **Dr. Donatien de Rochambeau** synthesized all the phosphoramidites in section 2.5.1. **Dr. Alexander Prinzen** helped designing the structure and the synthetic route of **Et**, **COO**, **Prop** and **Ser**.

Solid-phase synthesis:

The synthesis protocol was developed from the work of **Dr. Donatien de Rochambeau**. **Dr. Daniel Saliba** co-designed the constructs and the synthesis protocol for branched oligomer and levulinyl amidites.

Surface plasmon resonance:

Prof. Maureen McKeague and **Dr. Eiman Osman** performed and analyzed the results all SPR assay with target captured (section 2.4.4 and first part of section 2.4.2.2). **Dr. Eiman Osman**

assisted performing and analyzing the results of SPR assay with aptamer captured (second part of section 2.4.2.2).

2.2. Introduction

Aptamers are nucleoside sequences that bind specifically to target molecules. Aptamers are considered promising alternatives to antibodies due to their comparable high binding affinities with many types of targets. Moreover, aptamers possess some advantages over their protein counterparts, including the ease of chemical modification and the ability to undergo in vitro selection from a randomized pool. However, the limited chemical diversity of aptamers, with only four canonical nucleosidic bases, significantly narrow the range of targets they can efficiently bind. Adding unnatural building blocks might be a potential solution, but the generation of large libraries of unnatural sequence-defined oligomers is laborious. The requirement of a suitable high-throughput screening method is also a problem; thus, we propose the use of DNA-encoded library (DEL). Nevertheless, DEL technique requires organic reactions that are orthogonal to DNA-ligation chemistry and may not provide the high coupling yields necessary for making sequence-defined oligomers.

The Sleiman and McKeague labs introduced the Aptamer-Like ENcoded OligoMERS (Alenomers) library approach to overcome these obstacles. Here we include synthetic, non-nucleosidic building blocks to impart a wide variety of molecular interactions of the sequence-defined oligo strand. The aptamer was based on a rational design of thrombin binding aptamer (TBA). We also include a DNA code strand that is covalently linked to the oligomer through a nucleoside-based branching unit to identify the corresponding oligo strand. Solid-phase phosphoramidite synthesis and split-and-pool strategy were used to create a combinatorial library of nearly 300,000 alenomers in a

high coupling yield. Libraries were subject to biomolecule selection, separation, and code amplification. Alenomers identified from next-generation sequencing of the DNA code showed improvements in binding affinity and serum stability, underpinning our strategy as an effective method to identify new and useful sequence-defined oligomer for biomolecule binding.

In this section, our goal was to adapt the alenomer library design to make it more generalizable. We started with finding a new target with a reported aptamer that does not contain the common and highly stable G-quadruplex. Once a suitable model aptamer-target was revealed, we altered and tested the alenomer library design including the modification positions, the length of the code or the spacer and the types of branch unit we use. New types of monomers phosphoramidites were also synthesized and their coupling ability tested. Finally, the compatibility of library synthesis protocol to the new design was examined.

2.3. Identification of a non-G-quadruplex aptamer scaffold

In the previous library, the thrombin binding aptamer (TBA), which is the most extensively studied DNA aptamer that binds to thrombin, was used as a proof-of-concept to evaluate the alenomer approach.¹⁹⁰ The original TBA sequence, 5'-GGTTGGTGTGGTTGG-3', contained a unique anti-parallel G-quadruplex structure consisting of two G-tetrads with two TT loops and one TGT loop. Binding mainly occurred between the two TT loops and thrombin's exosite I, while the TGT loop was believed to have an electrostatic interaction with thrombin's exosite II.^{191, 192} To enhance the stability of the aptamer, an additional thymine was inserted at the 3' end, based on a previous report that recommended adding a guanine or thymine in this position.¹⁹³ Consequently, seven nucleotides, which we call variable positions, were targeted for modification while preserving the G-tetrads' framework.

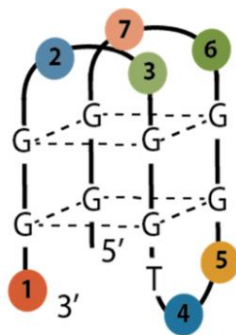


Figure 31: The TBA-based oligomer structure with seven modified positions

However, keeping the G-quadruplex core decreases the structural diversity of our library. Moreover, G-quadruplex is a thermodynamically stable secondary motif that appears in many other aptamers, particularly those that bind to proteins.¹⁹⁴ Therefore, to test the applicability of our method to diverse aptamer structures, we sought to identify a protein-binding aptamer known to form an alternate structure such as a stem-loop. Given that many aptamers reported to date fail to be reliably reproduced in the lab¹⁹⁵, each potential aptamer was first validated reported aptamers using a fluorescent anisotropy (FA) assay¹⁹⁶. In this assay, we tagged the aptamer with fluorescein (FAM) at its 5' end and mixed it with the protein in a binding buffer. The aptamer concentration was fixed below the reported K_D values, typically at half of the value, while the protein concentration varied within a range that included the reported K_D value. We then fitted the anisotropy differences between the bound and free states of the FAM-labelled aptamer into a "one-site specific" isothermal binding curve to determine the K_D values.

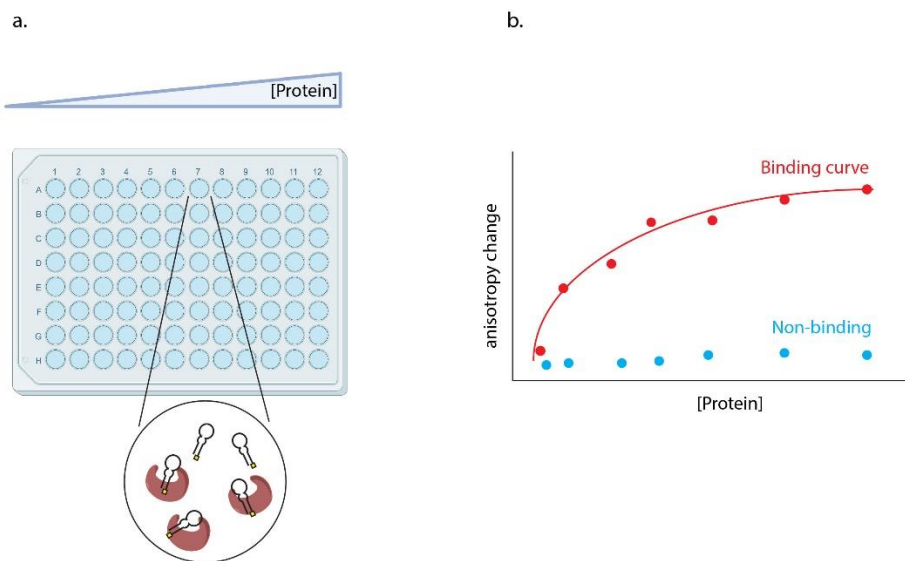


Figure 32: a. | FA experiment set-up on a 96-well plate (made by Biorender); b. | A typical FA binding curve.

Our first target protein was the programmed cell death protein 1 (PD-1), which plays a role in negatively regulating the immune response and promoting T cell apoptosis.¹⁹⁷ Gao *et al.* previously reported PD4S, a 45-mer PD-1 aptamer with a measured K_D value of 10.3 nM using flow cytometry with PD-1-attached cells.¹⁹⁷ However, in fluorescent anisotropy (FA) assay in **Figure 33c**, FAM-labelled PD4S with PD-1, with large error bars and therefore a poorly fitted dissociation constant. The second target was CD63, a transmembrane protein that regulates breast cancer malignancy. Song and colleagues previously reported CD63-1, a 42-mer CD63 aptamer with a reported K_D value of around 38.71 nM.⁹⁶ However, in FA assay in **Figure 33d**, no binding of CD63-1 to its target was observed.

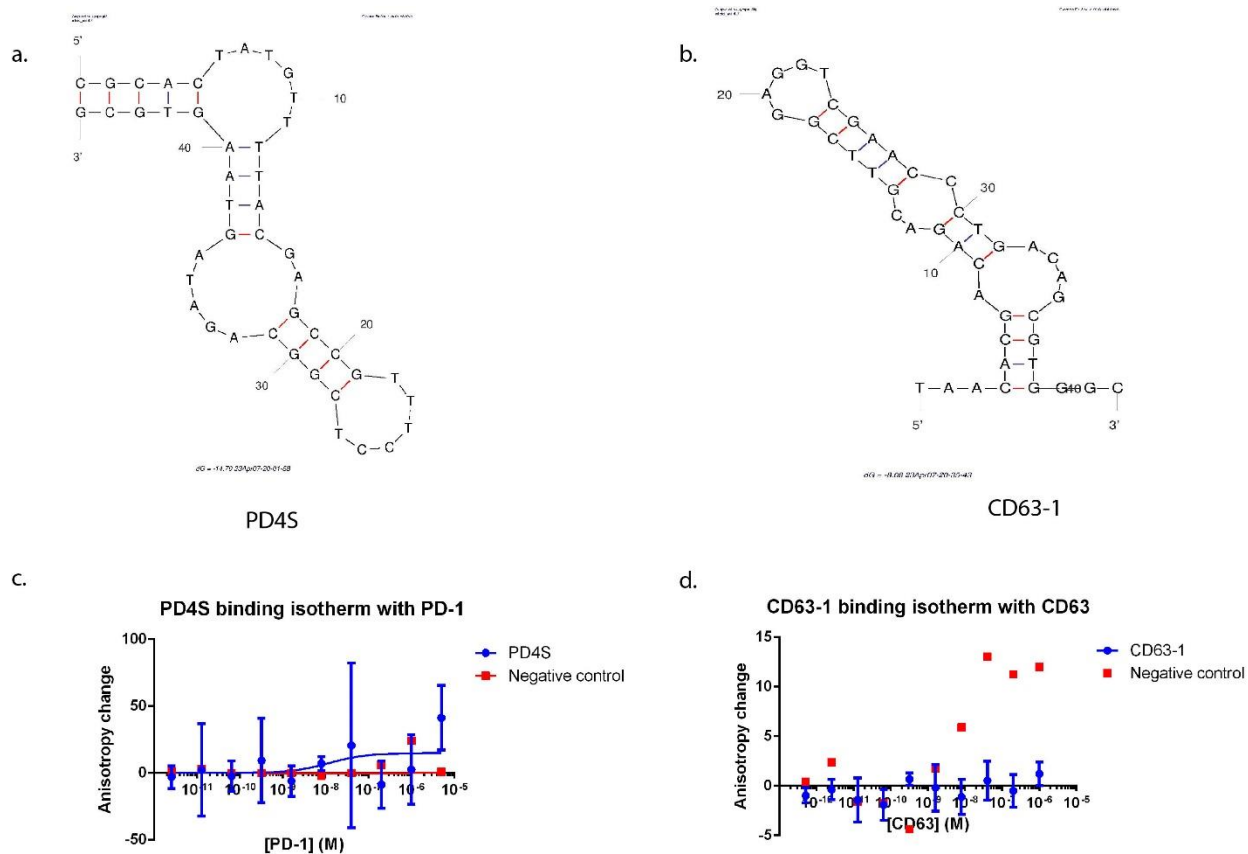


Figure 33: Predicted 2D structures (calculated by Unafold) of **a.** | PD4S and **b.** | CD63-1; FA binding assay result of **c.** | PD4S and **d.** | CD63-1 with their targets.

The third target was trastuzumab, an antibody drug that targets the human epidermal growth factor 2 receptor (HER2). Chen *et al.* previously identified CH1S-3 as an aptamer that binds to Fab-trastuzumab with a reported K_D value of 10.3 nM.¹⁹⁸ In fluorescent anisotropy (FA) assay, the binding affinity of CH1S-3 with trastuzumab was successfully confirmed, with a measured K_D value that closely matches the literature value. Importantly, the circular dichroism (CD) spectra of CH1S-3 in the binding buffer showed a minimum negative band at 240 nm and a maximum positive band around 275 nm, indicative of a B-form oligonucleotide conformation and ruling out any G-quadruplex structures.¹⁹⁹ The predicted 2D structure of CH1S-3 also suggested a simple stem-loop secondary structure. Moreover, at a length of 28 nucleotides, CH1S-3 might enable

good-yield solid-phase synthesis. Based on these findings, trastuzumab is a promising target for the new aptamer library.

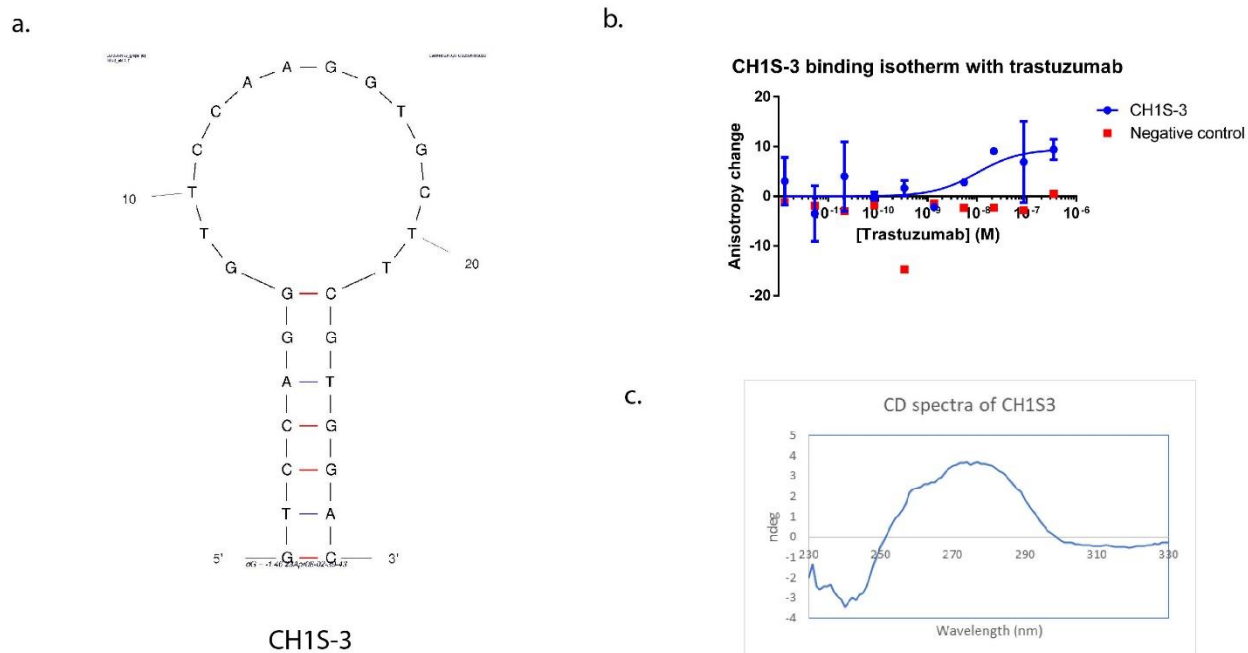


Figure 34: Trastuzumab-binding aptamer **CH1S-3**: a. | Predicted 2D structure of **CH1S-3** (obtained from Unafold); b. | FA assay result of **CH1S-3** to trastuzumab; c. | CD spectra of **CH1S-3** in binding buffer.

2.4. Design of the library member scaffold

2.4.1. The design and synthesis of model constructs

The general aptamer design currently consists of two strands, the aptamer (oligomer) and the code strand, that are covalently linked. To facilitate PCR amplification, two primer regions flank the code strand, and the branching point was found to be best situated in the reverse primer region based on studies of the TBA library. In the TBA library, a 4T spacer was included between the branch unit and the aptamer to prevent interference from the code strands with aptamer folding. However, since the **CH1S-3** aptamer is longer and has a less stable secondary structure than TBA,

a 10T spacer was added between the aptamer and the branching point to avoid any potential interaction between the aptamer and the code. To separate the entire molecule from the CPG, a 9T linker was added to the alenomer 3' end, as recommended by Horn *et al.*, who suggest keeping the branch point at least 20 nucleotides away from the CPG.²⁰⁰ To serve as the branch unit, a C5-modified uridine phosphoramidite with both DMT and Lev protecting groups was used (**BU**). Moreover, to explore the use of commercially available branched amidites, **BU2** was evaluated as another potential branch unit.

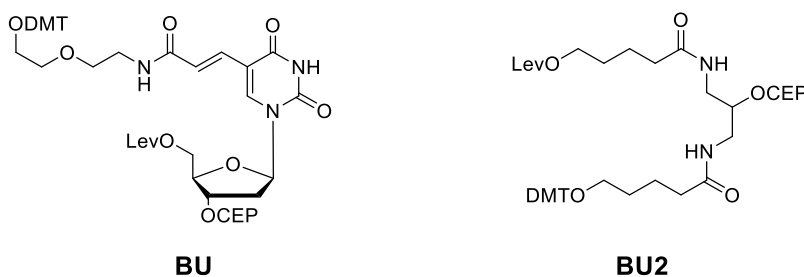


Figure 35: Structures of **BU** and **BU2** phosphoramidites.

The synthesis of **BU** phosphoramidites is shown in **Figure 36**. This synthesis was inspired by the work from Cook and Liu groups.¹⁴⁵ The synthetic route started with the Mizoroki-Heck coupling of iodouridine with methyl acrylate to form **1**, which could be hydrolyzed into **2**. The extended DMT arm **3** was synthesized from the DMT mono-insertion of 2-(2-amino)ethoxyethan-1-ol. The amide coupling of **2** and **3** created **4**, which could be levulinylate at 5' hydroxyl group to form **5**. Finally, the phosphorylation at 3' hydroxy group created **BU** amidite.

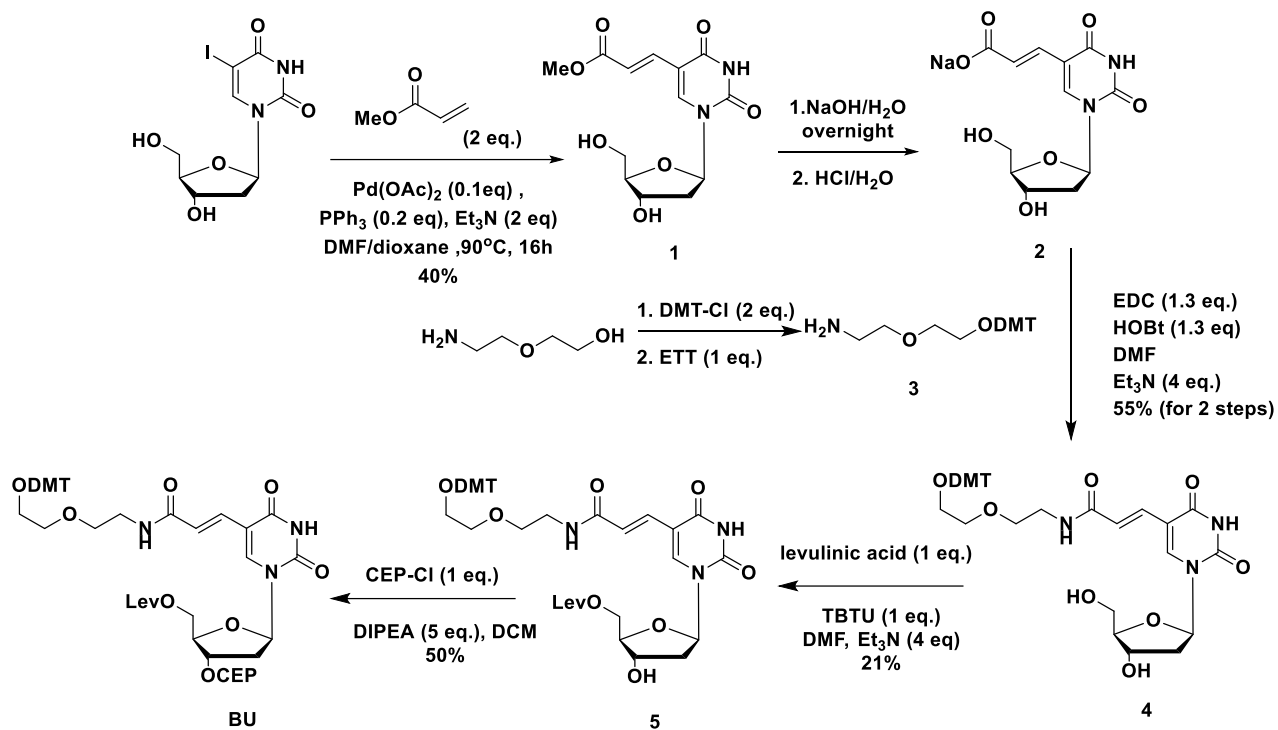


Figure 36: Synthetic route of BU phosphoramidite. The syntheses of 3, 4, 5 and BU were taken from Dr. de Rochambeau's work.

To examine the validity of the new alenomer design, we need to confirm the binding of model alenomer strands with this design to the target. A few model strands were synthesized, including **CH1S-3-1**, which served as a positive control and comprised the original **CH1S-3** aptamer with a 5'-end fluorescein (FAM). **CH1S-3-2** and **CH1S-3-3** are the full alenomer strands with **BU** and **BU2** as the branch units, respectively. FAM was attached to the 5'-end of the aptamer on both strands, and the code strand length was kept similar to that in the TBA library.

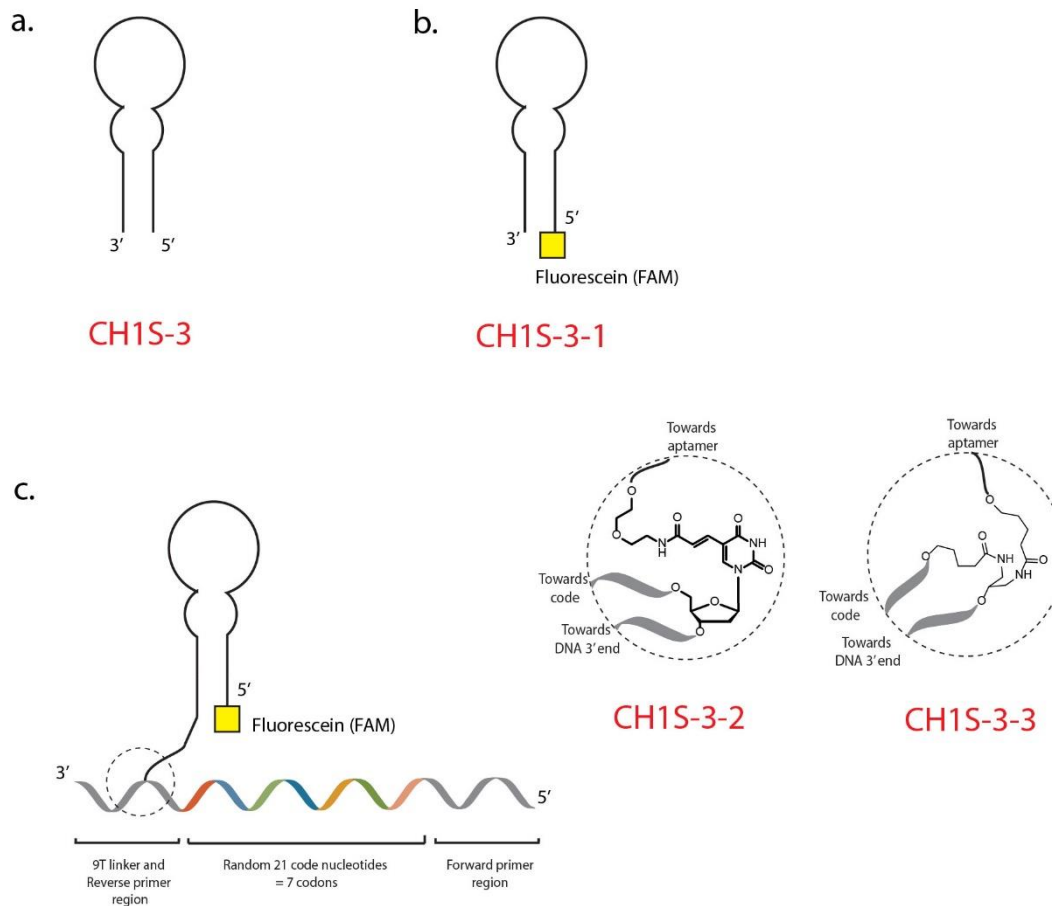


Figure 37: Design structures of test strands: **a.** | Original aptamer **CH1S-3**; **b.** | FAM-labelled aptamer **CH1S-3-1**; **c.** | FAM-labelled branched structure **CH1S-3-2** and **CH1S-3-3** with different branched units.

The synthesis of **CH1S-3-2** and **CH1S-3-3** were performed using the strand-by-strand technique on the Mermaid synthesizer, as shown in **Figure 38**. First, the 9T linker and reverse primer region were synthesized from the CPG before coupling the branch unit **BU** or **BU2** (step A). Next, the branch unit was de-tritylated, and the aptamer strand was added stepwise using DMT-amidites (step B). FAM was then added at the 5'-end of the aptamer (step C). After de-levulinylation of the branch unit, the code strand was synthesized using DMT-amidites (step D). Finally, the nucleobases were deprotected, and the strand was cleaved from the CPG by incubation in ammonium hydroxide (step E).

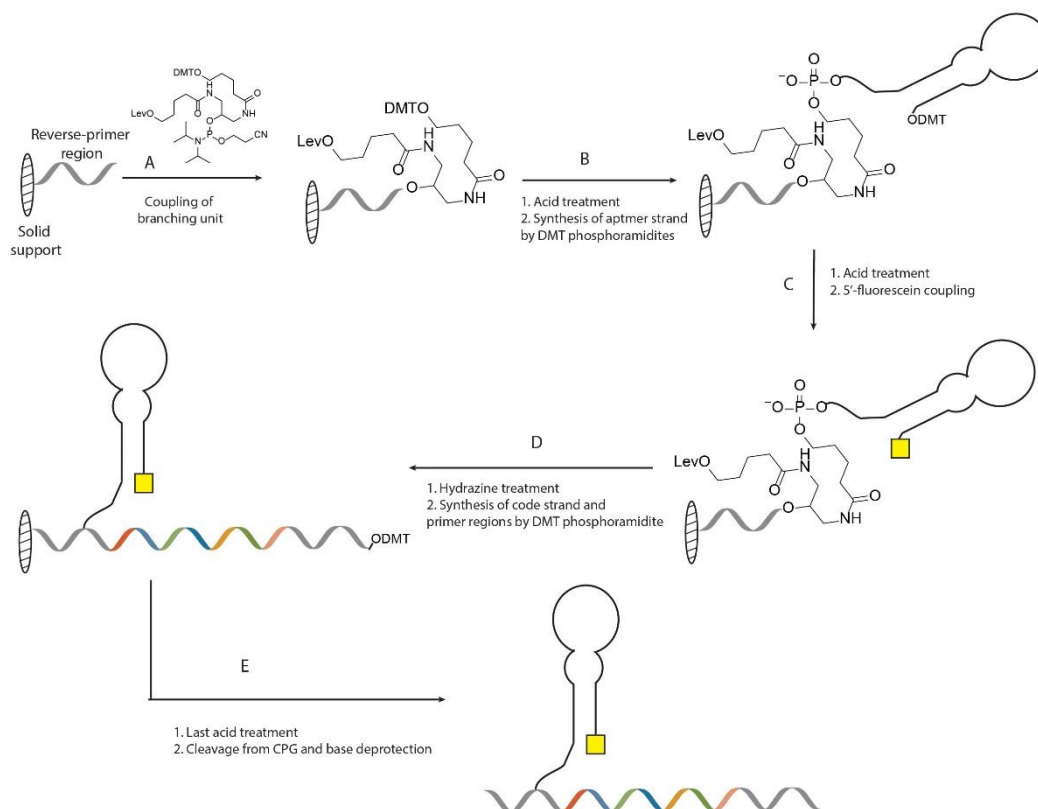


Figure 38: Strand-by-strand synthesis strategy of CH1S-3-3

Figure 39 shows the denaturing PAGE result of CH1S-3-2 and CH1S-3-3. The desired product bands were also confirmed by mass spectrometry. In CH1S-3-3 gel, there was also a short-strand band created by the unsuccessful coupling of BU2. On the other hand, many high mobility bands were observed in the gel of CH1S-3-2. Since BU amidite was synthesized in small amount and coupled immediately without purification, those bands might be the result of unsuccessful coupling or coupling of the active impurities. Both gels also showed a few bands above the product bands, which might contain the hyper-branched by-products. Hydrazine treatment could cleave the acetyl protecting group at cytosine nucleobase leaving a free amino group, which could act as another branching point for the following synthesis step.²⁰¹

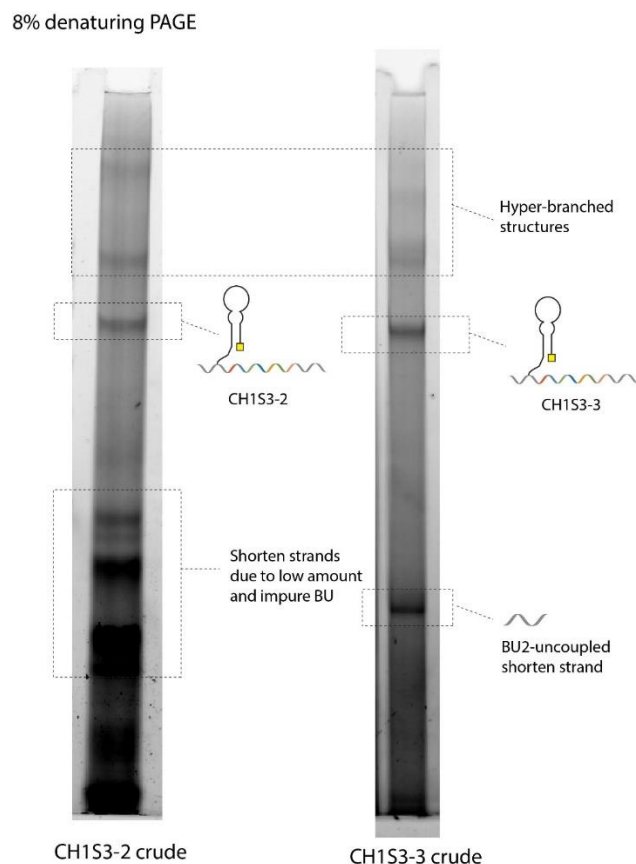


Figure 39: Denaturing PAGE of the crude products for the synthesis of CH1S-3-2 and CH1S-3-3

2.4.2. Binding comparison of model constructs

The screening process of the alenomer library consists of serial competition of library to target-immobilized column in increasing stringency binding condition. Each elution fractions compared to each other to identify the best alenomer binders. After the screening process, top candidates from the sequencing results are then re-synthesized code-free to study the actual binding affinity and other properties. However, it is important to ensure that the construction of the library does not alter the binding of any individual member.

In this section, we examined the binding of model alenomer constructs with trastuzumab. Our primary goal was to verify that with the new designs, the branched alenomers could still bind to

the target in normal binding conditions. If the new designs had significantly diminished the binding affinity, the majority of the library could be eliminated making it impossible to identify candidates based on elution comparison.

According to McKeague *et al.*, aptamer binding may vary depending on the sensitivity of the measurement techniques employed, as well as whether the target or aptamer is used in a solution or immobilized state.²⁰² As a result, we will utilize two methods, namely, fluorescence anisotropy (FA) and surface plasmon resonance (SPR), to investigate the binding of these aptamer models. Furthermore, in the SPR assays, we will study the binding in two fashions: target-immobilized and aptamer-immobilized to account for potential interference of immobilization on binding interactions.

2.4.2.1. Fluorescent anisotropy binding assay

The FA assay protocol used in this study was similar to Section 2.3 (as shown in **Figure 32**). 5'-FAM-tagged aptamers, with a fixed concentration of 10 nM, were mixed with varying concentrations of trastuzumab in binding buffer and incubated in a 96-well plate. The change in anisotropy of the mixture compared to the free fluorescent aptamers (delta anisotropy) was fitted into the binding isotherm curve. **Figure 40** showed the binding isotherm curve and the calculated K_D of **CHIS-3-1** (positive control), **CHIS-3-2** and **CHIS-3-3**. Each sample measurement was replicated twice. The FA result confirmed that both branched constructs bound to trastuzumab. Although their binding affinities were lower than the original aptamer, the K_D value obtained was still below micromolar range, indicating those were not weak binding.

CH1S-3 branched constructs binding isotherms

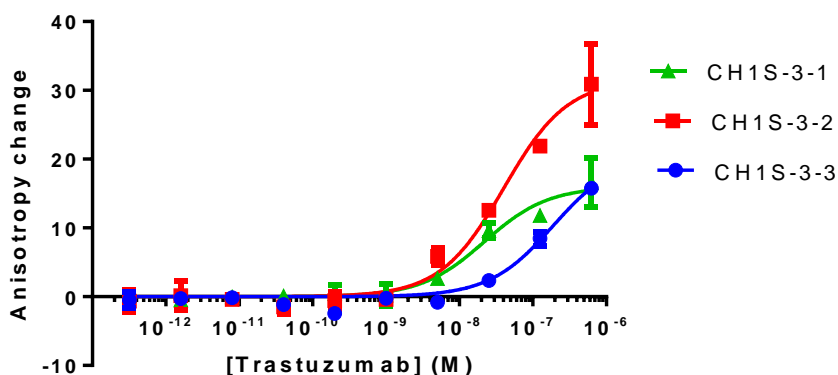
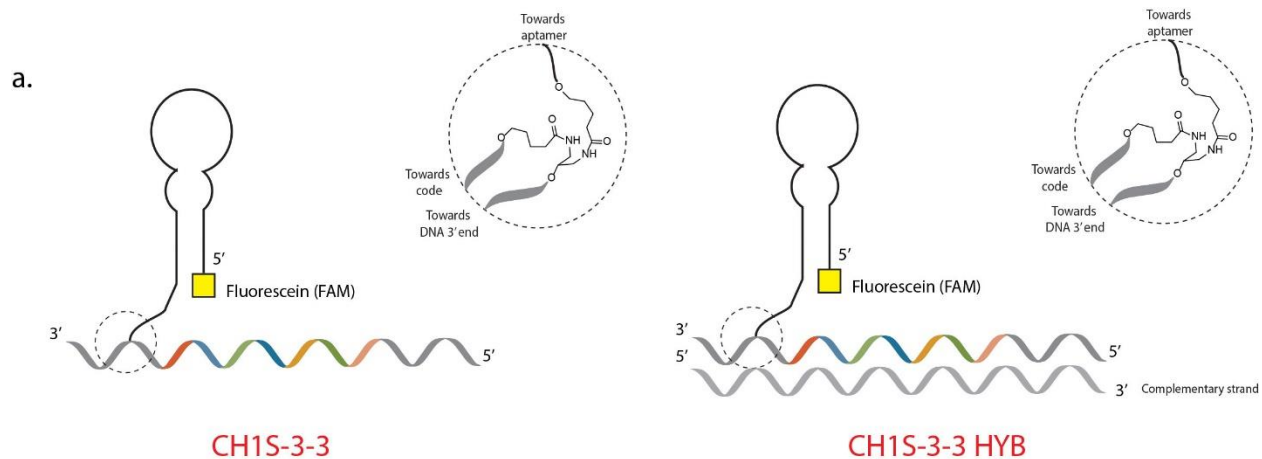


Figure 40: Fluorescent anisotropy result for the binding of branched constructs to trastuzumab

Constructs	K _D (nM)
CH1S-3-1	22 ± 11
CH1S-3-2	40 ± 18
CH1S-3-3	187 ± 106

Table 1: Calculated K_D values of three constructs on FA assay

One of the possible reasons for the decreased affinity of branched structures could be the interference of the code strand with aptamer folding. To test this hypothesis, we created **CH1S-3-3-HYD**, where an additional complementary strand was used to hybridize the code and primer strands. The FA assay was performed using the same protocol as the previous assay, with the exception that the experiments of the positive control (**CH1S-3-1**) and negative control were conducted only once (the rest were replicated twice for each construct). The FA result showed that **CH1S-3-3-HYD** had even lower binding affinity than **CH1S-3-3**, indicating that the interference of the code was not the cause of the decreased affinity of the branched constructs. another method besides FA should be utilized to examine the binding of those constructs.



b.

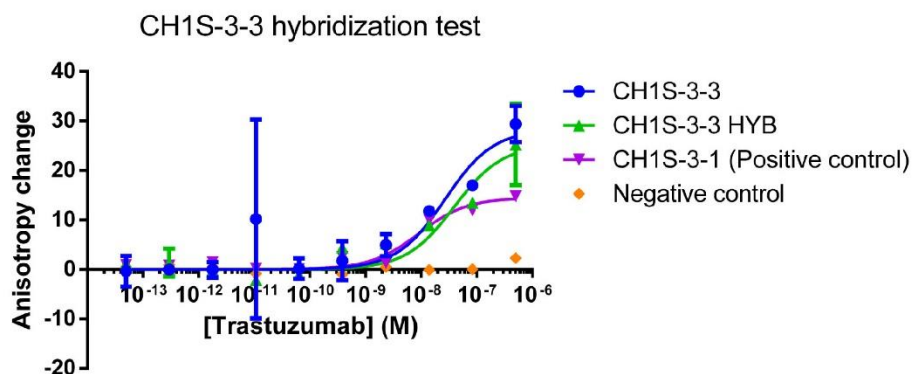


Figure 41: Hybridization binding test of CH1S-3-3. a. | CH1S-3-3 HYB structure; b. | FA isotherm of CH1S-3-3 and CH1S-3-3 HYB

Constructs	K_D (nM)
CH1S-3-1	9.1 ± 2.2
CH1S-3-3	27 ± 20
CH1S-3-3 HYB	39 ± 18

Table 2: Calculated K_D values of CH1S-3-1, CH1S-3-3 and CH1S-3-3-HYB

A noteworthy observation in the FA experiment of **Figure 40** and **Figure 41** is the magnitude of error bars, which tended to be larger at higher concentrations of the protein target. This

phenomenon could potentially be attributed to the protein aggregation during the aptamer-protein incubation process. Despite the use of surfactant, there still may be some aggregation and would be more pronounced at higher protein concentrations. Experimental error may also result in the large error bar in **Figure 41**. Finally, there was a difference between K_D values of CH1S-3-1 and CH1S-3-3 between the two experiments. The variation is likely attributed to the fact that the binding curves had not yet reached a plateau, resulting in differences in fitting the binding curve.

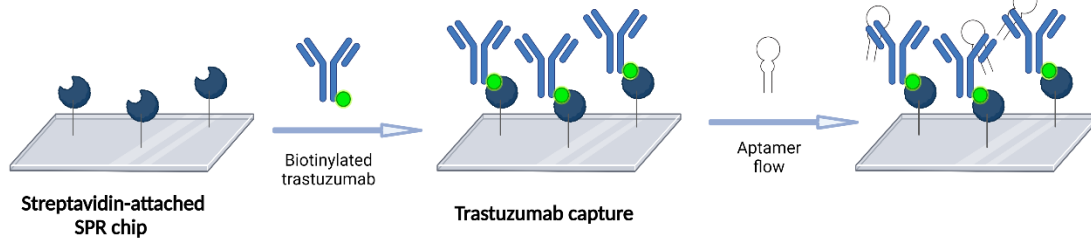
2.4.2.2 SPR binding assay

Two types of SPR experiments were carried out to examine the binding affinity of the new design with the target. In the target capture experiment, biotinylated trastuzumab was immobilized on the streptavidin-attached SPR chip, while the aptamers were added through the flow cell. We did the assay with five different concentrations of the branched constructs with a fixed trastuzumab concentration. Each experiment of each branched construct was replicated twice, and the SPR sensorgrams in **Figure 43** only showed the first trial for each construct. The original aptamer **CH1S-3** (positive control) and DNA scramble (negative control) were measured at one concentration only (250 nM) for two trials. The sensorgram of those controls in **Figure 42** are the average result of the two replications. The results of k_{on} , k_{off} and K_D are summarized in **Table 3**.

The K_D values of all constructs in this experiment are much higher than the corresponding data in the FA assay. This may be due to the immobilization of large antibody molecules, which limits the binding space for the aptamers. Moreover, the K_D values of **CH1S-3-2** and **CH1S-3-3** are lower than the positive control, which is a strange result. The lower K_D values primarily stem from the much lower k_{off} values of the branched constructs compared to the original aptamer. One of the possible reasons might be the non-specific interactions of branched aptamers with other trastuzumab molecules in the vicinity. These interactions might prevent the branched constructs

from dissociating quickly from the aptamer-target complexes, therefore decrease the dissociation constant values.

a. Target capture



b. Aptamer capture

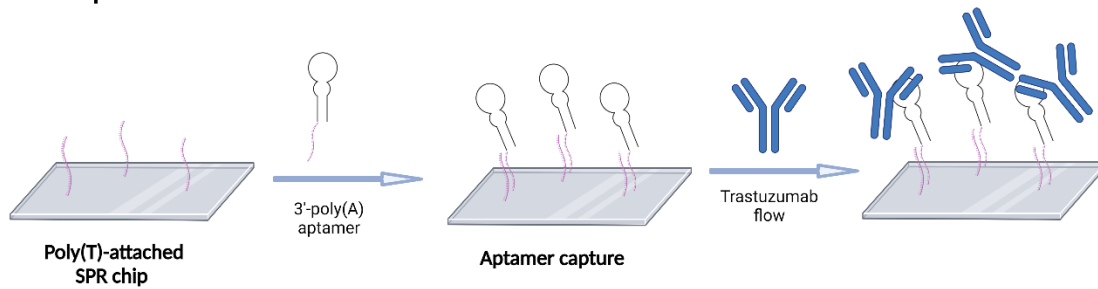


Figure 42: The set-up of two types of SPR assays (made by Biorender)

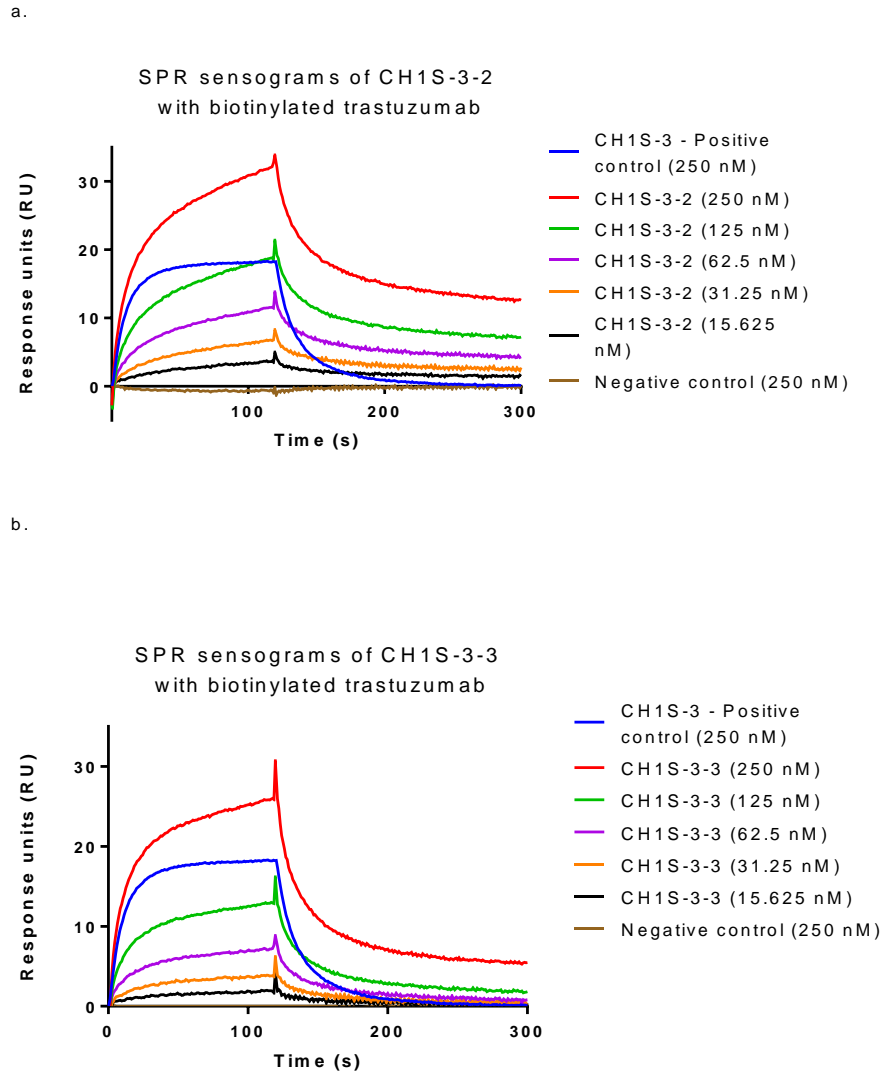


Figure 43: SPR sensorgrams of the binding of immobilized trastuzumab with branched constructs: a. | CH1S-3-2; b. | CH1S-3-3

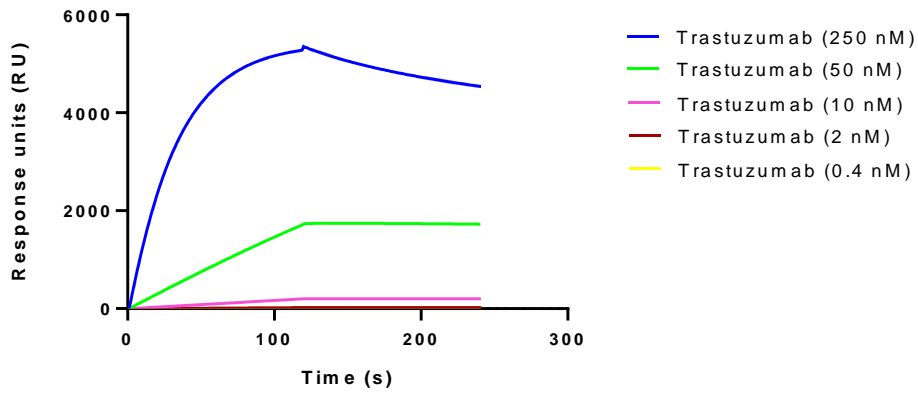
Constructs	$k_{on} (\cdot 10^{-4} \text{ nM}^{-1} \text{ s}^{-1})$	$k_{off} (\cdot 10^{-4} \text{ s}^{-1})$	K_D (nM)
CH1S-3	2.68 ± 1.95	910 ± 643	342 ± 9.05
CH1S-3-2	0.557 ± 0.510	46.9 ± 8.83	132 ± 105
CH1S-3-3	0.976 ± 0.00298	129 ± 41.9	139 ± 33.1

Table 3: SPR binding kinetics data of branched constructs with immobilized trastuzumab

For our “aptamer capture” SPR assays, **Poly(A)-CH1S-3-3** was synthesized by replacing the poly(T) at the 3'-end of the alenomer with 24A. Another 24A linker was also added to the 3'-end of **CH1S-3** to get the positive control **Poly(A)-CH1S-3**. **CH1S-3-2** was not studied in this experiment due to the unavailability of **BU** phosphoramidite by the time the experiment was conducted. Both the positive control and **Poly(A)-CH1S-3-3** were measured twice at five different concentrations, and the binding sensorgrams in **Figure 44** indicated the first trial for each construct only. The K_D results of these SPR experiments were closer to FA results and the reported results than the target capture SPR, probably because the immobilized species this time was smaller, and the binding space was more available. Also, **Poly(A)-CH1S-3-3** in this experiment had a much closer K_D value to the positive control, and both was also near the reported value of the original aptamer of 10.3 nM.

a.

SPR sensograms of Poly(A)-CH1S-3 vs. trastuzumab



b.

SPR sensograms of Poly(A)-CH1S-3-3 vs. trastuzumab

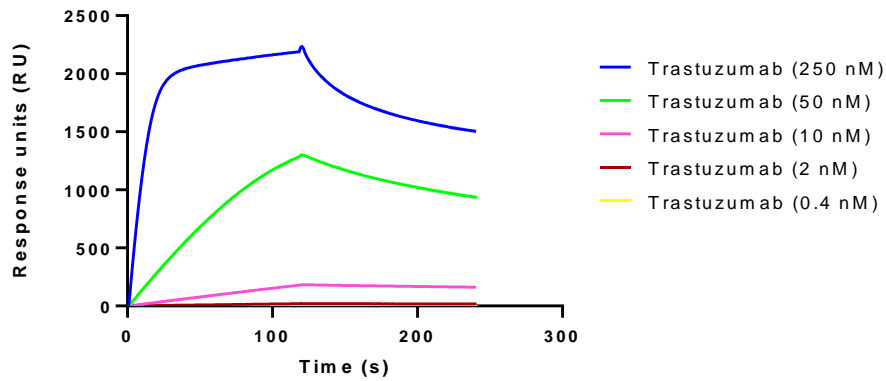


Figure 44: SPR sensorgrams of the binding of trastuzumab with poly(A) constructs. a. | Poly(A)-CH1S-3; b. |

Poly(A)-CH1S-3-3

Constructs	k_{on} ($\cdot 10^{-4} \text{ nM}^{-1}\text{s}^{-1}$)	k_{off} ($\cdot 10^{-4} \text{ s}^{-1}$)	K_D (nM)
Poly(A)-CH1S-3	1.43 ± 0.136	13.0 ± 1.05	9.11 ± 1.07
Poly(A)-CH1S-3-3	3.06 ± 0.153	37.3 ± 1.96	12.2 ± 0.264

Table 4: SPR binding kinetics and affinity data of immobilized constructs with trastuzumab

2.4.2.3. Conclusion for binding study

To summarize, the FA and the two SPR assays confirmed the binding of the branched alenomer containing the **CH1S-3** aptamer to the trastuzumab target. Although each type of assays showed a different affinity trend between different constructs, the calculated alenomer K_D values from all methods are equal or below sub-micromolar range. This result showed an adequately strong binding of the alenomer **CH1S-3-2** or **CH1S-3-3** to the target, suggesting that these designs are suitable for the new alenomer library.

2.4.4. Identification of potential positions in the aptamer that tolerate modifications.

Chen *et al.* used molecular dynamics (MD) to simulate the binding model between CH1S-3 and trastuzumab.¹⁹⁸ The binding site simulation with highlighted binding interaction was shown in **Figure 45a**. From MD simulation, the authors were able to identify the nucleotides that interact directly with the antibody and their binding amino acid partner (**Figure 45b**). These nucleotides can be great candidate for modification in our library.

The researchers also reported that point mutation of 5T, 6C, 8C, and 9T significantly decrease the binding of the aptamer, while 7C sequence only reduced about half of binding affinity. To gain more information about the importance of other positions, we examined the binding of a larger amount of point mutation sequences. The binding assay was the SPR assay with biotinylated trastuzumab (**Figure 42a**). Beside the three base-pairs at the 3rd, 4th and 5th nucleotides of **CH1S-3** which we believed that were crucial in maintaining the aptamer structure, we tried to mutate each of every other nucleotide in the aptamer. **Figure 45c** indicated the SPR result of all point mutation sequences with the original aptamer, while **Figure 45d** summarized the mutation that

either increases or decreases the binding affinity compared to **CHIS-3**. Other point mutation sequences that were not included in **Figure 45d** showed no binding at all.

From this work, we noted positions that should tolerate modification. The most potential position is the 7G, since this nucleotide interact directly with the antibody, and different point mutation results in different decreasing (7C) or increasing (7A, 7T) binding affinity. The 6G nucleotide is also promising because of the direct antibody interaction, the decrease affinity of point mutation (6A), and the position lying between two base-pairs. The 12C nucleotide can be a good choice as the 12T mutation sequence resulted in an increase affinity even though that position did not attend in the binding. Other possible variable positions are 5A, 7G, 18G, 21T and 24T. The 1G and 28C can also be chosen, but modification at those terminal positions might affect the folding of the aptamer.

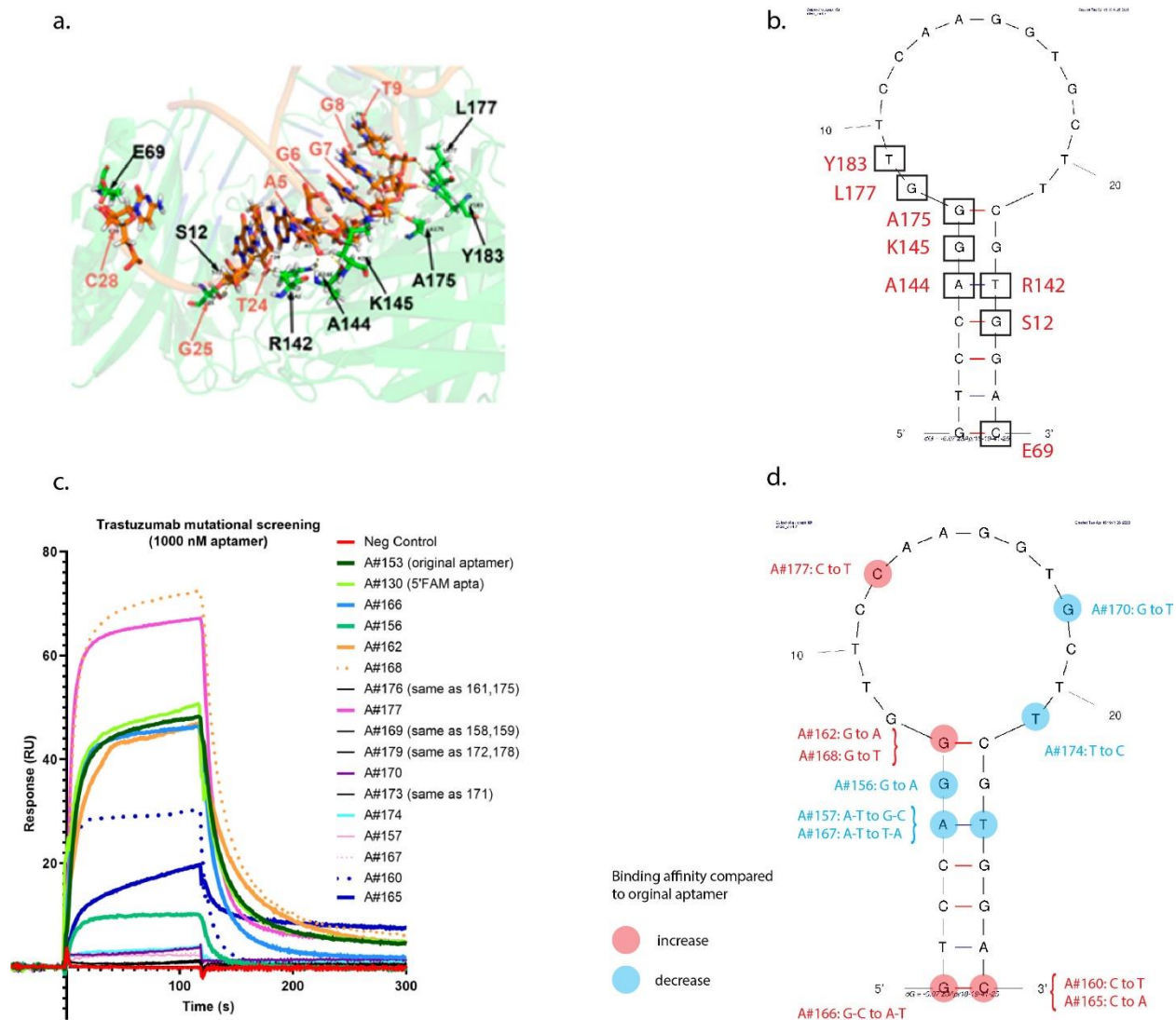


Figure 45: Mutation study of CH1S-3. **a.** | MD simulation of binding site between CH1S-3 and trastuzumab (adapted from reference 198) ¹⁹⁸; **b.** | The nucleotides (in square) that directly interact with trastuzumab and their corresponding binding amino acid partner (in red); **c.** | SPR sensorgram of point mutation sequences and original aptamer; **d.** | Summary the effect of point mutation on binding affinity (point mutations resulting in no binding are not shown).

2.5. Modified monomer amidites synthesis

2.5.1. Synthesis of phosphoramidites from TBA library

In previous work, Dr. Donatien de Rochambeau synthesized nine synthetic, non-nucleosidic phosphoramidites (**Figure 46**), with eight of them included in the TBA library. The remaining one, **Bal**, was only used in the early study to prevent racemic mixtures in the alenomer pool. Those nine phosphoramidites were designed to be synthesized easily and to carry various functional groups. For example, **His**, **Trp** and **Phe** carry the aromatic sidechains of amino acids that are favored by many proteins.⁸⁹ In the previous TBA library, **Phe** and **Trp** appeared in the most popular sequences, including **AlenA** and **AlenB** (**Figure 30a**). The three phosphoramidites can be synthesized from the same reagent (PT2a) by amide coupling reactions with different amine reagents. Similarly, the aromatic **Ant** and hydrophilic **Sug** can be synthesized from the CuAAC click reaction of the **PT1** with other azide reagents. The other reagents, **C12**, **Bal** and **Nap**, have the aliphatic and aromatic backbone and therefore are also good choices to target proteins. **Nap** was included in the sequence of both **AlenA** and **AlenB**, while **C12** was also found in **AlenA**.

Because the target trastuzumab is also a protein, **His**, **Trp**, **Phe**, **C12** and **Nap** should be included in the alenomer sequence. **Ant** should also be chosen due to its large aromatic sidechain, while **Alk** can help coupling of different functional groups in post-synthesis via click reaction. As in TBA library, **Bal** should not be incorporated in the alenomer pools due to its chirality. We will also exclude **Sug** from our CH1S-3 library because of its absence in the most popular sequences from the TBA library screening, particularly **AlenA** and **AlenB** in **Figure 30a**.

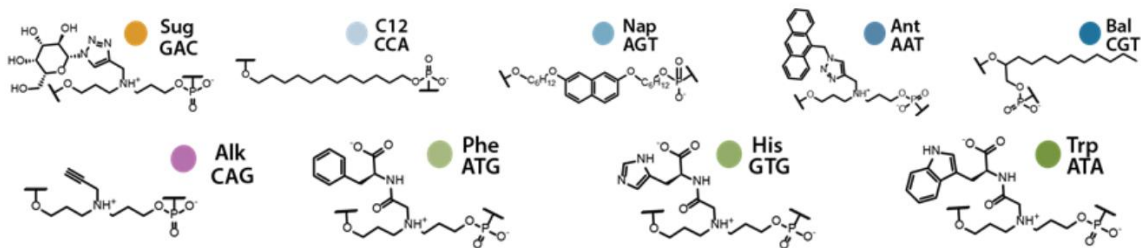


Figure 46: Nine synthetic phosphoramidites included in TBA alenomer library study.

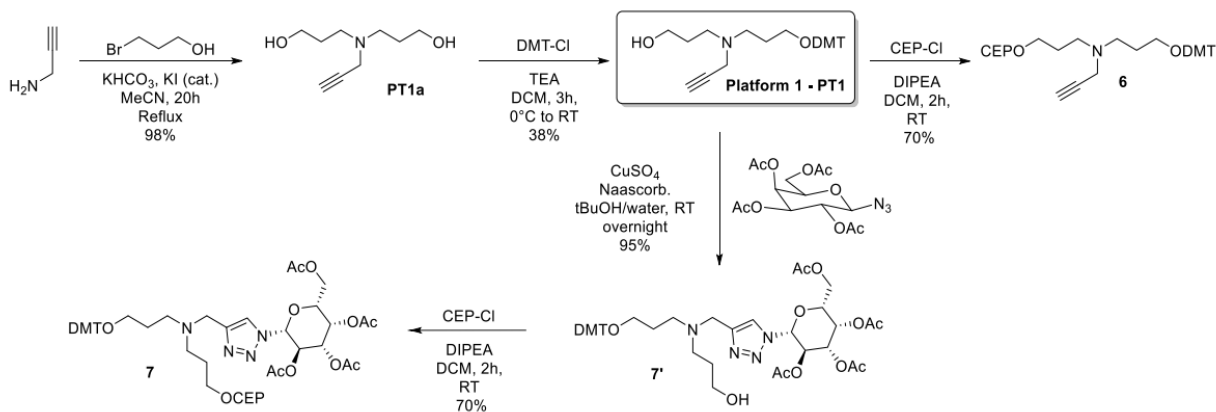


Figure 47: Synthetic route of Alk and Sug from PT1 (taken from Dr. de Rochambeau's work)

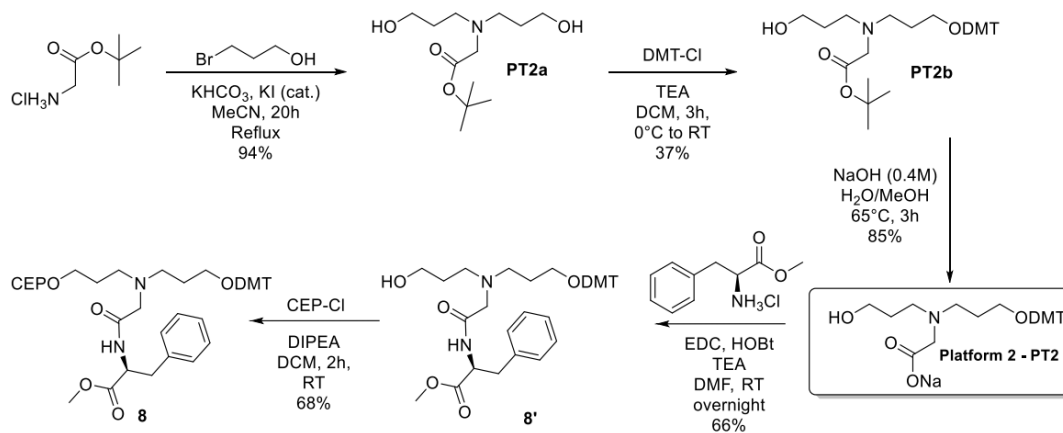


Figure 48: Synthetic route of Phe from PT2a (taken from Dr. de Rochambeau's work)

2.5.2. Synthesis of a new class of phosphoramidites

For many protein targets, hydrophobic and aromatic modifications are more likely to increase the binding affinity of the aptamers.^{89, 138} Moreover, the result from the screening of TBA library showed that the hydrophobic- and aromatic-cored monomers such as **C12** or **Nap** are more favored in the strong binders. Therefore, our goal is to integrate more types of such monomers into our new library. As a result, a new type of monomer amidites, which composes of methylbenzene core, may be suitable. These amidites can be synthesized from 2,6-di(hydroxymethyl)-4-methylphenol, which is a common reagent used in many calixarene syntheses. The synthetic route of those amidites is also simple with three steps: tritylation, substitution of functional groups and phosphorylation. With that design, we successfully synthesized four amidites with different functional groups. While **Et** contains a neutral alkyl group, **Ser** has a silyl ether group that can be deprotected to form a polar hydroxide side chain. Since OTBDMS is also used as a 2'-protecting group in RNA synthesis, its cleavage using fluoride salt such as TBAF should also be compatible with the whole SPS protocol. The other two monomers, **COO** and **Prop**, can be used as platforms to synthesize other monomers in similar way to PT2a and PT1 (**Figure 48** and **Figure 47**, respectively).

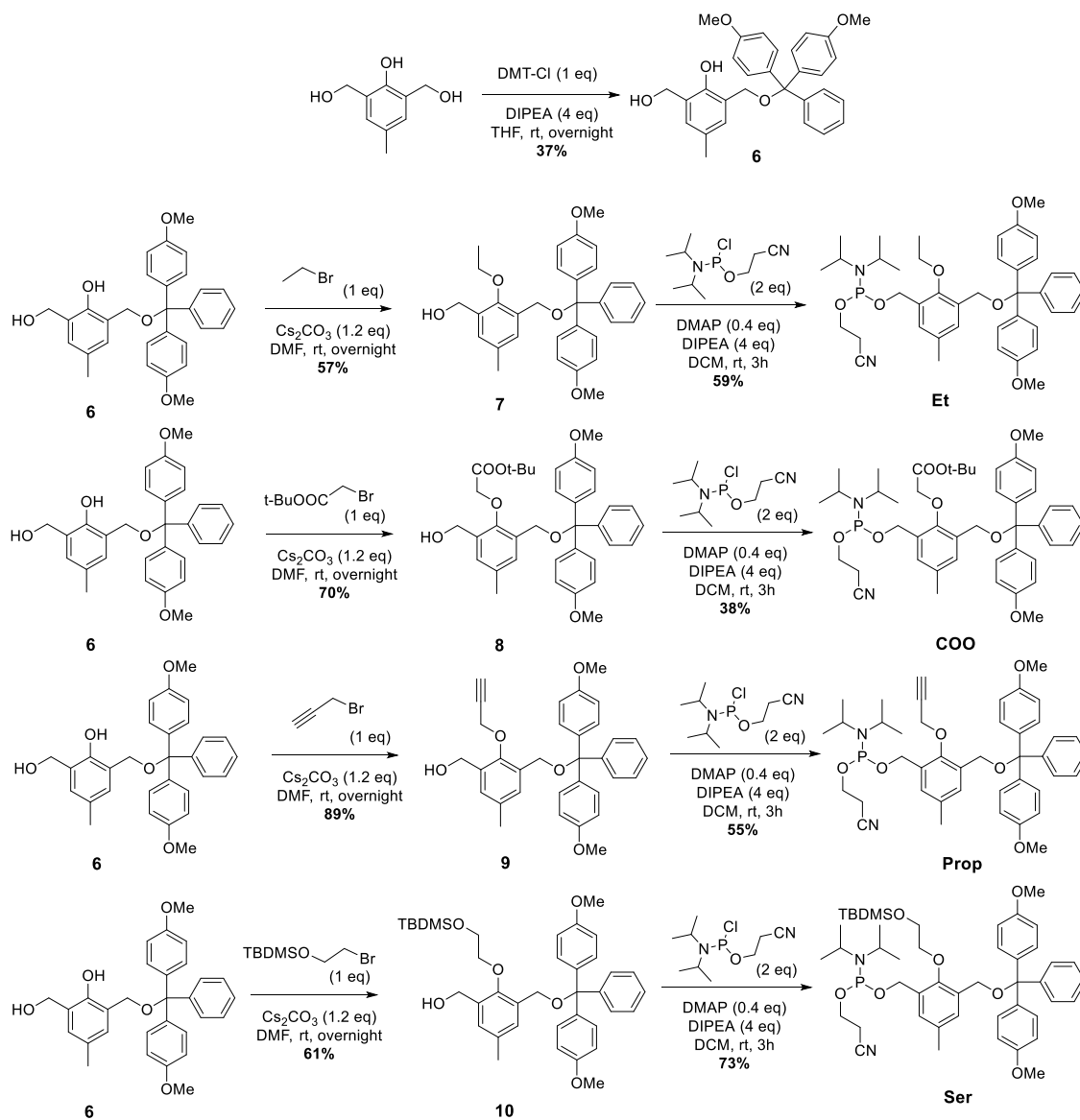


Figure 49: Synthetic routes of **Et**, **COO**, **Prop** and **Ser** phosphoramidites

The coupling yield of the four new amidites was tested by individually inserting each of them to the 5' end of a 19-mer DNA strand. In addition, each test strand was also treated with hydrazine treatment the same procedure used in the de-levulinylation. The crude products were analyzed in PAGE in **Figure 50**. From the PAGE result, hydrazine treatment did not affect the new modified monomers, as the bands patterns the two lanes of a single strand were similar. However, compared to normal 20mer normal DNA sample in lane 9 which has an intense single band, in each of the

other lanes, there were at least two bands with similar intensity. This result indicated the low coupling yield of the four phosphoramidites, leading to the significant appearance of uncoupled 19mer on each sample. HPLC and mass spectrometry were needed to draw the conclusion for the coupling yield of these phosphoramidites.

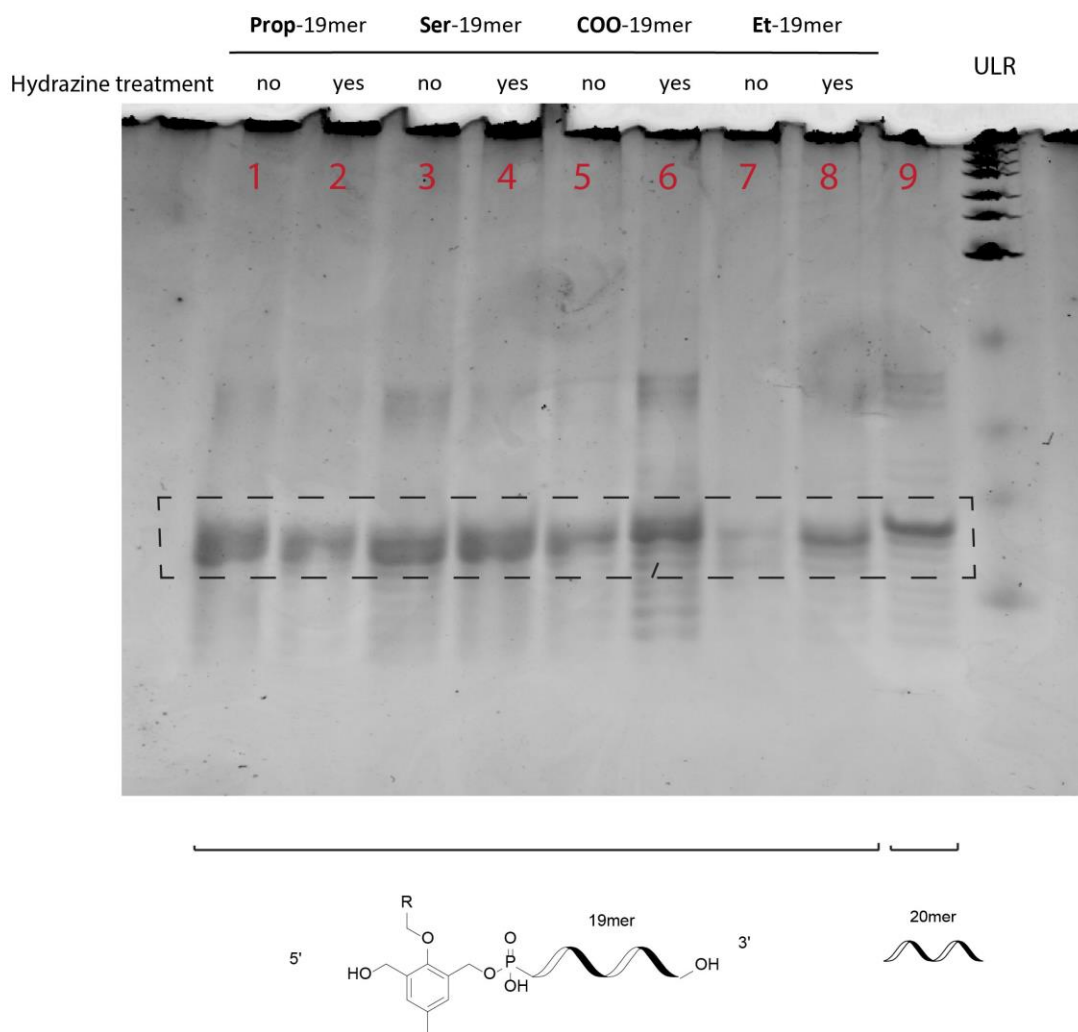


Figure 50: Crude PAGE result of the coupling of modified amidites. Lane 1 to 8 contained the 5'-X-19mer strands (X is **Prop**, **Ser**, **COO** or **Et**). In lane 2, 4, 6, 8, the strands were treated with hydrazine before final deprotection. Lane 9 contained a normal 20mer DNA strand. The dashed square showed the band region expected for 19mer and 20mer strands. Other high mobility bands come from the incomplete normal DNA syntheses, while low mobility bands might be the dimerization due to the low quality of cap reagents.

2.6. Library synthesis protocol

We next examined the library synthesis. First, a linear strand **Lev20T** was synthesized. This 20-mer strand was synthesized by adding consecutively four Lev-protected amidites followed by one DMT-protected amidites (**Figure 51**). The de-levulinylation step was similar to the previous TBA library protocol. Hydrazine was diluted into 0.5 M solution in pyridine/acetic acid buffer (3/2 v/v). The de-levulinylation was kept at 6 minutes, followed by a wash of the same pyridine/acetic acid buffer before acetonitrile washing. **Lev20T** was synthesized with a good yield, and the presence of the product was confirmed by mass spectrometry (**Section 2.8.6**). This result confirms the validity of de-levulinylation in linear SPS protocol.



Figure 51: Lev20T sequence from 5' to 3' (right) and synthesis procedure from 3' to 5' (left)

The next step is to synthesize a single member of the library. The purpose is to test the synthesis protocol in the synthesizer on a branched, long strand. The synthesis process will be the same as library synthesis protocol except for the lack of split-and-pool steps. Moreover, only four natural DMT-amidites were used in the aptamer strand to prevent the affect of different coupling yield from synthetic amidites. For cytosine amidites, the compatibility of both N-acetyl and N-benzoyl protecting group were also examined. From our previous study of TBA library, N4-benzoyl cytosine is less likely to form hyperbranched structure than N4-acetylcytosine when being treated with hydrazine.

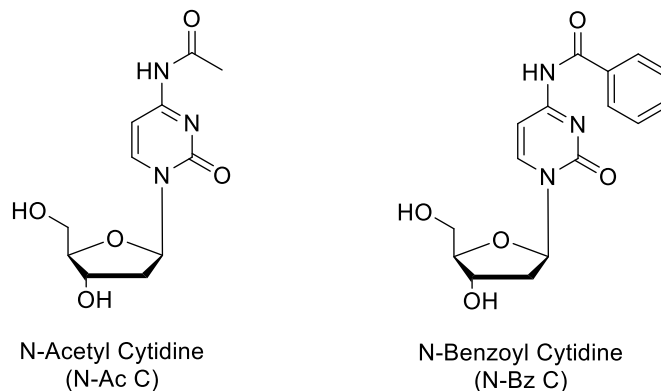


Figure 52: N-acetyl and N-benzoyl cytidine nucleoside structures

The design of this single member is the same as **CH1S-3-3** construct, with **BU2** was used instead of **BU**. From the mutation study in section 2.4.4, 6G, 7G and 12C were chosen as variable positions on the aptamer (colored in **Figure 53a**); those variables will be the actual modification monomers in the real library later. We decided to start with three variables only to simplify the synthesis process, the number of variables can be increased in the future experiments.

To ensure the compatibility with the library synthesis conditions, the single member must be synthesized by a parallel strategy utilizing the two orthogonal protecting groups in the two strands (**Figure 53b**). After coupling **BU2** (step A), the aptamer was grown with DMT amidites on one side of the branch unit. This synthesis was stopped at the first variable - the red-colored 12C - (step B) before the codon of cytidine was added into the other branch by Lev amidites (step C). The synthesis continued as each variable code was added immediately after the coupling of that variable. After the last variable – green-colored 6G – with its code were coupled into the two branches, the rest of the aptamer was synthesized by DMT amidites. Finally, the aptamer 5'-end was acetyl-capped, and the rest of the code strand was grown also by DMT amidites.

compatibility of the library synthesis protocol used in previous TBA library with our new Mermaid synthesizer and our new design.

8% denaturing PAGE

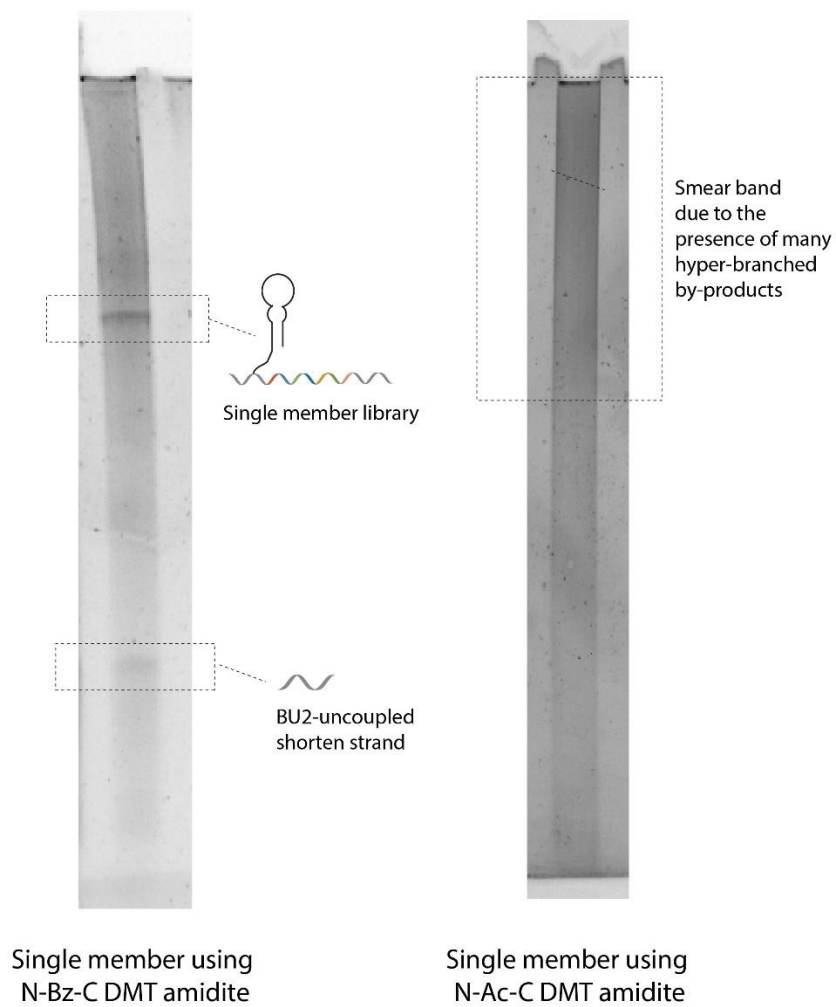


Figure 54: Denature PAGE of single member library synthesis using N-Bz and N-Ac DMT-protected cytidine

2.7. Conclusions and future work

2.7.1. Conclusion

This work examined the flexibility of design parameters of the alenomer library. First, a new target, trastuzumab was chosen, with a reported CH1S-3 aptamer that does not form any thermodynamically stable secondary structure. The aptamer is a vastly different sequence composition and is greater in length compared to the thrombin binding aptamer. As such, understanding how the alenomer library must be adapted for this aptamer will help ensure the strategy can be applied to numerous diverse aptamers reported to date. As a consequence of using this stem-loop and long aptamer, introducing modification into the aptamer might affect its folding significantly, leading to an increase in structural diversity in our aptamer pool. For the library, we introduced a new branch unit that is commercially available, therefore reducing the laborious synthesis of the uridine-based branch amidite. With the new target and the new branch unit, we examined the binding affinity of the new design by two methods: fluorescent anisotropy and surface plasmon resonance. All the model alenomers binds to the target, with the K_D values stayed below micromolar range. Although there was still a difference between the binding affinity measured by different methods, these results showed that the new design is good enough to be used in the screening process. Some of the monomer phosphoramidites were also synthesized. A new design of the monomers, the benzene-core phosphoramidites, was also examined, but the coupling affinity needed to be studied more. Finally, the library synthesis protocol was shown to be compatible with our new instrument and our new design.

2.7.2. Future work

2.7.2.1. For CH1S-3-based alenomer library

For the CH1S-3-based alenomer, a few more studies need to be completed before the finally library synthesis. For example, the compatibility of the split-and-pool process to the synthesis protocol on the new instrument with the new design needs to be considered. The coupling ability of the new monomer amidites (**Et**, **COO**, **Prop**, **Ser**) should also be confirmed before adding them into the library. In addition, since we can only appoint a certain number of modifiers in each variable position, we need to decide which monomer should be chosen by looking to the interaction between the original aptamer with trastuzumab. After library synthesis, the screening of the alenomer library with trastuzumab should be done the same way as in TBA library. PCR and next-generation sequencing can give us the information of the strong binders, and these single-stranded modified aptamers can be synthesized individually again for more detailed studies.

2.7.2.2. Further technique generalization

In the future, the alenomer technique can be improved to expand its application. A more diverse chemical space can be introduced into the alenomer library by adding new types of monomers. A wider range of targets, especially for small molecules, could be examined to build the new library. Moreover, beside the binding affinity and stability, other properties of alenomers should also be studied. For example, their binding specificity can be compared to original aptamer. The binding can also be study in different media, e.g., in different buffers or *in vivo* environment. In addition, the inhibitory activity of alenomer to the protein target also needs to be examined. The activity of an aptamer does not always depend solely on the binding affinity: a more active aptamer can have higher K_D value, but they are more stable, or their binding distort protein conformation more. In

the TBA library case, as thrombin participates in blood coagulation pathway that transforms fibrinogen into insoluble fibrin, a comparison study of clotting ability *in vivo* of thrombin in presence of original and modified TBA would likely to be interesting. In a similar way, an analytical assay such as ELISA can be used to identify the binding of HER2 with trastuzumab in the presence of original and modified CH1S-3. Moreover, beside aptamers, alenomer technique can be used for other functional oligomers. For example, a library of catalytic alenomers that mimic DNAzymes can be built to target certain substrates.

2.7.2.3. Technique improvement

Compared with other modified aptamer techniques such as SOMAmers or click-SELEX, alenomer's most significant advantage comes from the ability of incorporate any number of non-nucleosidic monomers thus substantially expanding the chemical diversity of the aptamers. However, there are still limitations, both in method basis and practical operation, that need to be improved. For example, the inclusion of code strand may induce non-specific binding that can affect the screening process. One way to minimize this effect is to hybridize the code strand by a complementary strand that is *in situ* synthesized enzymatically after library formation. Additionally, for an ideal alenomer library, the aptamer needed to be modified in every position to obtain all possible combination of monomers. While doing that is impractical due to the technical shortage, the variable positions for modification should be found with more detailed studies. For example, in the single mutation in section 2.4.4, each position could be modified with more than one mutation for better binding effect examination. In practical aspect, the SPS yield of alenomer synthesis is usually not very high (as can be seen from the "single member" synthesis in **Figure 52**) as the length of oligonucleotide is often very long. This yield can be even lower when incorporating non-nucleosidic monomers into the alenomer. A modern SPS synthesizer that allows

more efficient phosphoramidite coupling could be a solution. The low synthesis yield can also come from the steric hindrance created when a long oligonucleotide strand grows inside a small CPG pore. For now, the CPG pore size used is 2000 angstrom, which is one of the largest CPG pores available commercially. Rather than further increasing the CPG pore size which could make the solid support very fragile, a practical way to relieve this problem is to decrease the alenomer length, e.g., by shorten the linker or the primer region. The split-and-pool process can also be facilitated with more automated system that can divide CPG more evenly. Magnetic beads can also be integrated into the alenomer molecule to facilitate the split-and-pool process. Moreover, with the “one-bead-one-compound” strategy, the magnetic beads may help separate individual alenomer member from the pools, paving the way for even more types of activity-based alenomer screening.

2.8. Experimental Section

2.8.1 Chemicals

All starting materials were obtained from commercial suppliers and used without further purification unless otherwise noted. DMT-Cl was purchased from AK Scientifics. N,N-diisopropylamino cyanoethyl phosphonamidic-Cl (CEP-Cl) and 2-cyanoethyl N,N,N,N-tetraisopropyl phosphane were purchased from Chemgenes. Chloroform-d and dimethyl sulfoxide-d₆ were purchased from Sigma-Aldrich. The CPG UnylinkerTM Universal Supports 1000 Å and 2000 Å were purchased from Chemgenes. 5'-DMT-protected and 5'-levulinyl-protected canonical phosphoramidites were purchased from Chemgenes. Asymmetric doubler (Lev) phosphoramidite and 5'-6-fluorescein phosphoramidite were purchased from GlenResearch. Ammonium hydroxide

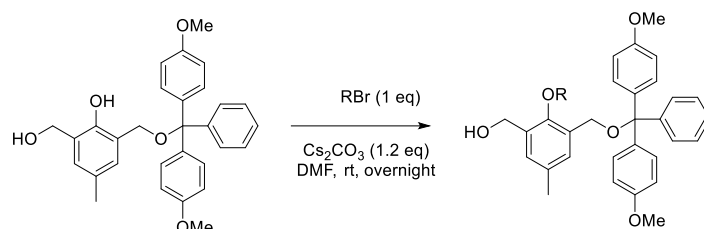
aqueous solution (28%) was purchased from Fischer Chemical. Sephadex G-25 (super fine, DNA grade) was purchased from GlenResearch. Acrylamide/Bis solution (19: 1), 40% (w/v) was purchased from Biobasics. Tris and urea were purchased from Biobasics, while boric acid and EDTA were purchased from BioShop. TBE solution 10x was prepared as an aqueous solution of Tris (890 mM), boric acid (890 mM) and EDTA (20 mM). GelRed™ 10000x in water was purchased from VWR. Triton X-100 was purchased from Bioshop. PBS buffer 10x (pH = 7.4, without calcium and without magnesium) was purchased from Bioshop. Filtered aqueous solution KCl 2M and MgCl₂ 1M were purchased from Invitrogen.

2.8.2. Instrumentation

Organic compounds were evaporated *in vacuo* in Buchi Rotavapor R-114 and were isolated by column chromatography using CombiFlash Rf system from Teledyne Isco. NMR spectra were taken from Bruker 500 MHz or Varian 300 MHz with chloroform-d or dimethyl sulfoxide-d₆ as internal locked solvents. Off-column solid-phase phosphoramidite coupling was performed in OMNI-lab glovebox from VAC. Automated oligonucleotide solid-phase synthesis was performed by Mermaid 6 synthesizer from Bioautomation. DNA and oligomers were quantified by UV absorbance with a NanoDrop Lite spectrophotometer from Thermo Scientific. Dry solvents were collected from an Innovation Technology device. Low resolution mass spectrometry (MS) was performed with an electron-spray ionization (ESI) ion trap MS on a Finnigan LCQ Duo device. PAGE was run with Hoefer 600 electrophoresis unit and Mini-PROTEAN electrophoresis units. The preparative gels were image using a ChemiDoc MP System from Bio-Rad Laboratories. Fluorescent anisotropy was carried out using BioTek Cytation 5 imaging reader system. SPR experiment was carried out in Biacore X100 SPR system.

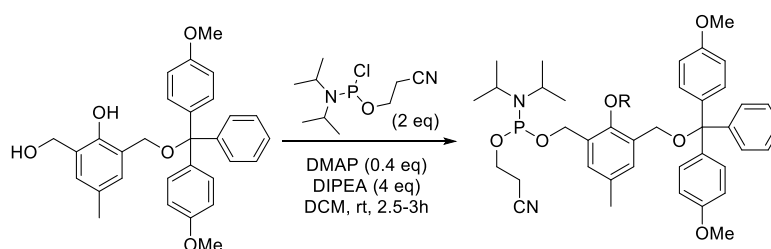
2.8.3. Small molecule synthesis

2.8.3.1. General procedure for phenolic nucleophilic substitution



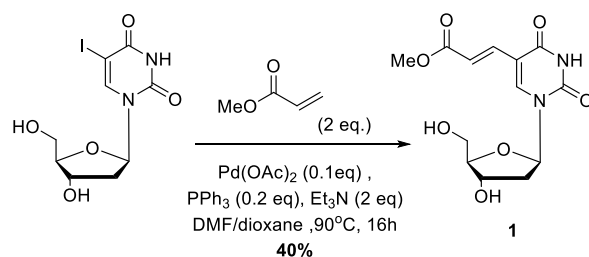
2-((bis(4-methoxyphenyl)(phenyl)methoxy)methyl)-6-(hydroxymethyl)-4-methylphenol (**6**) (1 equivalent) was diluted with 10 to 20 mL of DMF in a dry 100 mL RBF with a stir bar. After that, cesium carbonate Cs₂CO₃ (1.2 equivalent) was added into the solution while stirring. The color of the solution slightly changed. The solution was left stirring for about 1 minute before adding the bromide reagent (1 equivalent). The reaction was left stirring overnight at room temperature. The appearance of the product was confirmed by TLC. Water was added into the mixture to quench the reaction. After that, EtOAc and water was used to transfer the mixture into a separatory funnel. The crude product in EtOAc layer was washed three times with water and three times with brine to remove DMF. The combined organic layer then was dried with Na₂SO₄ and evaporated under reduced pressure (40°C). The crude product was loaded on celite and purified using the CombiFlash system.

2.8.3.2. General procedure for phosphoramidite formation from DMT-protected diol



DMT-monoprotected diol (1 equivalent) was diluted in DCM in an oven-dried RBF and solvent was evaporated under reduced pressure (60 °C). The dried compound was kept under high vacuum for at least 5 hours. After that, DMAP (0.4 equivalent) and a stir bar were added, and gas exchange with argon was done inside the flask. The mixture was then dissolved in anhydrous DCM (5 - 7 mL), and dry DIPEA (4 equivalents) was added under stirring. CEP-Cl (2 equivalents) was added slowly and the reaction was allowed to stir under inert gas at room temperature for 2.5-3 hours. Two fast extractions with DCM from a 10 % Na₂CO₃ aqueous solution were performed. Organic fractions were combined, dried over Na₂SO₄, filtered and the solvent was evaporated under reduced pressure (40 °C). The crude product was loaded on celite and purified using the CombiFlash system. Silica columns have been pretreated with a solution containing 1 % of triethylamine.

2.8.3.3. methyl (*E*)-3-(1-((2*R*,4*S*,5*R*)-4-hydroxy-5-(hydroxymethyl)tetrahydrofuran-2-yl)-2,4-dioxo-1,2,3,4-tetrahydropyrimidin-5-yl)acrylate (**1**)

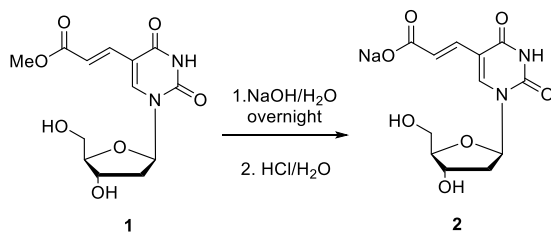


The following procedure was based on the protocol developed by Liu and colleague.¹⁴⁵ In an oven-dried RBF, 1.77 g (5 mmol, 1 equivalent) of 5'-deoxy-5-iodouridine, 262 mg (1.00 mmol, 0.2 equivalent) of triphenylphosphine and 1.4 mL (10.0 mmol, 2 equivalents) of triethylamine was dissolve in a mixture of dry DMF (14 mL) and dry dioxane (36 mL) at 25 °C under an argon atmosphere. Next, 0.9 mL (10 mmol, 2 equivalents) of methyl acrylate and 112 mg (0.50 mmol, 0.1 equivalent) of Pd(OAc)₂ were added to the flash. The mixture was then heated to 90 °C and

stirred for 16 hours. Afterward, the reaction mixture was evaporated under reduced pressure to remove the dioxane, followed by coevaporation with toluene until dryness. The resulting residue was purified by column chromatography (using SiO₂ and a solvent mixture of DCM/10% methanol in DCM, with a gradient of 0 to 70% over 7 column volumes). This purification process yielded 618 mg (2.0 mmol, 40% yield) of compound **1** as a white solid.

¹H NMR (300 MHz, DMSO-d₆) δ 11.66 (s, 1H), 8.41 (s, 1H), 7.36 (d, *J* = 15.8 Hz, 1H), 6.84 (d, *J* = 15.8 Hz, 1H), 6.12 (t, *J* = 6.4 Hz, 1H), 5.26 (d, *J* = 4.4 Hz, 1H), 5.19 (d, *J* = 5.2 Hz, 1H), 4.25 (q, *J* = 4.5 Hz, 1H), 3.78 (q, *J* = 3.6 Hz, 1H), 3.67 (s, 1H), 3.59 – 3.56 (m, 1H), 2.19 – 2.13 (m, 2H).

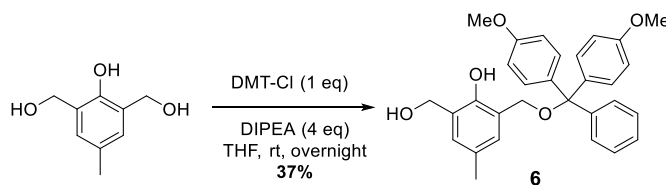
2.8.3.4. Sodium (*E*)-3-(1-((2*R*,4*S*,5*R*)-4-hydroxy-5-(hydroxymethyl)tetrahydrofuran-2-yl)-2,4-dioxo-1,2,3,4-tetrahydropyrimidin-5-yl)acrylate (**2**)



1 M aqueous NaOH solution was added to a flask of **1**, and the mixture was left stirring overnight. The reaction mixture was neutralized to pH of 7 with 1 M HCl aqueous solution and evaporated at high vacuum at 60°C to remove water. The residue was then resuspended in DMF to use for next reaction without further purification.

2.8.3.5. 2-((bis(4-methoxyphenyl)(phenyl)methoxy)methyl)-6-(hydroxymethyl)-4-methylphenol

(6)



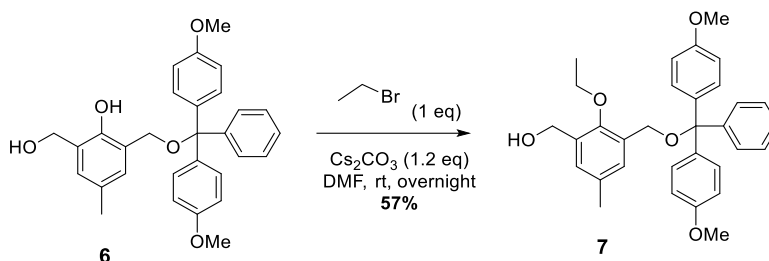
(2-hydroxy-5-methyl-1,3-phenylene)dimethanol (2.52 g, 15 mmol) was diluted with 30 mL of THF in a dry 250 mL RBF with a stir bar. After that, DIPEA (10.45 mL, 60 mmol) was added into the solution. In another flask, DMT-Cl (5.08 g, 15 mmol) was diluted with 20 mL of THF. The DMT-Cl solution was then added dropwise through a funnel into the reaction in 250 mL RBF while stirring at room temperature. The reaction was left stirring overnight. The appearance of the product was confirmed by TLC. The reaction mixture was then evaporated under reduced pressure (40°C). The crude product was loaded on celite and purified using the CombiFlash system. The solvent mixture used was hexanes/TEA (100:1 v/v) and EtOAc in a gradient of 15% to 90% EtOAc. The product appeared at around 10 CV. A brown oil was isolated with a mass of 2.56 g (37%).

^1H NMR (500 MHz, CDCl_3) δ 7.53 (d, $J = 7.5$ Hz, 2H), 7.45 – 7.40 (m, 4H), 7.33 (t, $J = 7.7$ Hz, 2H), 7.26 – 7.22 (m, 1H), 6.93 (d, $J = 2.2$ Hz, 1H), 6.89 – 6.85 (m, 5H), 4.72 (s, 2H), 4.33 (s, 2H), 3.78 (s, 6H), 2.26 (s, 3H).

^{13}C NMR (126 MHz, CDCl_3) δ 158.69, 151.71, 144.36, 135.44, 129.94, 128.68, 128.17, 128.07, 127.92, 127.80, 127.01, 126.70, 123.58, 113.36, 87.52, 64.52, 62.55, 55.13, 20.43.

2.8.3.6. (3-((bis(4-methoxyphenyl)(phenyl)methoxy)methyl)-2-ethoxy-5-methylphenyl)methanol

(7)

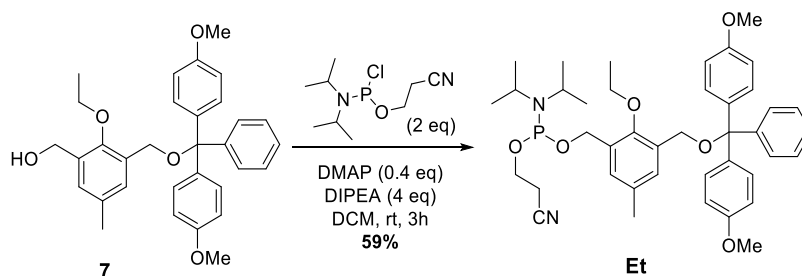


Reaction was set-up and perform from 779 mg (1.66 mmol) of **6**, 0.123 mL (1.66 mmol) of ethyl bromide, 647 mg of Cs₂CO₃ (2.00 mmol) in 10 mL of DMF as in Section 2.8.3.1. The solution mixture for the CombiFlash was hexane:TEA (1000:1) and EtOAc with the gradient from 15% to 85% EtOAc. The resulting colorless oily residue was recovered in 468 mg (57%).

¹H NMR (500 MHz, CDCl₃) δ 7.55 – 7.51 (m, 2H), 7.44 – 7.39 (m, 5H), 7.31 (dd, *J* = 8.4, 6.9 Hz, 2H), 7.26 – 7.21 (m, 1H), 7.10 (d, *J* = 2.3 Hz, 1H), 6.88 – 6.84 (m, 4H), 4.65 (s, 2H), 4.17 (s, 2H), 3.80 (s, 6H), 3.71 (q, *J* = 7.0 Hz, 2H), 2.38 (s, 3H), 1.15 (t, *J* = 7.0 Hz, 3H).

¹³C NMR (126 MHz, CDCl₃) δ 158.60, 152.96, 145.11, 136.39, 133.85, 133.51, 132.28, 130.24, 129.66, 128.84, 128.39, 127.95, 126.89, 113.24, 86.62, 70.40, 61.68, 60.75, 55.34, 21.19, 15.77.

2.8.3.7. 3-((bis(4-methoxyphenyl)(phenyl)methoxy)methyl)-2-ethoxy-5-methylbenzyl (2-cyanoethyl) diisopropylphosphoramidite (**Et**)

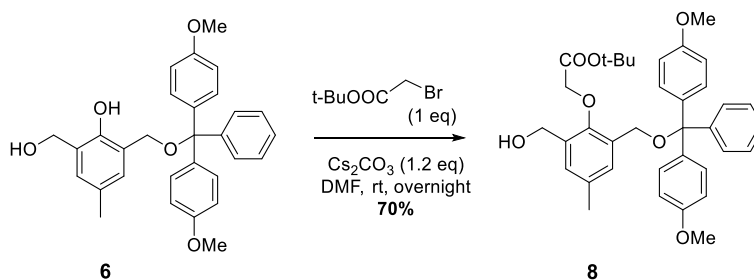


Reaction was set-up and perform from 375 mg (0.752 mmol) of **7**, 0.336 mL of CEP-Cl (1.50 mmol), 0.524 mL of DIPEA (3.01 mmol), 36.7 mg DMAP (0.300 mmol) in 5 mL dry DCM as in Section 2.8.3.2. The reaction was left stirring in 3 hours. The solution mixture for the CombiFlash was hexane:TEA (100:1) and EtOAc with 40% EtOAc. The resulting transparent oily residue was recovered in 310 mg (59%).

^1H NMR (500 MHz, CDCl_3) δ 7.56 – 7.52 (m, 2H), 7.45 – 7.41 (m, 4H), 7.40 (d, $J = 2.3$ Hz, 1H), 7.31 (dd, $J = 8.5, 7.0$ Hz, 2H), 7.25 – 7.19 (m, 2H), 6.88 – 6.84 (m, 4H), 4.71 (ddd, $J = 54.7, 12.5, 7.9$ Hz, 2H), 4.18 (s, 2H), 3.90 – 3.82 (m, 2H), 3.79 (s, 6H), 3.72 – 3.63 (m, 4H), 2.61 (td, $J = 6.4, 1.4$ Hz, 2H), 2.40 (s, 3H), 1.22 (dd, $J = 8.6, 6.8$ Hz, 12H), 1.14 (t, $J = 7.0$ Hz, 3H).

^{31}P NMR (203 MHz, CDCl_3) δ 148.39.

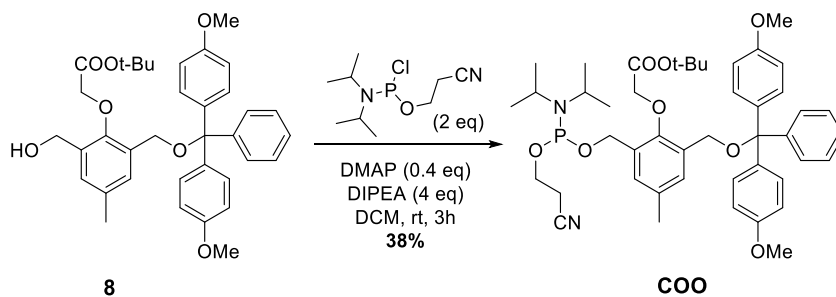
2.8.3.8. *tert*-butyl 2-(2-((bis(4-methoxyphenyl)(phenyl)methoxy)methyl)-6-(hydroxymethyl)-4-methylphenoxy)acetate (**8**)



Reaction was set-up and perform from 802 mg (1.70 mmol) of **6**, 0.252 mL (1.70 mol) of *tert*-butyl 2-bromoacetate, 667 mg of Cs₂CO₃ (2.05 mmol) in 15 mL of DMF as in Section 2.8.3.1. The solution mixture for the CombiFlash was hexane:TEA (1000:1) and EtOAc with the gradient from 15% to 85% EtOAc. The resulting pale-yellow oily residue was recovered in 698 mg (70%).

¹H NMR (300 MHz, CDCl₃) δ 7.50 (d, *J* = 7.4 Hz, 2H), 7.39 (d, *J* = 8.8 Hz, 4H), 7.30 (t, *J* = 7.3 Hz, 2H), 7.22 (d, *J* = 2.5 Hz, 2H), 7.05 (s, 1H), 6.85 (d, *J* = 8.8 Hz, 4H), 4.62 (d, *J* = 6.9 Hz, 2H), 4.24 (s, 2H), 4.12 (s, 2H), 3.80 (s, 6H), 2.34 (s, 3H), 1.44 (s, 9H).

2.8.3.9. *tert*-butyl 2-(2-((bis(4-methoxyphenyl)(phenyl)methoxy)methyl)-6-(((2-cyanoethoxy)(diisopropylamino)phosphanyl)oxy)methyl)-4-methylphenoxy)acetate (**COO**)

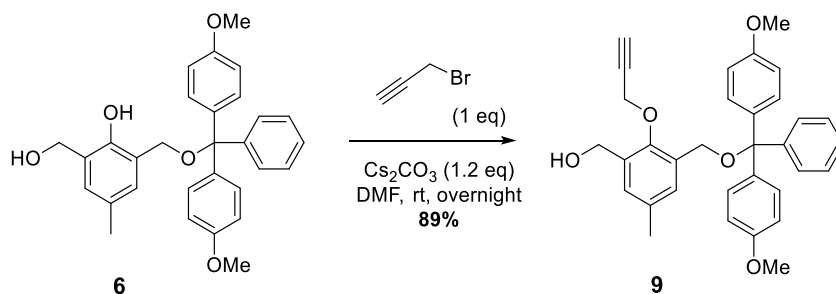


Reaction was set-up and perform from 218 mg (0.372 mmol) of **8**, 0.166 mL of CEP-Cl (0.745 mmol), 0.259 mL of DIPEA (1.49 mmol), 18.2 mg DMAP (0.149 mmol) in 5 mL dry DCM as in Section 2.8.3.2. The reaction was run in 3 hours. The solution mixture for the CombiFlash was hexane:TEA (100:1) and EtOAc with 40% EtOAc. The resulting transparent oily residue was recovered in 111 mg (38%).

¹H NMR (500 MHz, CDCl₃) δ 7.51 – 7.48 (m, 2H), 7.40 – 7.36 (m, 4H), 7.29 (dd, *J* = 8.4, 6.9 Hz, 2H), 7.23 – 7.19 (m, 2H), 7.16 (d, *J* = 2.2 Hz, 1H), 6.85 – 6.82 (m, 4H), 4.80 – 4.66 (m, 3H), 4.27 (s, 2H), 4.17 (s, 2H), 3.90 – 3.82 (m, 2H), 3.79 (s, 6H), 3.64 (m, 2H), 2.62 (t, *J* = 6.6 Hz, 2H), 2.34 (s, 3H), 1.42 (s, 9H), 1.19 (dd, *J* = 8.6, 6.8 Hz, 12H).

³¹P NMR (203 MHz, CDCl₃) δ 148.44.

2.8.3.10. (3-((bis(4-methoxyphenyl)(phenyl)methoxy)methyl)-5-methyl-2-(prop-2-yn-1-yloxy)phenyl)methanol (**9**)

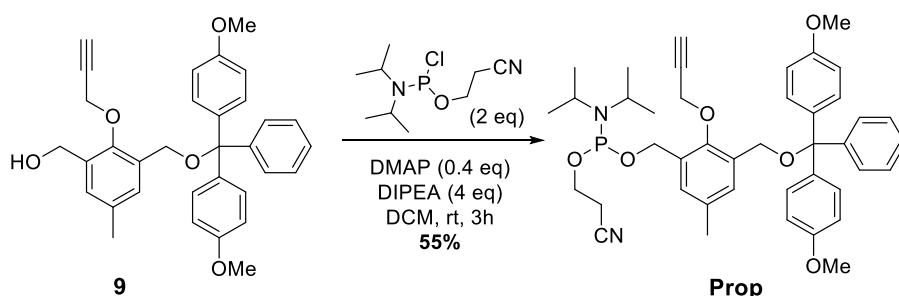


Reaction was set-up and perform from 782 mg (1.66 mmol) of **6**, 0.185 mL (1.66 mol) of 3-bromoprop-1-yne, 647 mg of Cs₂CO₃ (2.00 mmol) in 15 mL of DMF as in Section 2.8.3.1. The solution mixture for the CombiFlash was hexane:TEA (1000:1) and EtOAc with the gradient from 15% to 85% EtOAc. The resulting yellow oily residue was recovered in 755 mg (89%).

^1H NMR (500 MHz, CDCl_3) δ 7.54 – 7.50 (m, 2H), 7.43 – 7.39 (m, 4H), 7.33 – 7.29 (m, 3H), 7.25 – 7.21 (m, 1H), 7.14 (d, $J = 2.3$ Hz, 1H), 6.88 – 6.84 (m, 4H), 4.70 (s, 2H), 4.43 (d, $J = 2.4$ Hz, 2H), 4.20 (s, 2H), 3.80 (s, 6H), 2.42 (t, $J = 2.4$ Hz, 1H), 2.37 (s, 3H).

^{13}C NMR (126 MHz, CDCl_3) δ 158.63, 152.37, 145.07, 136.26, 134.66, 133.99, 132.21, 130.33, 130.25, 129.48, 128.34, 128.00, 126.92, 113.30, 86.78, 79.36, 75.67, 62.17, 61.38, 61.07, 55.34, 21.18.

2.8.3.11. 3-((bis(4-methoxyphenyl)(phenyl)methoxy)methyl)-5-methyl-2-(prop-2-yn-1-yloxy)benzyl (2-cyanoethyl) diisopropylphosphoramidite (**Prop**)



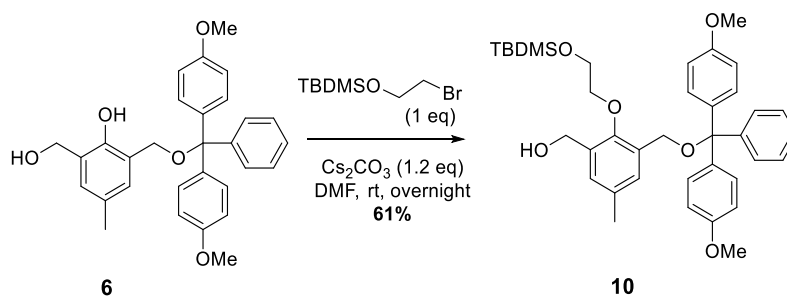
Reaction was set-up and perform from 208 mg (0.409 mmol) of **9**, 0.19 mL of CEP-Cl (0.817 mmol), 0.29 mL of DIPEA (1.63 mmol), 19.97 mg DMAP (0.163 mmol) in 5 mL dry DCM as in Section 2.8.3.2. The reaction was run in 3 hours. The solution mixture for the CombiFlash was hexane:TEA (100:1) and EtOAc with 40% EtOAc. The resulting transparent oily residue was recovered in 159 mg (55%).

^1H NMR (500 MHz, CDCl_3) δ 7.56 – 7.52 (m, 2H), 7.45 – 7.41 (m, 4H), 7.32 (m, 3H), 7.26 – 7.19 (m, 2H), 6.90 – 6.85 (m, 4H), 4.76 (ddd, $J = 53.1, 12.5, 7.8$ Hz, 2H), 4.43 (d, $J = 2.4$ Hz, 2H), 4.23

(s, 2H), 3.92 – 3.85 (m, 2H), 3.82 (s, 6H), 3.67 (dtd, $J = 13.5, 8.2, 5.0$ Hz, 2H), 2.65 (t, $J = 6.6$ Hz, 2H), 2.39 (m, 4H), 1.23 (t, $J = 6.8$ Hz, 12H).

^{31}P NMR (203 MHz, CDCl_3) δ 148.39.

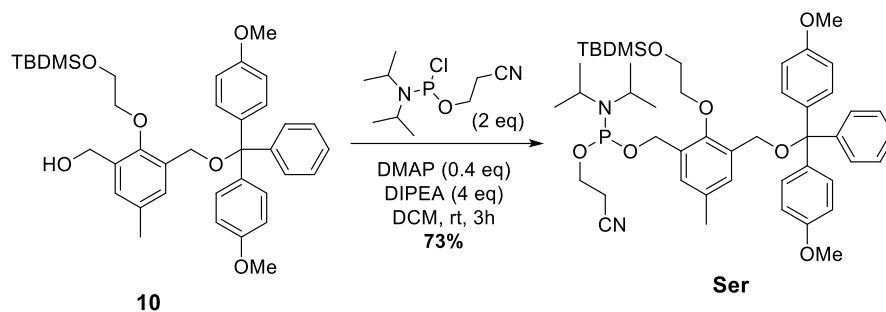
2.8.3.12. (3-((bis(4-methoxyphenyl)(phenyl)methoxy)methyl)-2-(2-((tert-butyl)dimethylsilyloxy)ethoxy)-5-methylphenyl)methanol (**10**)



Reaction was set-up and perform from 683 mg (1.45 mmol) of **6**, 0.311 mL (1.45 mol) of (2-bromoethoxy)(tert-butyl)dimethylsilane, 567 mg of Cs₂CO₃ (1.74 mmol) in 15 mL of DMF as in Section 2.8.3.1. The solution mixture for the CombiFlash was hexane:TEA (1000:1) and EtOAc with the gradient from 15% to 85% EtOAc. The resulting yellow oily residue was recovered in 555 mg (61%).

^1H NMR (500 MHz, CDCl_3) δ 7.56 – 7.52 (m, 2H), 7.45 – 7.40 (m, 4H), 7.35 – 7.30 (m, 3H), 7.25 – 7.22 (m, 1H), 7.05 (d, $J = 2.3$ Hz, 1H), 6.89 – 6.85 (m, 4H), 4.64 (s, 2H), 4.19 (s, 2H), 3.80 – 3.76 (m, 8H), 3.70 (dd, $J = 5.4, 3.3$ Hz, 2H), 2.37 (s, 3H), 0.93 (s, 9H), 0.11 (s, 6H).

2.8.3.13. 3-((bis(4-methoxyphenyl)(phenyl)methoxy)methyl)-2-(2-((tert-butyl-dimethylsilyl)oxy)ethoxy)-5-methylbenzyl (2-cyanoethyl) diisopropylphosphoramidite (**Ser**)



Reaction was set-up and perform from 222 mg (0.353 mmol) of **10**, 0.158 mL of CEP-Cl (0.706 mmol), 0.25 mL of DIPEA (1.41 mmol), 17.2 mg DMAP (0.141 mmol) in 5 mL dry DCM as in Section 2.8.3.2. The reaction was run in 3 hours. The solution mixture for the CombiFlash was hexane:TEA (100:1) and EtOAc with 40% EtOAc. The resulting pale-yellow oily residue was recovered in 217 mg (73%).

^1H NMR (500 MHz, CDCl_3) δ 7.53 – 7.50 (m, 2H), 7.43 – 7.39 (m, 4H), 7.36 (d, $J = 2.3$ Hz, 1H), 7.33 – 7.28 (m, 2H), 7.26 – 7.20 (m, 2H), 6.87 – 6.84 (m, 4H), 4.75 (ddd, $J = 60.0, 12.7, 8.2$ Hz, 2H), 4.18 (s, 2H), 3.89 – 3.82 (m, 2H), 3.80 (s, 6H), 3.73 – 3.63 (m, 6H), 2.61 (td, $J = 6.6, 2.0$ Hz, 2H), 2.39 (s, 3H), 1.21 (dd, $J = 9.7, 6.8$ Hz, 12H), 0.88 (s, 9H), 0.02 (s, 6H).

^{31}P NMR (203 MHz, CDCl_3) δ 148.84.

2.8.4. Solid phase synthesis

2.8.4.1. General procedure for SPS in Mermaid synthesizer

The protocol followed the original protocol from Dr. Donatien de Rochambeau with a few modifications. For linear oligomers, synthesis was performed on a 1 μmol scale, starting from a universal 1000 Å UnyLinker CPG solid support. 5'-DMT and 5'-Lev protected nucleoside phosphoramidites (benzoyl protected adenosine, benzoyl protected cytidine, acetyl protected cytidine, isobutyryl protected guanosine and thymidine) were dissolved in dry acetonitrile and coupling times of 3 minutes were used. Molecular trap packs were used to maintain the acetonitrile, the activator and the phosphoramidite solutions dry. In each coupling cycle, the coupling followed by the cap, oxidation and 5'-deprotection. For DMT-protected strand, the deprotection was carried out using 3 % dichloroacetic acid in DCM. For Lev-protected strand the cleavage of levulinyl protecting group was carried out using hydrazine hydrate (50-60 %) diluted to 0.5M in a 3:2 (v:v) pyridine/acetic acid solution. Hydrazine treatment lasts 6 minutes with three injections of 2 minutes each unless otherwise noted. For branched oligomers, synthesis was performed similarly but with a universal 2000 Å Unylinker CPG solid support.

2.8.4.2. General procedure for off-column coupling

CPG containing 5'-unprotected strand was plugged into a syringe through an adapter. The CPG and the phosphoramidite were transferred into the glove box. Here the phosphoramidite was diluted into 0.1 M solution with dry acetonitrile. For each coupling, 200 μL of 0.1 M phosphoramidite and 200 μL of 0.5 M activator in acetonitrile were added into the CPG. The CPG was left in 15 minutes in the glovebox. The solution was mixed several times by the syringe before and during the coupling. After the coupling, the CPG was taken out. The cap, oxidation and de-tritylation steps were carried out in the Mermaid synthesizer.

2.8.4.3. General procedure for deprotection

Post-synthesis CPG was incubated in 28 % aqueous ammonium hydroxide solution for 16-18 hours at 65 °C. This process deprotected the nucleobases as well as cleaved the DNA or oligomer strands from the solid support. After removal of ammonium hydroxide solution under reduced pressure at 60°C, the crude product was suspended in Millipore water. The product was purified by preparative PAGE and de-salted with Sephadex column. The final product was stored with autoclaved Millipore water at 4°C for further uses.

2.8.4.4. Strand sequences

*Amidites: underline = levulinyl-protected amidite, normal = DMT-protected amidites

*Color: **blue** = aptamer region, **green** = code region, **red** = primer region, **red in bold** = branch unit, **orange** = spacer between branch unit and aptamer

Strands	Sequence (5'-3')
CH1S-3	GTCCAGGGTTCCAAGGTGCTTCGTGGAC
CH1S-3-1	6FAM-GTCCAGGGTTCCAAGGTGCTTCGTGGAC
CH1S-3-2	CGTCGAGGCCCTTCTTCTTCGTCTTCTTCTTAGGA- BU- ACACGTCACGCCTTTTTTTTT Branch: 6FAM- GTCCAGGGTTCCAAGGTGCTTCGTGGACTTTTTTTTT
CH1S-3-3	CGTCGAGGCCCTTCTTCTTCGTCTTCTTCTTAGGA- BU2- ACACGTCACGCCTTTTTTTTT Branch: 6FAM- GTCCAGGGTTCCAAGGTGCTTCGTGGACTTTTTTTTT

CH1S-3-3 HYB	<p>CGTCGAGGCCCTTCTTCTTCGTCTTCTTCTTAGGA-BU2-</p> <p>ACACGTCACGCCTTTTTTTTT</p> <p>Branch: 6FAM-</p> <p>GTCCAGGGTTCCAAGGTGCTTCGTGGACTTTTTTTTTT</p> <p>Complementary strand: AAAAAAAAAAGGCGTGACGTGTATCCTAAGA</p> <p>AGAAGACGAAGAAGAAGGGGCCTCGACG</p>
Poly(A) CH1S-3	<p>GTCCAGGGTTCCAAGGTGCTTCGTGGACAAAAAAAAAAAAAAAAAAAA</p> <p>AAAAAA</p>
Poly(A) CH1S-3-3	<p>CGTCGAGGCCCTTCTTCTTCGTCTTCTTCTTAGGA-BU2-</p> <p>ACACGTCACGCCAAAAAAAAAAAAAAAAAAAAAAAAAAAA</p> <p>Branch: 6FAM-</p> <p>GTCCAGGGTTCCAAGGTGCTTCGTGGACTTTTTTTTTT</p>
Lev20T	<p><u>CTTTTTTTTTGTTTTATTTT</u></p>

2.8.5. Gel electrophoresis

Denaturing poly-acrylamide gel electrophoresis (PAGE) was carried out in room temperature using big glass plates. TBE 1x solution was used as buffer for running denature PAGE. For analytical gel, each sample was prepared in 10 μ L of 12 pmol and added 10 μ L of urea 8M. For preparative gel, the mixture of crude aqueous solution and urea 8M solution in 1:1 (v/v) ratio was loaded with maximum 150 μ L per lane.

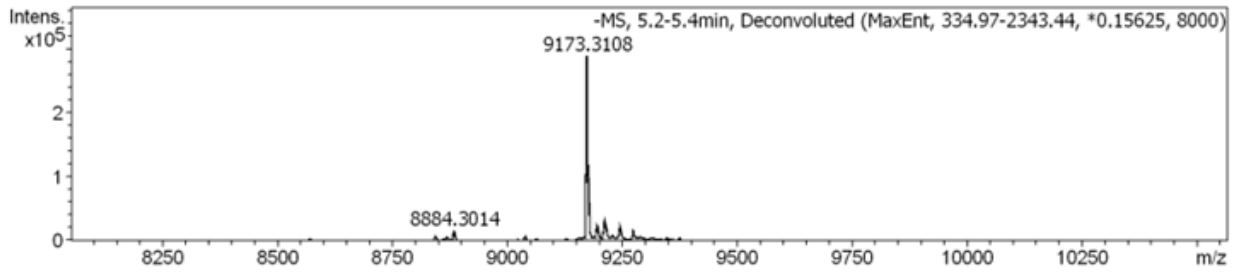
Initially, the gel was “pre-run” without any sample for 1 hour at 500 V. After sample loading, the gel was run at 250 V for 30 minutes and then at 500 V for 45 minutes. Analytical gel was stained by GelRed 1x in TBE 1x solution for 15-20 minutes and imaged by BioRad Imaging System.

2.8.6. LC-MS

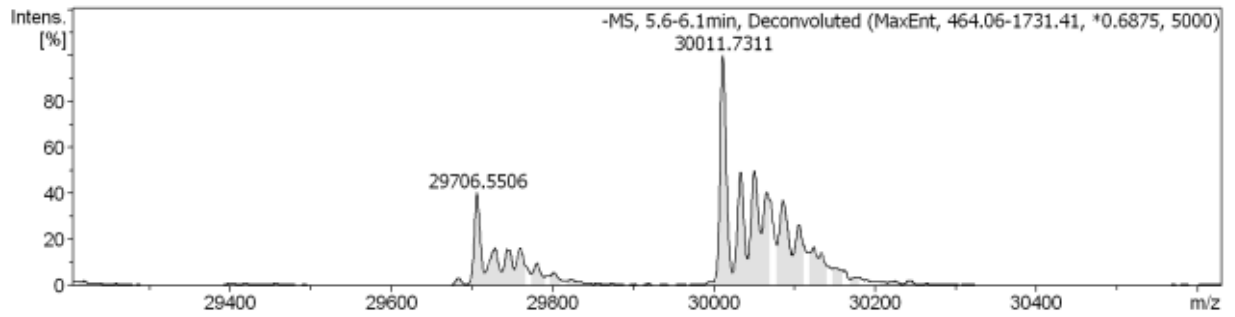
The protocol was taken from Dr. de Rochambeau work. The oligomers were analyzed by LC-ESI-MS in negative ESI mode. Samples (~60 pmols in water) were run through an Acclaim RSLC 120 C18 column (2.2 μ m, 120 \AA 2.1 x 50 mm) using a gradient of mobile phase A (100 mM 1,1,1,3,3,3-hexafluoro-2-propanol and 5 mM triethylamine in water) and mobile phase B (Methanol) in 8 minutes (2 % to 100 % B). Liquid chromatography was performed as a control for strand purity which was found to be superior to 90 % in all cases.

Strand	Expected molecular weight (g/mol)	Found peak (g/mol)
CH1S-3-1	9174.07	9173.3108
CH1S-3-2	30011.48	30011.7311
CH1S-3-3	29916.46	29917.7415
Poly(A)-CH1S-3-3	34695.75	34734.8025 (K ⁺ adduct)
Lev20T	6040.95	6039.9532

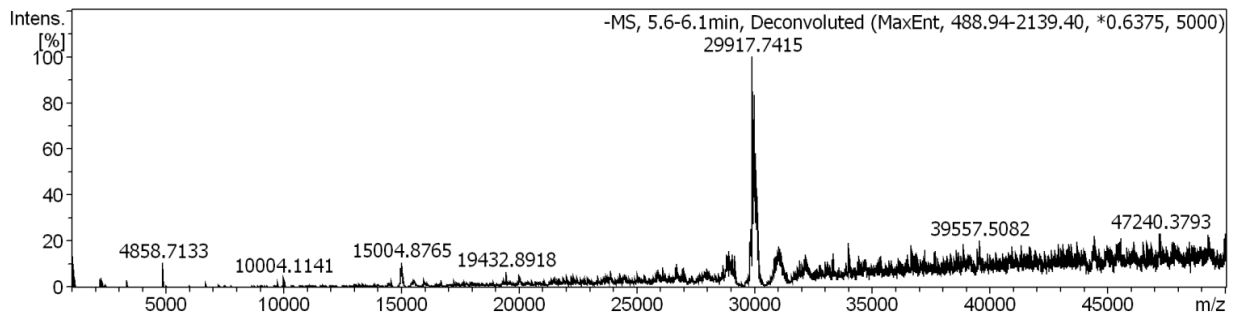
CH1S-3-1 (after gel purification)



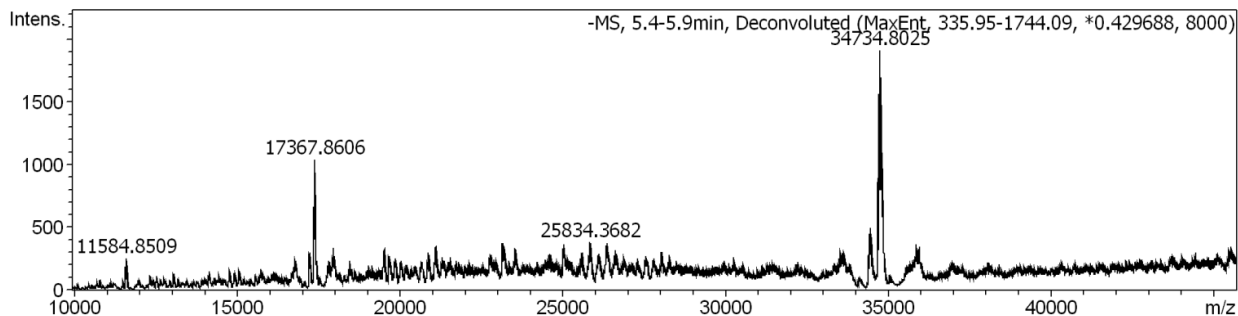
CH1S-3-2 (after gel purification)



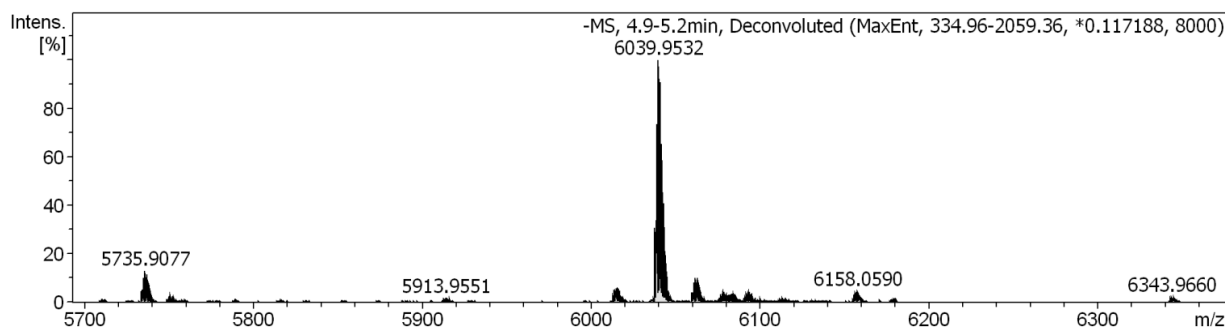
CH1S-3-3 (after gel purification)



Poly(A)-CH1S-3-3 (after gel purification)



Lev20T (after gel purification)



2.8.7. Fluorescence anisotropy

2.8.7.1. General procedure of fluorescence anisotropy

The fluorescence anisotropy assay was followed the previously described protocol.¹⁹⁶ All model strands were synthesized as described above or ordered directly from IDT with a fluorescein attached on the 5-prime-end. Each oligomer was dissolved in the corresponding binding buffer of its target (containing 0.1% surfactant v/v Triton X) to a concentration of 10 nM and stored in freezer in the dark until further use. For the assay, the oligomers were thawed, heated at 95 °C for 5 minutes, then cooled at 4 °C for 15 minutes. Protein solution was prepared fresh each time at a concentration of C_0 μ M by dissolving in binding buffer. Concentration was confirmed on the

NanoDrop Lite spectrophotometer and dilutions were made at a range of concentrations in selection buffer and were kept on ice before use.

After preparing the oligomers and target dilution, 30 μL of each were mixed separately in a 96-well microplate. The microplate used was RNase and DNase-free. For each trial of aptamer, its mixtures with different protein concentrations were placed in a single row. The plate was shaken at a certain time and temperature depending on the target. The anisotropy of each sample was then measured using a plate reader, with excitation at 485 nm and emission at 528 nm. The change in anisotropy, which was defined as the difference between the polarization values measured in the absence and presence of protein, was plotted against the total concentration of protein. A binding isotherm was fitted using GraphPad Prism 6 with a one-site binding (hyperbola) fit, and the K_D values were reported as the mean and standard deviation of three independent experiments.

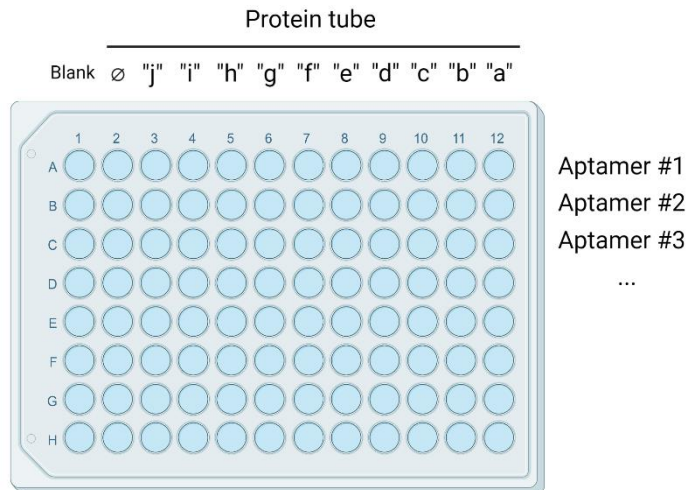
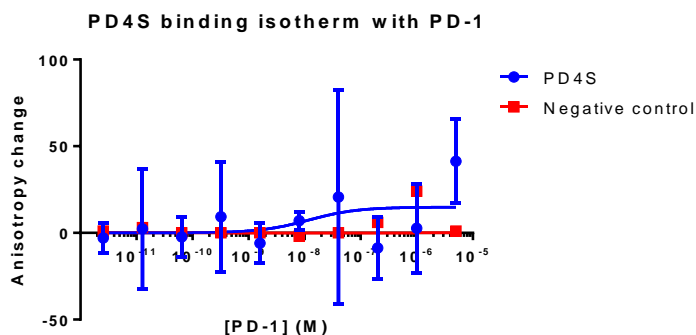


Figure 55: Diagram of the sample in each well of the 96-well plate (made by BioRender)

2.8.7.2. FA assay: PD4S vs PD-1

The fluorescent anisotropy assay between 5'-FAM-PD4S and PD-1 was proceeded as in general procedure in section 2.8.7.1. 5'-FAM-TBA sequence was used as a negative control sequence. The

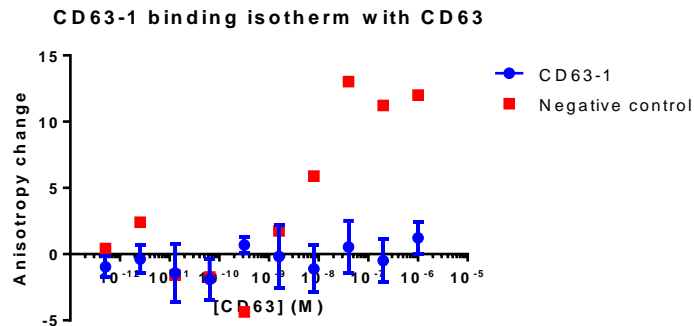
binding buffer was PBS (without magnesium and calcium) containing 4.5 g/L glucose and 5 mM MgCl₂. Stock PD-1 (Biotechne) was prepared in 180 μL of 10 μM. The serial five-fold dilution of PD-1 was done by taking 40 μL from the previous tube and adding 160 μL of buffer to the following tube. The anisotropy of 5'-FAM-PD4S was measured in three replicates, while the negative control was only measured once. The plate was incubated at 4°C for 1 hour.



Constructs	Fitted K _D (nM)
PD4S	12 ± 45

2.8.7.3. FA assay: CD63-1 vs CD63

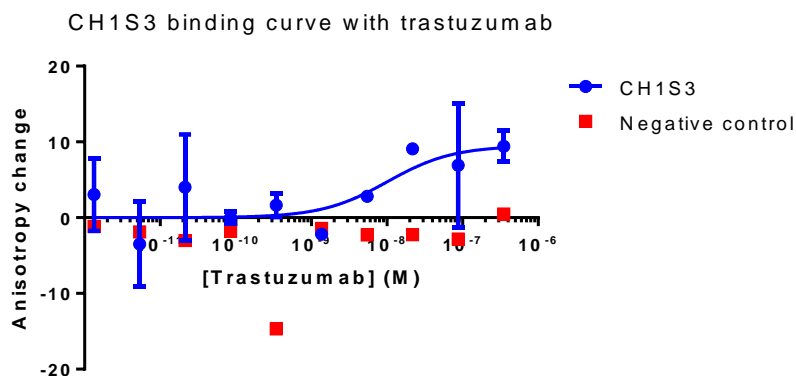
The fluorescent anisotropy assay between 5'-FAM-CD63-1 and CD-63 was proceeded as in general procedure in section 2.8.7.1. A strand of 5'-FAM-GGGTGGAGGGGTGGGGTGGTCGCCTTTT TAGGAAGTTTG-3' was used as a negative control sequence. The binding buffer was PBS (without magnesium and calcium) containing 2.0 mM MgCl₂. Stock CD63 (Sino Biological) was prepared in 180 μL of 10.96 μM. The serial five-fold dilution of CD63 was done to prepare the target solutions with concentration ranging from 2 μM to 1 pM. The anisotropy of 5'-FAM-CD63-1 was measured in three replicates, while the negative control was only measured once. The plate was incubated at 37°C for 1 hour.



Constructs	Fitted K_D (nM)
CD63-1	N/A (no binding)

2.8.7.4. FA assay: CH1S-3 vs trastuzumab

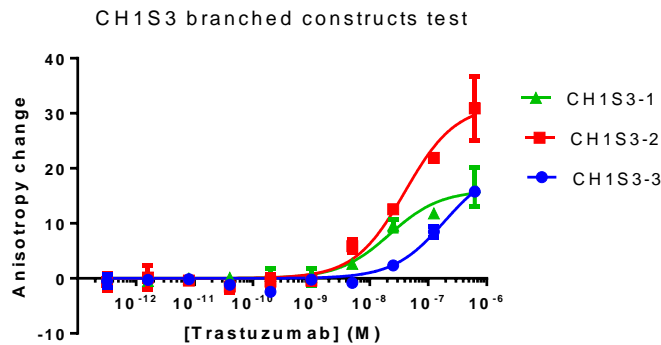
The fluorescent anisotropy assay between 5'-FAM-CH1S-3 and trastuzumab was proceeded as in general procedure in section 2.8.7.1. A G-quadruplex strand (5'-FAM-GGTTGGTGTGGTAGG-3') was used as a negative control sequence. The binding buffer was PBS (without magnesium and calcium) containing 0.55 mM MgCl₂. Stock trastuzumab (Cedarlane Labs) was prepared in 150 μL of 1.38 μM. The serial five-fold dilution of trastuzumab was done to prepare the target solutions with concentration ranging from 0.2 μM to 0.1 pM. The anisotropy of 5'-FAM-CH1S-3 was measured in three replicates, while the negative control was only measured once. The plate was incubated at 37°C for 1 hour.



Constructs	Fitted K_D (nM)
CH1S-3	12 ± 45

2.8.7.5. FA assay: CH1S-3 branched construct binding comparison.

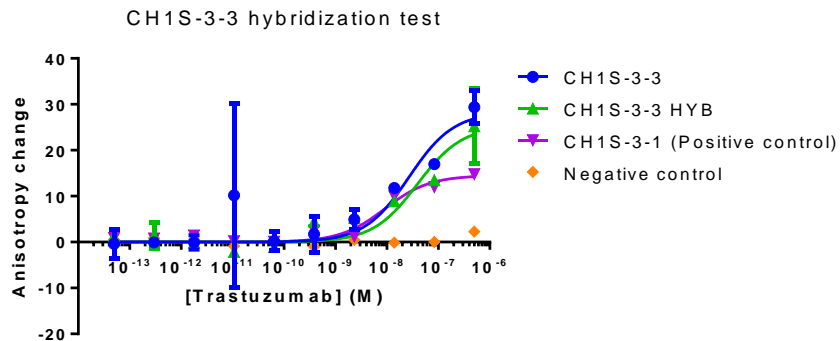
The fluorescent anisotropy assay between 5'-FAM aptamers and trastuzumab was proceeded as in general procedure in section 2.8.7.1. A G-quadruplex strand (5'-FAM-GGTTGGTGTGGTAGG-3') was used as a negative control sequence. The binding buffer was PBS (without magnesium and calcium) containing 0.55 mM MgCl₂. Stock trastuzumab (Cedarlane Labs) was prepared in 150 μL of 3.38 μM. The serial five-fold dilution of trastuzumab was done to prepare the target solutions with concentration ranging from 0.2 μM to 0.1 pM. The anisotropy of 5'-FAM aptamers (CH1S-3-1 CH1S-3-2 and CH1S-3-3) was measured in two replicates, while the anisotropy of negative control was only measured once. The plate was incubated at 37°C for 1 hour.



Constructs	K_D (nM)
CH1S-3-1	22 ± 11
CH1S-3-2	40 ± 18
CH1S-3-3	187 ± 106

2.8.7.6. FA assay: CH1S-3-3 hybridization test

The fluorescent anisotropy assay between 5'-FAM aptamers and trastuzumab was proceeded as in general procedure in section 2.8.7.1. The binding buffer was PBS (without magnesium and calcium) containing 0.55 mM MgCl₂. Stock trastuzumab (Cedarlane Labs) was prepared in 150 μ L of 3.38 μ M. The serial five-fold dilution of trastuzumab was done to prepare the target solutions with concentration ranging from 0.2 μ M to 0.1 pM. The anisotropy of 5'-FAM aptamers (CH1S-3-3, CH1S-3-3 HYB) was measured in three replicates. The plate was incubated at 37°C for 1 hour.



Constructs	K _D (nM)
CH1S-3-1	9.1 ± 2.2
CH1S-3-3	27 ± 20
CH1S-3-3 HYB	39 ± 18

2.8.8. Surface plasmon resonance

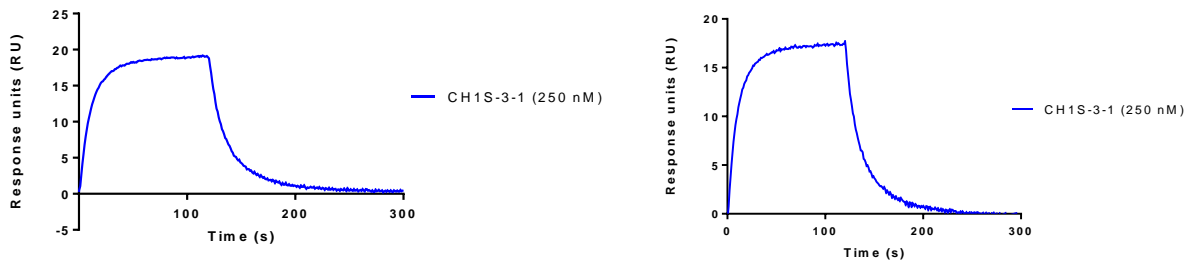
2.8.8.1. Target captured with streptavidin-coated SPR chip.

The experiment was done on Biacore X-100 surface plasmon resonance biosensor. The streptavidin chip was prepared by washing with solution of 1 M NaCl and 50 mM NaOH. 50 μ L of biotinylated trastuzumab (100 tests, ordered from CedarLane Labs, Canada) was prepared in 200 μ L of HBS-EP+ buffer for immobilization. Oligomers were diluted into the HBS-EP+ buffer with. Oligomers were prepared in binding buffer (HBS-EP+ buffer with 20 mM KCl, 1 mM CaCl₂ and 1 mM MgCl₂) at concentrations ranging from 100 to 1000 nM. The Biacore X100 instrument was primed three times with running buffer prior to all binding assays and injected over both flow cells at a flow rate of 30 μ L/min for 120 s to monitor target association, and running buffer was injected over both flow cells at a flow rate of 30 μ L/min for 180 s to monitor target dissociation.

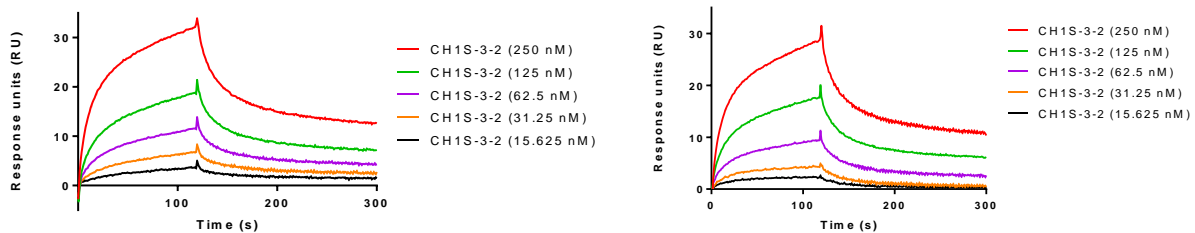
Oligomer was removed from the sensor surface by injecting 2 M NaCl for 30 s at a flow rate of 30 $\mu\text{L}/\text{min}$ over both flow cells.

Data processing and analysis were performed using Biacore X100 Evaluation Software version 2.0 (GE Healthcare). A double-referencing method was performed to process all datasets. Data from the sample flow cell (FC2) were referenced first by subtracting data from the reference flow cell (FC1) to correct for bulk refractive index changes, nonspecific binding, injection noise, matrix effects, and baseline drift. Reference-subtracted data (FC2–FC1) were double-referenced with a blank injection of running buffer to account for any systematic drift over the course of the injection. Double-referenced data were fit to a 1:1 binding model for kinetic analysis.

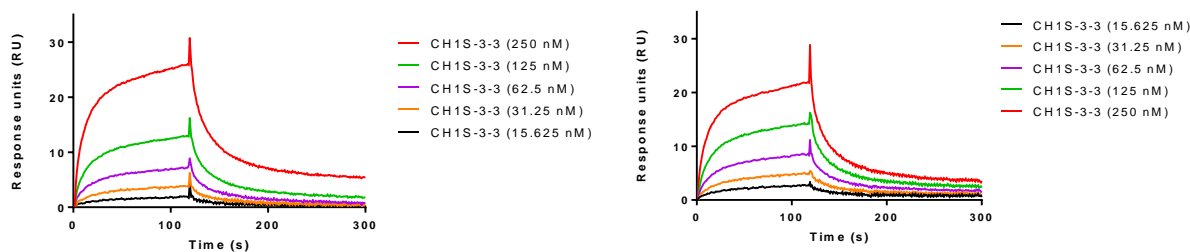
a. Positive control (CH1S-3) (2 replicates)



b. CH1S-3-2 (2 replicates)



c. CH1S-3-3 (2 replicates)

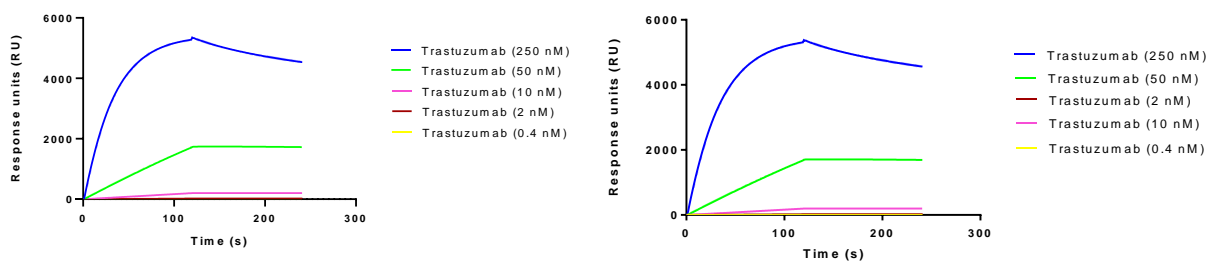


2.8.8.2. Aptamer captured with poly-T chip.

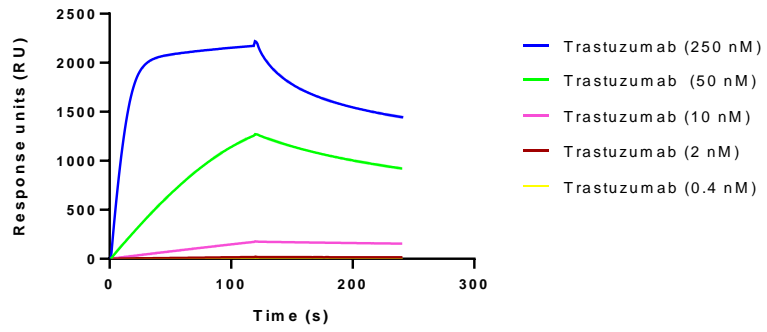
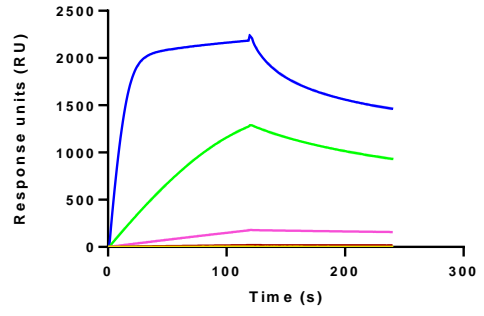
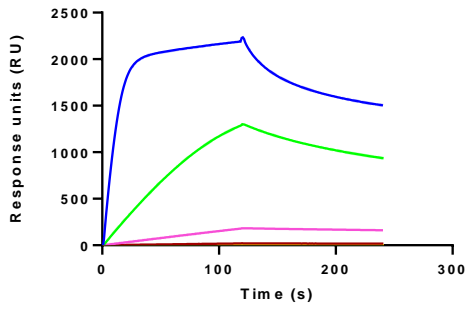
The experiment was done in Biacore X-100 surface plasmon resonance biosensor. The amino-poly(T) DNA sequence of 5'-NH₂-TTTTTTTTTTTTTTTTTTTTTTTTTTTTTTT-3' was suspended in 10 mM HEPES buffer into a 40 μM poly(T)-DNA solution. The surfactant CTAB was suspended in 10 mM HEPES buffer into a 1.2 mM CTAB solution. A “pre-concentration” test was run with COOH-attached CM5 Biacore chip and a mixture of CTAB and poly(T)-DNA to ensure the interaction of DNA strand on the surface of the chip. Next, the poly(T) DNA strand (in mixture of CTAB) was immobilized into the chip in the presence of EDC, NHS and ethanolamine. The signal of poly(T) immobilization was kept around 3000 RU. The poly(A)-aptamers were diluted in binding buffer (HBS-EP+ buffer with 20 mM KCl, 1 mM CaCl₂ and 1 mM MgCl₂) to make 3 μM solutions. Trastuzumab was also diluted in binding buffer in a range of solution from 250 nM to 0.4 nM. The Biacore X100 instrument was primed three times with running buffer prior to all binding assays and injected over both flow cells at a flow rate of 30 μL/min for 120 s to monitor target association, and running buffer was injected over both flow cells at a flow rate of 30 μL/min for 180 s to monitor target dissociation. Poly(A)-aptamers was removed from the sensor surface by injecting 25 mM NaOH for 30 s at a flow rate of 30 μL/min over both flow cells.

Data processing and analysis were performed using Biacore X100 Evaluation Software version 2.0 (GE Healthcare). A double-referencing method was performed to process all datasets. Data from the sample flow cell (FC2) were referenced first by subtracting data from the reference flow cell (FC1) to correct for bulk refractive index changes, nonspecific binding, injection noise, matrix effects, and baseline drift. Reference-subtracted data (FC2–FC1) were double-referenced with a blank injection of running buffer to account for any systematic drift over the course of the injection. Double-referenced data were fit to a 1:1 binding model for kinetic analysis.

a. Poly(A)-CH1S-3 (2 replicates)



b. Poly(A)-CH1S-3-3 (3 replicates)



References

- (1) Voet, D.; Voet, J. G. *Biochemistry*; John Wiley & Sons, **2011**.
- (2) Watson, J. D. *Molecular biology of the gene*; Benjamin Cummings, **2003**.
- (3) Dahm, R. Discovering DNA: Friedrich Miescher and the early years of nucleic acid research. *Hum Genet* **2008**, *122* (6), 565-581.
- (4) Levine, P. A. The structure of yeast nucleic acid: IV. Ammonia hydrolysis *J Biol Chem* **1919**, *40* (4), 415-424.
- (5) Watson, J. D.; Crick, F. H. Molecular structure of nucleic acids; a structure for deoxyribose nucleic acid. *Nature* **1953**, *171* (4356), 737-738.
- (6) Minchin, S.; Lodge, J. Understanding biochemistry: structure and function of nucleic acids. *Essays Biochem* **2019**, *63* (4), 433-456.
- (7) Yakovchuk, P.; Protozanova, E.; Frank-Kamenetskii, M. D. Base-stacking and base-pairing contributions into thermal stability of the DNA double helix. *Nucleic Acids Res* **2006**, *34* (2), 564-574.
- (8) Neidle, S. Beyond the double helix: DNA structural diversity and the PDB. *J Biol Chem* **2021**, *296*, 100553.
- (9) Dickerson, R. E. DNA structure from A to Z. *Methods Enzymol* **1992**, *211*, 67-111.
- (10) Drew, H. R.; Wing, R. M.; Takano, T.; Broka, C.; Tanaka, S.; Itakura, K.; Dickerson, R. E. Structure of a B-DNA dodecamer: conformation and dynamics. *Proc Natl Acad Sci U S A* **1981**, *78* (4), 2179-2183.
- (11) Lim, G. F.; Merz, G. E.; McCann, M. D.; Gruskiewicz, J. M.; Serra, M. J. Stability of single-nucleotide bulge loops embedded in a GAAA RNA hairpin stem. *RNA* **2012**, *18* (4), 807-814.
- (12) Kankia, B. I.; Marky, L. A. DNA, RNA, and DNA/RNA Oligomer Duplexes: A Comparative Study of Their Stability, Heat, Hydration, and Mg²⁺ Binding Properties. *J Phys Chem B* **1999**, *103* (41), 8759-8767.
- (13) Saenger, W. *Principles of nucleic acid structure*; Springer-Verlag, **1984**.
- (14) Merrifield, R. B. Solid-Phase Peptide Synthesis. 1. The Synthesis of a Tetrapeptide. *J Am Chem Soc* **1963**, *85*, 2149-2154.

- (15) Beaucage, S. L.; Caruthers, M. H. Deoxynucleoside Phosphoramidites - a New Class of Key Intermediates for Deoxypolynucleotide Synthesis. *Tetrahedron Lett* **1981**, *22* (20), 1859-1862.
- (16) Yu, G. W.; Kang, Y. H. Solid-Phase Synthesis of 2'-O-Methoxyethyl Oligonucleotides Using Dimeric Phosphoramidite Blocks. *Bull Korean Chem Soc* **2016**, *37* (11), 1754-1759.
- (17) Molina, A. G.; Sanghvi, Y. S. Liquid-Phase Oligonucleotide Synthesis: Past, Present, and Future Predictions. *Curr Protoc Nucleic Acid Chem* **2019**, *77* (1), e82.
- (18) Ballico, M.; Drioli, S.; Morvan, F.; Xodo, L.; Bonora, G. M. Triple, MPEG-conjugated, helix-forming oligonucleotides (TRIEGXs): liquid-phase synthesis of natural and chimeric "all-purine" sequences linked to high molecular weight poly(ethylene glycols). *Bioconjug Chem* **2001**, *12* (5), 719-725.
- (19) Donga, R. A.; Khaliq-Uz-Zaman, S. M.; Chan, T. H.; Damha, M. J. A novel approach to oligonucleotide synthesis using an imidazolium ion tag as a soluble support. *J Org Chem* **2006**, *71* (20), 7907-7910.
- (20) Molina, A. G.; Kungurtsev, V.; Virta, P.; Lonngberg, H. Acetylated and methylated beta-cyclodextrins as viable soluble supports for the synthesis of short 2'-oligodeoxyribo-nucleotides in solution. *Molecules* **2012**, *17* (10), 12102-12120.
- (21) Kim, J. F.; Gaffney, P. R. J.; Valtcheva, I. B.; Williams, G.; Buswell, A. M.; Anson, M. S.; Livingston, A. G. Organic Solvent Nanofiltration (OSN): A New Technology Platform for Liquid-Phase Oligonucleotide Synthesis (LPOS). *Org Process Res Dev* **2016**, *20* (8), 1439-1452.
- (22) Gaffney, P. R.; Kim, J. F.; Valtcheva, I. B.; Williams, G. D.; Anson, M. S.; Buswell, A. M.; Livingston, A. G. Liquid-Phase Synthesis of 2'-Methyl-RNA on a Homostar Support through Organic-Solvent Nanofiltration. *Chemistry* **2015**, *21* (26), 9535-9543.
- (23) Takahashi, D.; Inomata, T.; Fukui, T. AJIPHASE(R): A Highly Efficient Synthetic Method for One-Pot Peptide Elongation in the Solution Phase by an Fmoc Strategy. *Angew Chem Int Ed Engl* **2017**, *56* (27), 7803-7807.

- (24) Yoo, E.; Choe, D.; Shin, J.; Cho, S.; Cho, B. K. Mini review: Enzyme-based DNA synthesis and selective retrieval for data storage. *Comput Struct Biotechnol J* **2021**, *19*, 2468-2476.
- (25) Mathews, A. S.; Yang, H.; Montemagno, C. Photo-cleavable nucleotides for primer free enzyme mediated DNA synthesis. *Org Biomol Chem* **2016**, *14* (35), 8278-8288.
- (26) Seeman, N. C. Nucleic acid junctions and lattices. *J Theor Biol* **1982**, *99* (2), 237-247.
- (27) Tintore, M.; Eritja, R.; Fabrega, C. DNA nanoarchitectures: steps towards biological applications. *Chembiochem* **2014**, *15* (10), 1374-1390.
- (28) Li, X.; Yang, X.; Qi, J.; Seeman, N. C. Antiparallel DNA Double Crossover Molecules As Components for Nanoconstruction. *J Am Chem Soc* **1996**, *118* (26), 6131-6140.
- (29) LaBean, T. H.; Yan, H.; Kopatsch, J.; Liu, F.; Winfree, E.; Reif, J. H.; Seeman, N. C. Construction, Analysis, Ligation, and Self-Assembly of DNA Triple Crossover Complexes. *J Am Chem Soc* **2000**, *122* (9), 1848-1860.
- (30) Zhang, X.; Yan, H.; Shen, Z.; Seeman, N. C. Paranemic cohesion of topologically-closed DNA molecules. *J Am Chem Soc* **2002**, *124* (44), 12940-12941.
- (31) Winfree, E.; Liu, F.; Wenzler, L. A.; Seeman, N. C. Design and self-assembly of two-dimensional DNA crystals. *Nature* **1998**, *394* (6693), 539-544.
- (32) Shih, W. M.; Quispe, J. D.; Joyce, G. F. A 1.7-kilobase single-stranded DNA that folds into a nanoscale octahedron. *Nature* **2004**, *427* (6975), 618-621.
- (33) Rothemund, P. W. Folding DNA to create nanoscale shapes and patterns. *Nature* **2006**, *440* (7082), 297-302.
- (34) Douglas, S. M.; Dietz, H.; Liedl, T.; Hogberg, B.; Graf, F.; Shih, W. M. Self-assembly of DNA into nanoscale three-dimensional shapes. *Nature* **2009**, *459* (7245), 414-418.
- (35) Zhang, F.; Jiang, S.; Wu, S.; Li, Y.; Mao, C.; Liu, Y.; Yan, H. Complex wireframe DNA origami nanostructures with multi-arm junction vertices. *Nat Nanotechnol* **2015**, *10* (9), 779-784.

- (36) Tikhomirov, G.; Petersen, P.; Qian, L. Fractal assembly of micrometre-scale DNA origami arrays with arbitrary patterns. *Nature* **2017**, *552* (7683), 67-71.
- (37) Wei, B.; Dai, M.; Yin, P. Complex shapes self-assembled from single-stranded DNA tiles. *Nature* **2012**, *485* (7400), 623-626.
- (38) Ke, Y.; Ong, L. L.; Shih, W. M.; Yin, P. Three-dimensional structures self-assembled from DNA bricks. *Science* **2012**, *338* (6111), 1177-1183.
- (39) Park, S.-J.; Lazarides, A. A.; Storhoff, J. J.; Pesce, L.; Mirkin, C. A. The Structural Characterization of Oligonucleotide-Modified Gold Nanoparticle Networks Formed by DNA Hybridization. *J Phys Chem B* **2004**, *108* (33), 12375-12380.
- (40) Park, S. Y.; Lytton-Jean, A. K.; Lee, B.; Weigand, S.; Schatz, G. C.; Mirkin, C. A. DNA-programmable nanoparticle crystallization. *Nature* **2008**, *451* (7178), 553-556.
- (41) Auyeung, E.; Li, T. I.; Senesi, A. J.; Schmucker, A. L.; Pals, B. C.; de la Cruz, M. O.; Mirkin, C. A. DNA-mediated nanoparticle crystallization into Wulff polyhedra. *Nature* **2014**, *505* (7481), 73-77.
- (42) Mitra, D.; Di Cesare, N.; Sleiman, H. F. Self-assembly of cyclic metal-DNA nanostructures using ruthenium tris(bipyridine)-branched oligonucleotides. *Angew Chem Int Ed Engl* **2004**, *43* (43), 5804-5808.
- (43) Yang, H.; Rys, A. Z.; McLaughlin, C. K.; Sleiman, H. F. Templated ligand environments for the selective incorporation of different metals into DNA. *Angew Chem Int Ed Engl* **2009**, *48* (52), 9919-9923.
- (44) Yang, H.; Altvater, F.; de Bruijn, A. D.; McLaughlin, C. K.; Lo, P. K.; Sleiman, H. F. Chiral metal-DNA four-arm junctions and metalated nanotubular structures. *Angew Chem Int Ed Engl* **2011**, *50* (20), 4620-4623.
- (45) Aldaye, F. A.; Lo, P. K.; Karam, P.; McLaughlin, C. K.; Cosa, G.; Sleiman, H. F. Modular construction of DNA nanotubes of tunable geometry and single- or double-stranded character. *Nat Nanotechnol* **2009**, *4* (6), 349-352.
- (46) Hariri, A. A.; Hamblin, G. D.; Gidi, Y.; Sleiman, H. F.; Cosa, G. Stepwise growth of surface-grafted DNA nanotubes visualized at the single-molecule level. *Nat Chem* **2015**, *7* (4), 295-300.

- (47) Lo, P. K.; Karam, P.; Aldaye, F. A.; McLaughlin, C. K.; Hamblin, G. D.; Cosa, G.; Sleiman, H. F. Loading and selective release of cargo in DNA nanotubes with longitudinal variation. *Nat Chem* **2010**, *2* (4), 319-328.
- (48) Lee, H.; Lytton-Jean, A. K.; Chen, Y.; Love, K. T.; Park, A. I.; Karagiannis, E. D.; Sehgal, A.; Querbes, W.; Zurenko, C. S.; Jayaraman, M.; et al. Molecularly self-assembled nucleic acid nanoparticles for targeted in vivo siRNA delivery. *Nat Nanotechnol* **2012**, *7* (6), 389-393.
- (49) Wiraja, C.; Zhu, Y.; Lio, D. C. S.; Yeo, D. C.; Xie, M.; Fang, W.; Li, Q.; Zheng, M.; Van Steensel, M.; Wang, L.; et al. Framework nucleic acids as programmable carrier for transdermal drug delivery. *Nat Commun* **2019**, *10* (1), 1147.
- (50) Turek, V. A.; Chikkaraddy, R.; Cormier, S.; Stockham, B.; Ding, T.; Keyser, U. F.; Baumberg, J. J. Thermo-Responsive Actuation of a DNA Origami Flexor. *J Adv Funct Mater* **2018**, *28* (25), 1706410.
- (51) Liu, D.; Bruckbauer, A.; Abell, C.; Balasubramanian, S.; Kang, D. J.; Klenerman, D.; Zhou, D. A reversible pH-driven DNA nanoswitch array. *J Am Chem Soc* **2006**, *128* (6), 2067-2071.
- (52) Di Fusco, D.; Dinallo, V.; Marafini, I.; Figliuzzi, M. M.; Romano, B.; Monteleone, G. Antisense Oligonucleotide: Basic Concepts and Therapeutic Application in Inflammatory Bowel Disease. *Front Pharmacol* **2019**, *10*, 305.
- (53) Rinaldi, C.; Wood, M. J. A. Antisense oligonucleotides: the next frontier for treatment of neurological disorders. *Nat Rev Neurol* **2018**, *14* (1), 9-21.
- (54) Watts, J. K.; Corey, D. R. Silencing disease genes in the laboratory and the clinic. *J Pathol* **2012**, *226* (2), 365-379.
- (55) Dana, H.; Chalbatani, G. M.; Mahmoodzadeh, H.; Karimloo, R.; Rezaiean, O.; Moradzadeh, A.; Mehmandoost, N.; Moazzen, F.; Mazraeh, A.; Marmari, V.; et al. Molecular Mechanisms and Biological Functions of siRNA. *Int J Biomed Sci* **2017**, *13* (2), 48-57.

- (56) Egli, M.; Manoharan, M. Chemistry, structure and function of approved oligonucleotide therapeutics. *Nucleic Acids Res* **2023**, *51* (6), 2529-2573.
- (57) Zhou, Y.; Peng, J.; Shen, W.; Li, X. Psoralen as an interstrand DNA crosslinker in the selection of DNA-Encoded dynamic chemical library. *Biochem Biophys Res Commun* **2020**, *533* (2), 215-222.
- (58) Brenner, S.; Lerner, R. A. Encoded combinatorial chemistry. *Proc Natl Acad Sci U S A* **1992**, *89* (12), 5381-5383.
- (59) Nielsen, J.; Brenner, S.; Janda, K. D. Synthetic methods for the implementation of encoded combinatorial chemistry. *J Am Chem Soc* **1993**, *115* (21), 9812-9813.
- (60) Favalli, N.; Bassi, G.; Scheuermann, J.; Neri, D. DNA-encoded chemical libraries - achievements and remaining challenges. *FEBS Lett* **2018**, *592* (12), 2168-2180.
- (61) Madsen, D.; Azevedo, C.; Micco, I.; Petersen, L. K.; Hansen, N. J. V. An overview of DNA-encoded libraries: A versatile tool for drug discovery. *Prog Med Chem* **2020**, *59*, 181-249.
- (62) Leimbacher, M.; Zhang, Y.; Mannocci, L.; Stravs, M.; Geppert, T.; Scheuermann, J.; Schneider, G.; Neri, D. Discovery of small-molecule interleukin-2 inhibitors from a DNA-encoded chemical library. *Chemistry* **2012**, *18* (25), 7729-7737.
- (63) Li, Y.; De Luca, R.; Cazzamalli, S.; Pretto, F.; Bajic, D.; Scheuermann, J.; Neri, D. Versatile protein recognition by the encoded display of multiple chemical elements on a constant macrocyclic scaffold. *Nat Chem* **2018**, *10* (4), 441-448.
- (64) Li, Y.; Zhao, P.; Zhang, M.; Zhao, X.; Li, X. Multistep DNA-templated synthesis using a universal template. *J Am Chem Soc* **2013**, *135* (47), 17727-17730.
- (65) Melkko, S.; Scheuermann, J.; Dumelin, C. E.; Neri, D. Encoded self-assembling chemical libraries. *Nat Biotechnol* **2004**, *22* (5), 568-574.

- (66) Wichert, M.; Krall, N.; Decurtins, W.; Franzini, R. M.; Pretto, F.; Schneider, P.; Neri, D.; Scheuermann, J. Dual-display of small molecules enables the discovery of ligand pairs and facilitates affinity maturation. *Nat Chem* **2015**, *7* (3), 241-249.
- (67) Arico-Muendel, C.; Zhu, Z.; Dickson, H.; Parks, D.; Keicher, J.; Deng, J.; Aquilani, L.; Coppo, F.; Graybill, T.; Lind, K.; et al. Encoded library technology screening of hepatitis C virus NS4B yields a small-molecule compound series with in vitro replicon activity. *Antimicrob Agents Chemother* **2015**, *59* (6), 3450-3459.
- (68) Maianti, J. P.; McFedries, A.; Foda, Z. H.; Kleiner, R. E.; Du, X. Q.; Leissring, M. A.; Tang, W. J.; Charron, M. J.; Seeliger, M. A.; Saghatelian, A.; et al. Anti-diabetic activity of insulin-degrading enzyme inhibitors mediated by multiple hormones. *Nature* **2014**, *511* (7507), 94-98.
- (69) Clark, M. A.; Acharya, R. A.; Arico-Muendel, C. C.; Belyanskaya, S. L.; Benjamin, D. R.; Carlson, N. R.; Centrella, P. A.; Chiu, C. H.; Creaser, S. P.; Cuzzo, J. W.; et al. Design, synthesis and selection of DNA-encoded small-molecule libraries. *Nat Chem Biol* **2009**, *5* (9), 647-654.
- (70) Hunter, J. H.; Prendergast, L.; Valente, L. F.; Madin, A.; Pairaudeau, G.; Waring, M. J. High Fidelity Suzuki-Miyaura Coupling for the Synthesis of DNA Encoded Libraries Enabled by Micelle Forming Surfactants. *Bioconjug Chem* **2020**, *31* (1), 149-155.
- (71) Ji, Y.; Dai, D.; Luo, H.; Shen, S.; Fan, J.; Wang, Z.; Chen, M.; Wan, J.; Li, J.; Ma, H.; et al. C-S Coupling of DNA-Conjugated Aryl Iodides for DNA-Encoded Chemical Library Synthesis. *Bioconjug Chem* **2021**, *32* (4), 685-689.
- (72) Graham, J. S.; Hunter, J. H.; Waring, M. J. Micellar Buchwald-Hartwig Coupling of Aryl and Heteroarylamines for the Synthesis of DNA-Encoded Libraries. *J Org Chem* **2021**, *86* (23), 17257-17264.
- (73) Chheda, P. R.; Simmons, N.; Schuman, D. P.; Shi, Z. Palladium-Mediated Carbonylative Suzuki Coupling for DNA-Encoded Library Synthesis. *Org Lett* **2022**, *24* (28), 5214-5219.

- (74) Phelan, J. P.; Lang, S. B.; Sim, J.; Berritt, S.; Peat, A. J.; Billings, K.; Fan, L.; Molander, G. A. Open-Air Alkylation Reactions in Photoredox-Catalyzed DNA-Encoded Library Synthesis. *J Am Chem Soc* **2019**, *141* (8), 3723-3732.
- (75) Badir, S. O.; Lipp, A.; Krumb, M.; Cabrera-Afonso, M. J.; Kammer, L. M.; Wu, V. E.; Huang, M.; Csakai, A.; Marcaurelle, L. A.; Molander, G. A. Photoredox-mediated hydroalkylation and hydroarylation of functionalized olefins for DNA-encoded library synthesis. *Chem Sci* **2021**, *12* (36), 12036-12045.
- (76) Jetson, R. R.; Krusemark, C. J. Sensing Enzymatic Activity by Exposure and Selection of DNA-Encoded Probes. *Angew Chem Int Ed Engl* **2016**, *55* (33), 9562-9566.
- (77) Cochrane, W. G.; Malone, M. L.; Dang, V. Q.; Cavett, V.; Satz, A. L.; Paegel, B. M. Activity-Based DNA-Encoded Library Screening. *ACS Comb Sci* **2019**, *21* (5), 425-435.
- (78) Zhou, Y.; Li, C.; Peng, J.; Xie, L.; Meng, L.; Li, Q.; Zhang, J.; Li, X. D.; Li, X.; Huang, X.; et al. DNA-Encoded Dynamic Chemical Library and Its Applications in Ligand Discovery. *J Am Chem Soc* **2018**, *140* (46), 15859-15867.
- (79) Petersen, L. K.; Christensen, A. B.; Andersen, J.; Folkesson, C. G.; Kristensen, O.; Andersen, C.; Alzu, A.; Slok, F. A.; Blakskjaer, P.; Madsen, D.; et al. Screening of DNA-Encoded Small Molecule Libraries inside a Living Cell. *J Am Chem Soc* **2021**, *143* (7), 2751-2756.
- (80) Zhou, J.; Rossi, J. Aptamers as targeted therapeutics: current potential and challenges. *Nat Rev Drug Discov* **2017**, *16* (3), 181-202.
- (81) Kalra, P.; Dhiman, A.; Cho, W. C.; Bruno, J. G.; Sharma, T. K. Simple Methods and Rational Design for Enhancing Aptamer Sensitivity and Specificity. *Front Mol Biosci* **2018**, *5*, 41.
- (82) Keefe, A. D.; Pai, S.; Ellington, A. Aptamers as therapeutics. *Nat Rev Drug Discov* **2010**, *9* (7), 537-550.
- (83) Dunn, M. R.; Jimenez, R. M.; Chaput, J. C. Analysis of aptamer discovery and technology. *Nature Reviews Chemistry* **2017**, *1* (10), 0076.

- (84) Kratschmer, C.; Levy, M. Effect of Chemical Modifications on Aptamer Stability in Serum. *Nucleic Acid Ther* **2017**, *27* (6), 335-344.
- (85) Li, Z.; Fu, X.; Huang, J.; Zeng, P.; Huang, Y.; Chen, X.; Liang, C. Advances in Screening and Development of Therapeutic Aptamers Against Cancer Cells. *Front Cell Dev Biol* **2021**, *9*, Review.
- (86) Kong, H. Y.; Byun, J. Nucleic Acid aptamers: new methods for selection, stabilization, and application in biomedical science. *Biomol Ther (Seoul)* **2013**, *21* (6), 423-434.
- (87) Chai, C.; Xie, Z.; Grotewold, E. SELEX (Systematic Evolution of Ligands by EXponential Enrichment), as a powerful tool for deciphering the protein-DNA interaction space. *Methods Mol Biol* **2011**, *754*, 249-258.
- (88) Catuogno, S.; Esposito, C. L. Aptamer Cell-Based Selection: Overview and Advances. *Biomedicines* **2017**, *5* (3).
- (89) Gold, L.; Ayers, D.; Bertino, J.; Bock, C.; Bock, A.; Brody, E. N.; Carter, J.; Dalby, A. B.; Eaton, B. E.; Fitzwater, T.; et al. Aptamer-based multiplexed proteomic technology for biomarker discovery. *PLoS One* **2010**, *5* (12), e15004.
- (90) Sakamoto, T.; Ennifar, E.; Nakamura, Y. Thermodynamic study of aptamers binding to their target proteins. *Biochimie* **2018**, *145*, 91-97.
- (91) Hayashi, T.; Oshima, H.; Mashima, T.; Nagata, T.; Katahira, M.; Kinoshita, M. Binding of an RNA aptamer and a partial peptide of a prion protein: crucial importance of water entropy in molecular recognition. *Nucleic Acids Res* **2014**, *42* (11), 6861-6875.
- (92) Zhao, Q.; Tao, J.; Feng, W.; Uppal, J. S.; Peng, H.; Le, X. C. Aptamer binding assays and molecular interaction studies using fluorescence anisotropy - A review. *Anal Chim Acta* **2020**, *1125*, 267-278.
- (93) Bassani, G. F.; Liedl, G. L.; Wyder, P. *Encyclopedia of condensed matter physics*; Elsevier, 2005.
- (94) Zhang, D.; Lu, M.; Wang, H. Fluorescence anisotropy analysis for mapping aptamer-protein interaction at the single nucleotide level. *J Am Chem Soc* **2011**, *133* (24), 9188-9191.

- (95) Kanakaraj, I.; Chen, W. H.; Poongavanam, M.; Dhamane, S.; Stagg, L. J.; Ladbury, J. E.; Kourentzi, K.; Strych, U.; Willson, R. C. Biophysical characterization of VEGF-aHt DNA aptamer interactions. *Int J Biol Macromol* **2013**, *57*, 69-75.
- (96) Song, Z.; Mao, J.; Barrero, R. A.; Wang, P.; Zhang, F.; Wang, T. Development of a CD63 Aptamer for Efficient Cancer Immunochemistry and Immunoaffinity-Based Exosome Isolation. *Molecules* **2020**, *25* (23).
- (97) Gokulrangan, G.; Unruh, J. R.; Holub, D. F.; Ingram, B.; Johnson, C. K.; Wilson, G. S. DNA aptamer-based bioanalysis of IgE by fluorescence anisotropy. *Anal Chem* **2005**, *77* (7), 1963-1970.
- (98) Zhao, Q.; Lv, Q.; Wang, H. Identification of allosteric nucleotide sites of tetramethylrhodamine-labeled aptamer for noncompetitive aptamer-based fluorescence anisotropy detection of a small molecule, ochratoxin A. *Anal Chem* **2014**, *86* (2), 1238-1245.
- (99) Samokhvalov, A. V.; Safenkova, I. V.; Eremin, S. A.; Zherdev, A. V.; Dzantiev, B. B. Measurement of (Aptamer-Small Target) K(D) Using the Competition between Fluorescently Labeled and Unlabeled Targets and the Detection of Fluorescence Anisotropy. *Anal Chem* **2018**, *90* (15), 9189-9198.
- (100) Li, Y.; Sun, L.; Zhao, Q. Competitive fluorescence anisotropy/polarization assay for ATP using aptamer as affinity ligand and dye-labeled ATP as fluorescence tracer. *Talanta* **2017**, *174*, 7-13.
- (101) Liu, Y.; Zhao, Q. Direct fluorescence anisotropy assay for cocaine using tetramethylrhodamine-labeled aptamer. *Anal Bioanal Chem* **2017**, *409* (16), 3993-4000.
- (102) Bakhtiar, R. Surface Plasmon Resonance Spectroscopy: A Versatile Technique in a Biochemist's Toolbox. *J Chem Educ* **2013**, *90* (2), 203-209.
- (103) Chang, A. L.; McKeague, M.; Liang, J. C.; Smolke, C. D. Kinetic and equilibrium binding characterization of aptamers to small molecules using a label-free, sensitive, and scalable platform. *Anal Chem* **2014**, *86* (7), 3273-3278.
- (104) Sun, L.; Shen, K.; Zhang, J.; Wan, W.; Cao, W.; Wang, Z.; Guo, C. Aptamer based surface plasma resonance assay for direct detection of neuron specific enolase and progastrin-releasing peptide (31-98). *RSC Adv* **2021**, *11* (51), 32135-32142.

- (105) Potty, A. S.; Kourentzi, K.; Fang, H.; Jackson, G. W.; Zhang, X.; Legge, G. B.; Willson, R. C. Biophysical characterization of DNA aptamer interactions with vascular endothelial growth factor. *Biopolymers* **2009**, *91* (2), 145-156.
- (106) Eremeeva, E.; Herdewijn, P. PCR Amplification of Base-Modified DNA. *Curr Protoc Chem Biol* **2018**, *10* (1), 18-48.
- (107) Kimoto, M.; Hirao, I. Genetic alphabet expansion technology by creating unnatural base pairs. *Chem Soc Rev* **2020**, *49* (21), 7602-7626.
- (108) Elskens, J. P.; Elskens, J. M.; Madder, A. Chemical Modification of Aptamers for Increased Binding Affinity in Diagnostic Applications: Current Status and Future Prospects. *Int J Mol Sci* **2020**, *21* (12).
- (109) Elliott, D.; Lodomery, M. *Molecular biology of RNA*; Oxford University Press, 2016.
- (110) Green, L. S.; Jellinek, D.; Bell, C.; Beebe, L. A.; Feistner, B. D.; Gill, S. C.; Jucker, F. M.; Janjic, N. Nuclease-resistant nucleic acid ligands to vascular permeability factor/vascular endothelial growth factor. *Chem Biol* **1995**, *2* (10), 683-695.
- (111) Burmeister, P. E.; Lewis, S. D.; Silva, R. F.; Preiss, J. R.; Horwitz, L. R.; Pendergrast, P. S.; McCauley, T. G.; Kurz, J. C.; Epstein, D. M.; Wilson, C.; et al. Direct in vitro selection of a 2'-O-methyl aptamer to VEGF. *Chem Biol* **2005**, *12* (1), 25-33.
- (112) Ruckman, J.; Green, L. S.; Beeson, J.; Waugh, S.; Gillette, W. L.; Henninger, D. D.; Claesson-Welsh, L.; Janjic, N. 2'-Fluoropyrimidine RNA-based aptamers to the 165-amino acid form of vascular endothelial growth factor (VEGF165). Inhibition of receptor binding and VEGF-induced vascular permeability through interactions requiring the exon 7-encoded domain. *J Biol Chem* **1998**, *273* (32), 20556-20567.
- (113) Lauridsen, L. H.; Rothnagel, J. A.; Veedu, R. N. Enzymatic recognition of 2'-modified ribonucleoside 5'-triphosphates: towards the evolution of versatile aptamers. *ChemBiochem* **2012**, *13* (1), 19-25.

- (114) Pinheiro, V. B.; Taylor, A. I.; Cozens, C.; Abramov, M.; Renders, M.; Zhang, S.; Chaput, J. C.; Wengel, J.; Peak-Chew, S. Y.; McLaughlin, S. H.; et al. Synthetic genetic polymers capable of heredity and evolution. *Science* **2012**, *336* (6079), 341-344.
- (115) Anosova, I.; Kowal, E. A.; Dunn, M. R.; Chaput, J. C.; Van Horn, W. D.; Egli, M. The structural diversity of artificial genetic polymers. *Nucleic Acids Res* **2016**, *44* (3), 1007-1021.
- (116) Verbeure, B.; Lescrinier, E.; Wang, J.; Herdewijn, P. RNase H mediated cleavage of RNA by cyclohexene nucleic acid (CeNA). *Nucleic Acids Res* **2001**, *29* (24), 4941-4947.
- (117) Sau, S. P.; Kumar, T. S.; Hrdlicka, P. J. Invader LNA: efficient targeting of short double stranded DNA. *Org Biomol Chem* **2010**, *8* (9), 2028-2036.
- (118) Li, F.; Sarkhel, S.; Wilds, C. J.; Wawrzak, Z.; Prakash, T. P.; Manoharan, M.; Egli, M. 2'-Fluoroarabino- and arabinonucleic acid show different conformations, resulting in deviating RNA affinities and processing of their heteroduplexes with RNA by RNase H. *Biochemistry* **2006**, *45* (13), 4141-4152.
- (119) Darfeuille, F.; Hansen, J. B.; Orum, H.; Di Primo, C.; Toulme, J. J. LNA/DNA chimeric oligomers mimic RNA aptamers targeted to the TAR RNA element of HIV-1. *Nucleic Acids Res* **2004**, *32* (10), 3101-3107.
- (120) Schmidt, K. S.; Borkowski, S.; Kurreck, J.; Stephens, A. W.; Bald, R.; Hecht, M.; Friebe, M.; Dinkelborg, L.; Erdmann, V. A. Application of locked nucleic acids to improve aptamer in vivo stability and targeting function. *Nucleic Acids Res* **2004**, *32* (19), 5757-5765.
- (121) Rose, K. M.; Alves Ferreira-Bravo, I.; Li, M.; Craigie, R.; Ditzler, M. A.; Holliger, P.; DeStefano, J. J. Selection of 2'-Deoxy-2'-Fluoroarabino Nucleic Acid (FANA) Aptamers That Bind HIV-1 Integrase with Picomolar Affinity. *ACS Chem Biol* **2019**, *14* (10), 2166-2175.
- (122) Zhang, L.; Chaput, J. C. In Vitro Selection of an ATP-Binding TNA Aptamer. *Molecules* **2020**, *25* (18).
- (123) Dunn, M. R.; McCloskey, C. M.; Buckley, P.; Rhea, K.; Chaput, J. C. Generating Biologically Stable TNA Aptamers that Function with High Affinity and Thermal Stability. *J Am Chem Soc* **2020**, *142* (17), 7721-7724.

- (124) Ghassemi, K. M.; Demelenne, A.; Crommen, J.; Servais, A. C.; Fillet, M. Improvement of chemo- and stereoselectivity for phosphorothioate oligonucleotides in capillary electrophoresis by addition of cyclodextrins. *J Chromatogr A* **2022**, *1676*, 463270.
- (125) Jahns, H.; Taneja, N.; Willoughby, J. L. S.; Akabane-Nakata, M.; Brown, C. R.; Nguyen, T.; Bisbe, A.; Matsuda, S.; Hettinger, M.; Manoharan, R. M.; et al. Chirality matters: stereo-defined phosphorothioate linkages at the termini of small interfering RNAs improve pharmacology in vivo. *Nucleic Acids Res* **2022**, *50* (3), 1221-1240.
- (126) Volk, D. E.; Lokesh, G. L. R. Development of Phosphorothioate DNA and DNA Thioaptamers. *Biomedicines* **2017**, *5* (3).
- (127) Huang, Y.; Knouse, K. W.; Qiu, S.; Hao, W.; Padial, N. M.; Vantourout, J. C.; Zheng, B.; Mercer, S. E.; Lopez-Ogalla, J.; Narayan, R.; et al. A P(V) platform for oligonucleotide synthesis. *Science* **2021**, *373* (6560), 1265-1270.
- (128) Yang, Z.; Sismour, A. M.; Benner, S. A. Nucleoside alpha-thiotriphosphates, polymerases and the exonuclease III analysis of oligonucleotides containing phosphorothioate linkages. *Nucleic Acids Res* **2007**, *35* (9), 3118-3127.
- (129) Zaitseva, M.; Kaluzhny, D.; Shchylkina, A.; Borisova, O.; Smirnov, I.; Pozmogova, G. Conformation and thermostability of oligonucleotide d(GGTTGGTGGTGG) containing thiophosphoryl internucleotide bonds at different positions. *Biophys Chem* **2010**, *146* (1), 1-6.
- (130) Somasunderam, A.; Thiviyathan, V.; Tanaka, T.; Li, X.; Neerathilingam, M.; Lokesh, G. L.; Mann, A.; Peng, Y.; Ferrari, M.; Klostergaard, J.; et al. Combinatorial selection of DNA thioaptamers targeted to the HA binding domain of human CD44. *Biochemistry* **2010**, *49* (42), 9106-9112.
- (131) Vaillant, A.; Juteau, J. M.; Lu, H.; Liu, S.; Lackman-Smith, C.; Ptak, R.; Jiang, S. Phosphorothioate oligonucleotides inhibit human immunodeficiency virus type 1 fusion by blocking gp41 core formation. *Antimicrob Agents Chemother* **2006**, *50* (4), 1393-1401.

- (132) Higashimoto, Y.; Matsui, T.; Nishino, Y.; Taira, J.; Inoue, H.; Takeuchi, M.; Yamagishi, S. Blockade by phosphorothioate aptamers of advanced glycation end products-induced damage in cultured pericytes and endothelial cells. *Microvasc Res* **2013**, *90*, 64-70. DOI: 10.1016/j.mvr.2013.08.010 From NLM Medline.
- (133) Yang, X.; Gorenstein, D. G. Progress in thioaptamer development. *Curr Drug Targets* **2004**, *5* (8), 705-715.
- (134) Chen, J.; Xiang, Y.; Wang, P.; Liu, J.; Lai, W.; Xiao, M.; Pei, H.; Fan, C.; Li, L. Ensemble Modified Aptamer Based Pattern Recognition for Adaptive Target Identification. *Nano Lett* **2022**, *22* (24), 10057-10065.
- (135) Dong, Y. *Aptamers for Analytical Applications : Affinity Acquisition and Method Design*; Wiley-VCH, 2018.
- (136) Odeh, F.; Nsairat, H.; Alshaer, W.; Ismail, M. A.; Esawi, E.; Qaqish, B.; Bawab, A. A.; Ismail, S. I. Aptamers Chemistry: Chemical Modifications and Conjugation Strategies. *Molecules* **2019**, *25* (1).
- (137) Chan, K. Y.; Kinghorn, A. B.; Hollenstein, M.; Tanner, J. A. Chemical Modifications for a Next Generation of Nucleic Acid Aptamers. *Chembiochem* **2022**, *23* (15), e202200006.
- (138) Gawande, B. N.; Rohloff, J. C.; Carter, J. D.; von Carlowitz, I.; Zhang, C.; Schneider, D. J.; Janjic, N. Selection of DNA aptamers with two modified bases. *Proc Natl Acad Sci U S A* **2017**, *114* (11), 2898-2903.
- (139) He, W.; Elizondo-Riojas, M. A.; Li, X.; Lokesh, G. L.; Somasunderam, A.; Thiviyathan, V.; Volk, D. E.; Durland, R. H.; Englehardt, J.; Cavaotto, C. N.; et al. X-aptamers: a bead-based selection method for random incorporation of druglike moieties onto next-generation aptamers for enhanced binding. *Biochemistry* **2012**, *51* (42), 8321-8323.
- (140) Yoshikawa, A. M.; Rangel, A.; Feagin, T.; Chun, E. M.; Wan, L.; Li, A.; Moeckl, L.; Wu, D.; Eisenstein, M.; Pitteri, S.; et al. Discovery of indole-modified aptamers for highly specific recognition of protein glycoforms. *Nat Commun* **2021**, *12* (1), 7106.

- (141) Pfeiffer, F.; Tolle, F.; Rosenthal, M.; Brandle, G. M.; Ewers, J.; Mayer, G. Identification and characterization of nucleobase-modified aptamers by click-SELEX. *Nat Protoc* **2018**, *13* (5), 1153-1180.
- (142) Siegl, J.; Pluckthun, O.; Mayer, G. Dependence of click-SELEX performance on the nature and average number of modified nucleotides. *RSC Chem Biol* **2022**, *3* (3), 288-294.
- (143) Pluckthun, O.; Siegl, J.; Bryant, L. L.; Mayer, G. Dynamic changes in DNA populations revealed by split-combine selection. *Chem Sci* **2020**, *11* (35), 9577-9583.
- (144) Movahedi, M.; Khamissi, N.; Hili, R. Ligase-Catalyzed Oligonucleotide Polymerization (LOOPER): Evolution of chemically diverse aptamer libraries. *Aptamers* **2021**, *5*, 22-30.
- (145) Chen, Z.; Lichtor, P. A.; Berliner, A. P.; Chen, J. C.; Liu, D. R. Evolution of sequence-defined highly functionalized nucleic acid polymers. *Nat Chem* **2018**, *10* (4), 420-427.
- (146) Lei, Y.; Kong, D.; Hili, R. A High-Fidelity Codon Set for the T4 DNA Ligase-Catalyzed Polymerization of Modified Oligonucleotides. *ACS Comb Sci* **2015**, *17* (12), 716-721.
- (147) Lei, Y.; Washington, J.; Hili, R. Efficiency and fidelity of T3 DNA ligase in ligase-catalysed oligonucleotide polymerisations. *Org Biomol Chem* **2019**, *17* (7), 1962-1965.
- (148) Kong, D.; Movahedi, M.; Mahdavi-Amiri, Y.; Yeung, W.; Tiburcio, T.; Chen, D.; Hili, R. Evolutionary Outcomes of Diversely Functionalized Aptamers Isolated from in Vitro Evolution. *ACS Synth Biol* **2020**, *9* (1), 43-52.
- (149) Kimoto, M.; Kawai, R.; Mitsui, T.; Yokoyama, S.; Hirao, I. An unnatural base pair system for efficient PCR amplification and functionalization of DNA molecules. *Nucleic Acids Res* **2009**, *37* (2), e14.
- (150) Kimoto, M.; Yamashige, R.; Matsunaga, K.; Yokoyama, S.; Hirao, I. Generation of high-affinity DNA aptamers using an expanded genetic alphabet. *Nat Biotechnol* **2013**, *31* (5), 453-457.
- (151) Sefah, K.; Yang, Z.; Bradley, K. M.; Hoshika, S.; Jimenez, E.; Zhang, L.; Zhu, G.; Shanker, S.; Yu, F.; Turek, D.; et al. In vitro selection with artificial expanded genetic information systems. *Proc Natl Acad Sci U S A* **2014**, *111* (4), 1449-1454.

- (152) Zumrut, H.; Yang, Z.; Williams, N.; Arizala, J.; Batool, S.; Benner, S. A.; Mallikaratchy, P. Ligand-Guided Selection with Artificially Expanded Genetic Information Systems against TCR-CD3epsilon. *Biochemistry* **2020**, *59* (4), 552-562.
- (153) Vorobyeva, M. A.; Davydova, A. S.; Vorobjev, P. E.; Venyaminova, A. G. Key Aspects of Nucleic Acid Library Design for in Vitro Selection. *Int J Mol Sci* **2018**, *19* (2).
- (154) Shampo, M. A.; Kyle, R. A.; Steensma, D. P. Sidney Altman--Nobel laureate for work with RNA. *Mayo Clin Proc* **2012**, *87* (10), e73.
- (155) Walter, N. G.; Engelke, D. R. Ribozymes: catalytic RNAs that cut things, make things, and do odd and useful jobs. *Biologist (London)* **2002**, *49* (5), 199-203.
- (156) Hollenstein, M. DNA Catalysis: The Chemical Repertoire of DNAzymes. *Molecules* **2015**, *20* (11), 20777-20804.
- (157) Huang, P. J.; Liu, J. In vitro Selection of Chemically Modified DNAzymes. *ChemistryOpen* **2020**, *9* (10), 1046-1059.
- (158) Seelig, B.; Keiper, S.; Stuhlmann, F.; Jaschke, A. Enantioselective Ribozyme Catalysis of a Bimolecular Cycloaddition Reaction. *Angew Chem Int Ed Engl* **2000**, *39* (24), 4576-4579.
- (159) Helm, M.; Petermeier, M.; Ge, B.; Fiammengo, R.; Jaschke, A. Allosterically activated Diels-Alder catalysis by a ribozyme. *J Am Chem Soc* **2005**, *127* (30), 10492-10493.
- (160) Zhou, C.; Avins, J. L.; Klauser, P. C.; Brandsen, B. M.; Lee, Y.; Silverman, S. K. DNA-Catalyzed Amide Hydrolysis. *J Am Chem Soc* **2016**, *138* (7), 2106-2109.
- (161) Ray, P.; Viles, K. D.; Soule, E. E.; Woodruff, R. S. Application of aptamers for targeted therapeutics. *Arch Immunol Ther Exp (Warsz)* **2013**, *61* (4), 255-271.
- (162) Kim, D. H.; Seo, J. M.; Shin, K. J.; Yang, S. G. Design and clinical developments of aptamer-drug conjugates for targeted cancer therapy. *Biomater Res* **2021**, *25* (1), 42.

- (163) Ni, S.; Zhuo, Z.; Pan, Y.; Yu, Y.; Li, F.; Liu, J.; Wang, L.; Wu, X.; Li, D.; Wan, Y.; et al. Recent Progress in Aptamer Discoveries and Modifications for Therapeutic Applications. *ACS Appl Mater Interfaces* **2021**, *13* (8), 9500-9519.
- (164) Jakobsen, M. R.; Haasnoot, J.; Wengel, J.; Berkhout, B.; Kjems, J. Efficient inhibition of HIV-1 expression by LNA modified antisense oligonucleotides and DNAzymes targeted to functionally selected binding sites. *Retrovirology* **2007**, *4*, 29.
- (165) Sadiq, M. A.; Hanout, M.; Sarwar, S.; Hassan, M.; Agarwal, A.; Sepah, Y. J.; Do, D. V.; Nguyen, Q. D. Platelet-Derived Growth Factor Inhibitors: A Potential Therapeutic Approach for Ocular Neovascularization. *Dev Ophthalmol* **2016**, *55*, 310-316.
- (166) Cosmi, B. ARC-1779, a PEGylated aptamer antagonist of von Willebrand factor for potential use as an anticoagulant or antithrombotic agent. *Curr Opin Mol Ther* **2009**, *11* (3), 322-328.
- (167) Halawa, O. A.; Lin, J. B.; Miller, J. W.; Vavvas, D. G. A Review of Completed and Ongoing Complement Inhibitor Trials for Geographic Atrophy Secondary to Age-Related Macular Degeneration. *J Clin Med* **2021**, *10* (12).
- (168) Povsic, T. J.; Vavalle, J. P.; Aberle, L. H.; Kasprzak, J. D.; Cohen, M. G.; Mehran, R.; Bode, C.; Buller, C. E.; Montalescot, G.; Cornel, J. H.; et al. A Phase 2, randomized, partially blinded, active-controlled study assessing the efficacy and safety of variable anticoagulation reversal using the REG1 system in patients with acute coronary syndromes: results of the RADAR trial. *Eur Heart J* **2013**, *34* (31), 2481-2489.
- (169) Winkler, W.; Nahvi, A.; Breaker, R. R. Thiamine derivatives bind messenger RNAs directly to regulate bacterial gene expression. *Nature* **2002**, *419* (6910), 952-956.
- (170) Winkler, W. C.; Cohen-Chalamish, S.; Breaker, R. R. An mRNA structure that controls gene expression by binding FMN. *Proc Natl Acad Sci U S A* **2002**, *99* (25), 15908-15913.

- (171) Mironov, A. S.; Gusarov, I.; Rafikov, R.; Lopez, L. E.; Shatalin, K.; Kreneva, R. A.; Perumov, D. A.; Nudler, E. Sensing small molecules by nascent RNA: a mechanism to control transcription in bacteria. *Cell* **2002**, *111* (5), 747-756.
- (172) Nahvi, A.; Sudarsan, N.; Ebert, M. S.; Zou, X.; Brown, K. L.; Breaker, R. R. Genetic control by a metabolite binding mRNA. *Chem Biol* **2002**, *9* (9), 1043.
- (173) Wachter, A.; Tunc-Ozdemir, M.; Grove, B. C.; Green, P. J.; Shintani, D. K.; Breaker, R. R. Riboswitch control of gene expression in plants by splicing and alternative 3' end processing of mRNAs. *Plant Cell* **2007**, *19* (11), 3437-3450.
- (174) Breaker, R. R. Prospects for riboswitch discovery and analysis. *Mol Cell* **2011**, *43* (6), 867-879.
- (175) Winkler, W. C.; Nahvi, A.; Sudarsan, N.; Barrick, J. E.; Breaker, R. R. An mRNA structure that controls gene expression by binding S-adenosylmethionine. *Nat Struct Biol* **2003**, *10* (9), 701-707.
- (176) Huang, W.; Kim, J.; Jha, S.; Aboul-ela, F. The impact of a ligand binding on strand migration in the SAM-I riboswitch. *PLoS Comput Biol* **2013**, *9* (5), e1003069.
- (177) Savinov, A.; Block, S. M. Self-cleavage of the glmS ribozyme core is controlled by a fragile folding element. *Proc Natl Acad Sci U S A* **2018**, *115* (47), 11976-11981.
- (178) Ketzer, P.; Kaufmann, J. K.; Engelhardt, S.; Bossow, S.; von Kalle, C.; Hartig, J. S.; Ungerechts, G.; Nettelbeck, D. M. Artificial riboswitches for gene expression and replication control of DNA and RNA viruses. *Proc Natl Acad Sci U S A* **2014**, *111* (5), E554-562.
- (179) Dincer, C.; Bruch, R.; Costa-Rama, E.; Fernandez-Abedul, M. T.; Merkoci, A.; Manz, A.; Urban, G. A.; Guder, F. Disposable Sensors in Diagnostics, Food, and Environmental Monitoring. *Adv Mater* **2019**, *31* (30), e1806739.
- (180) McConnell, E. M.; Cozma, I.; Mou, Q.; Brennan, J. D.; Lu, Y.; Li, Y. Biosensing with DNazymes. *Chem Soc Rev* **2021**, *50* (16), 8954-8994.

- (181) Idili, A.; Gerson, J.; Parolo, C.; Kippin, T.; Plaxco, K. W. An electrochemical aptamer-based sensor for the rapid and convenient measurement of L-tryptophan. *Anal Bioanal Chem* **2019**, *411* (19), 4629-4635.
- (182) Ferguson, B. S.; Hoggarth, D. A.; Maliniak, D.; Ploense, K.; White, R. J.; Woodward, N.; Hsieh, K.; Bonham, A. J.; Eisenstein, M.; Kippin, T. E.; et al. Real-time, aptamer-based tracking of circulating therapeutic agents in living animals. *Sci Transl Med* **2013**, *5* (213), 213ra165.
- (183) Lu, Z.; Xiong, W.; Wang, P.; Li, X.; Zhai, K.; Shi, R.; Xiang, D. Simultaneous detection of lead (II) and mercury (II) ions using nucleic acid aptamer molecular beacons. *J Environ Anal Chem* **2021**, *101* (13), 1922-1934.
- (184) Liu, X.; Hou, Y.; Chen, S.; Liu, J. Controlling dopamine binding by the new aptamer for a FRET-based biosensor. *Biosens Bioelectron* **2020**, *173*, 112798. DOI: 10.1016/j.bios.2020.112798 From NLM Publisher.
- (185) Yamamoto, R.; Baba, T.; Kumar, P. K. Molecular beacon aptamer fluoresces in the presence of Tat protein of HIV-1. *Genes Cells* **2000**, *5* (5), 389-396.
- (186) Sapkota, K.; Dhakal, S. FRET-Based Aptasensor for the Selective and Sensitive Detection of Lysozyme. *Sensors (Basel)* **2020**, *20* (3).
- (187) Liu, M.; Song, J.; Shuang, S.; Dong, C.; Brennan, J. D.; Li, Y. A graphene-based biosensing platform based on the release of DNA probes and rolling circle amplification. *ACS Nano* **2014**, *8* (6), 5564-5573.
- (188) He, Y.; Chen, D.; Huang, P. J.; Zhou, Y.; Ma, L.; Xu, K.; Yang, R.; Liu, J. Misfolding of a DNAzyme for ultrahigh sodium selectivity over potassium. *Nucleic Acids Res* **2018**, *46* (19), 10262-10271.
- (189) de Rochambeau, D.; Hirka, S.; Saliba, D.; Anderson, S.; Toader, V.; Dore, M.; Rizzuto, F.; McKeague, M.; Sleiman, H. F. Orthogonal DNA barcodes enable the high-throughput screening of sequence-defined polymers. **2022**.
- (190) Bock, L. C.; Griffin, L. C.; Latham, J. A.; Vermaas, E. H.; Toole, J. J. Selection of single-stranded DNA molecules that bind and inhibit human thrombin. *Nature* **1992**, *355* (6360), 564-566.

- (191) Nagatoishi, S.; Isono, N.; Tsumoto, K.; Sugimoto, N. Loop residues of thrombin-binding DNA aptamer impact G-quadruplex stability and thrombin binding. *Biochimie* **2011**, *93* (8), 1231-1238.
- (192) Russo Krauss, I.; Merlino, A.; Randazzo, A.; Novellino, E.; Mazzarella, L.; Sica, F. High-resolution structures of two complexes between thrombin and thrombin-binding aptamer shed light on the role of cations in the aptamer inhibitory activity. *Nucleic Acids Res* **2012**, *40* (16), 8119-8128.
- (193) Smirnov, I.; Shafer, R. H. Effect of loop sequence and size on DNA aptamer stability. *Biochemistry* **2000**, *39* (6), 1462-1468.
- (194) Roxo, C.; Kotkowiak, W.; Pasternak, A. G-Quadruplex-Forming Aptamers-Characteristics, Applications, and Perspectives. *Molecules* **2019**, *24* (20).
- (195) McKeague, M.; Calzada, V.; Cerchia, L.; DeRosa, M.; Heemstra, J. M.; Janjic, N.; Johnson, P. E.; Kraus, L.; Limson, J.; Mayer, G.; et al. The minimum aptamer publication standards (MAPS guidelines) for *de novo* aptamer selection. *Aptamers* **2022**, *6*, 10-18.
- (196) Hirka, S.; McKeague, M. Quantification of aptamer-protein binding with fluorescence anisotropy. *Aptamers* **2021**, *5*, 1-6.
- (197) Gao, T.; Pei, R. Isolation of DNA Aptamer Targeting PD-1 with an Antitumor Immunotherapy Effect. *ACS Appl Bio Mater* **2020**, *3* (10), 7080-7086.
- (198) Chen, K.; Zhou, J.; Shao, Z.; Liu, J.; Song, J.; Wang, R.; Li, J.; Tan, W. Aptamers as Versatile Molecular Tools for Antibody Production Monitoring and Quality Control. *J Am Chem Soc* **2020**, *142* (28), 12079-12086.
- (199) Kypr, J.; Kejnovska, I.; Renciuik, D.; Vorlickova, M. Circular dichroism and conformational polymorphism of DNA. *Nucleic Acids Res* **2009**, *37* (6), 1713-1725.
- (200) Horn, T.; Chang, C. A.; Urdea, M. S. An improved divergent synthesis of comb-type branched oligodeoxyribonucleotides (bDNA) containing multiple secondary sequences. *Nucleic Acids Res* **1997**, *25* (23), 4835-4841.

(201) *Glen Report 24.18: Technical Brief – Compatibility of UltraMild Monomers or Ac-dC with Hydrazine Reagent.* <https://www.glenresearch.com/reports/gr24-18> (accessed 2023-06-13).

(202) McKeague, M.; De Girolamo, A.; Valenzano, S.; Pascale, M.; Ruscito, A.; Velu, R.; Frost, N. R.; Hill, K.; Smith, M.; McConnell, E. M.; et al. Comprehensive analytical comparison of strategies used for small molecule aptamer evaluation. *Anal Chem* **2015**, *87* (17), 8608-8612.